Study of the effect of nonlocal hopping and resetting in asymmetric exclusion process

A thesis submitted

in partial fulfillment for the award of the degree of

Doctor of Philosophy

by

Karthika S.

Department of Physics

Indian Institute of Space Science and Technology

Thiruvananthapuram, India

March 8, 2021

Certificate

This is to certify that the thesis titled ***Study of the effect of nonlocal hopping and resetting in asymmetric exclusion process*** submitted by **Karthika S.**, to the Indian Institute of Space Science and Technology, Thiruvananthapuram, in partial fulfillment for the award of the degree of **Doctor of Philosophy** in **Physics** is a bonafide record of the original work carried out by her under my supervision. The contents of this thesis, in full or in parts, have not been submitted to any other Institute or University for the award of any degree or diploma.

Dr. Apoorva Nagar
Research supervisor
Department of Physics

Counter signature of HOD with Seal

Place: Thiruvananthapuram
Date: March 8, 2021

Declaration

I declare that this thesis titled ***Study of the effect of nonlocal hopping and resetting in asymmetric exclusion process*** submitted in partial fulfillment for the award of the degree of **Doctor of Philosophy** in **Physics** is a record of the original work carried out by me under the supervision of **Dr. Apoorva Nagar** and has not formed the basis for the award of any degree, diploma, associateship, fellowship, or other titles in this or any other Institution or University of higher learning. In keeping with the ethical practice in reporting scientific information, due acknowledgements have been made wherever the findings of others have been cited.

Place: Thiruvananthapuram
Date: March 8, 2021

Karthika S.
SC13D014

To Amma and Achan.

Acknowledgements

Firstly, I would like to express my sincere gratitude to my advisor Dr. Apoorva Nagar for the continuous support of my research, for his patience, motivation and immense knowledge. His guidance helped me in all the time of research and writing of this thesis. I could not have imagined having a better advisor and mentor for my research career. Without his consistent support throughout the research, this thesis work might be impossible.

Besides my advisor, I would like to thank the rest of my thesis committee members: Dr. Punyabrata Pradhan, Dr. Sreedhar B Dutta, Dr. S. Murugesh, Dr. Naveen Surendran and Dr. Resmi Lekhmi for their insightful comments and encouragement, but also for the hard question which incented me to widen my research from various perspectives. I should mention special thanks to Dr. Naveen Surendran in the initial days of research, his assistance in learning the theory is appreciable.

I take this opportunity to sincerely acknowledge IIST for providing financial assistance and the necessary infrastructure and resources to accomplish my research work.

I am indebted to many of my friends for providing a stimulating and fun-filled atmosphere. My thanks go to Deepak, Sarath and Sajith they are always willing to rectify my doubts related to simulation. I am ever indebted to Soumya and I admired her distinguished helping nature. My special appreciation goes to Pavithra for her friendship and encouragement. I wish to thank my friends Reshmi, Devi and Meegle for their love care and moral support. I am also thankful to Randeep, Najeeb, Viji, Deepthi, Veena, Praveen, Rahul, Anu, Gayathri, Neema, Preethi, Richa, Anvy, Neethu, Ani and Ram. I wish to thank my best friend Newton Nath for his valuable care and support during my research.

I would like to thank my family: my parents and to my brothers for supporting me spiritually throughout writing this thesis. Last but not least I would like to mention a great thanks to Rohith my better half he helped me in all my research and supported me without any complaint and regret that enabled me to complete my thesis. Besides this, I would like to express my sincere gratitude to all people who knowingly or unknowingly helped me in the successful completion of this research.

Karthika S.

Abstract

The totally asymmetric simple exclusion process (TASEP) is a paradigmatic model of nonequilibrium statistical mechanics. It describes a system of particles interacting with each other via hard-core repulsions, undergoing driven diffusive dynamics. The one dimensional version of the model is simple to define and has been used to model various phenomena like mRNA translation, molecular motors and traffic flow. With periodic boundaries, it has been shown that the steady state has a solution with all microstates being equally probable. When the boundaries are open, the model shows interesting behaviour with the existence of three different phases determined by the input and output rates of the particles. Due to its simplicity of definition and non-trivial but well understood phase behaviour, the TASEP has been adapted to model various physical phenomena by varying the particle and boundary dynamics. In this thesis, our motivation is to study the effect of two different kinds of dynamics on driven diffusive systems and we have chosen TASEP as the basic system to study these effects.

In the first part of the thesis, we will describe our results on the effect of nonlocal hopping dynamics on the phase behaviour of driven diffusive systems. Here we considered a model where in addition to the normal TASEP dynamics of moving to the nearest neighbour site, the particle is also allowed to make a long hop all the way to the next unoccupied site before an occupied site. The non-local hopping dynamics is characterized by a parameter p with $p = 0$ corresponding to the usual TASEP. The introduction of finite p in a model with open boundaries leads to the possibility of a new phase called empty road (ER) phase, where the particles clear out of the lattice soon after entry, leading to a zero bulk density. We have studied the full phase diagram in the three dimensional phase space of entry rate α, exit rate β and the nonlocal hopping parameter p. Using numerical simulations and mean field arguments, we studied the transitions between four possible phases; the three usual TASEP phases: low density (LD), high density (HD) and maximal current (MC), as well as the new ER phase. We mapped out the full phase diagram and showed that the ER and HD phases come to dominate the phase space at large values of p. In addition to the open boundary system, we also studied the effect of nonlocal hopping in a system with periodic boundaries and defects. When the defect is static, we see that the long hop dynamics introduces a phase transition into the system between two different kinds of shock

phases, which we have named LD-HD and ER-HD. While the defect always produces a shock between a high and a low density region, the long hop dynamics opens up the possibility of the density becoming zero on the low density side. When the impurity considered is dynamic (one slow particle), we see a transition between a homogeneous density phase and a shock phase. Increasing the value of p increases the tendency of shock formation and we have mapped out the complete phase diagram of the system in the $\mu - p$ space, where the parameter μ is the hopping probability of the slower particle. The mean field approximation works well qualitatively and correctly identifies the possible phases, while the quantitative agreement with numerics varies depending on parameter values.

In the second part of the thesis, we have studied the effect of stochastic resetting to the initial empty state on a TASEP with open boundaries. The problem of resetting in dynamical systems has invited much recent attention. Resetting involves a sudden large change in the state of the system, in addition to the usual continuous dynamics. TASEP being a paradigmatic model is an obvious choice for the study of such dynamical effects on nonequilibrium driven diffusive systems. In addition to this, we are also motivated by mRNA translation where the resetting dynamics models the observed stochastic decay of mRNA-ribosome machinery. Using numerics and approximate expressions of the time evolution of density in TASEP, we studied the effect of stochastic resetting to an initial, empty lattice state on all the phases of the system. We considered two possibilities for the distribution of the time intervals (τ) between successive resets - a power law $\tau^{-(1+\gamma)}$ where $\gamma > 0$, and an exponential distribution $\lambda e^{-\lambda\tau}$. We find that the system achieves a steady-state in the large time limit for $\gamma > 1$ while for $\gamma < 1$ we see a time dependant scaling function. The large time behaviour of density function shows a power-law decay at the boundaries in all the phases except at the HD phase, where it shows a non-monotonic behaviour. For the exponential resetting case, the monotonic behaviour persists and the system always attains a steady state in the long time limit. The results from numerics show good agreement with the theory.

Contents

List of Figures

Abbreviations

DDS	Driven diffusive system
TASEP	Totally asymmetric simple exclusion process
LD	Low density phase
HD	High density phase
MC	Maximal current phase
ER	Empty rod phase
CDA model	Chipping diffusion aggregation model
MC simulation	Monte Carlo simulation
KPZ model	Kardar Parisi Zang model
EW model	Edward Wilkinson model

Nomenclature

L	Size of the one dimensional discrete lattice
N	Total number of particle on the lattice
i	Lattice site in the discrete lattice space
τ_i	Particle occupation of site i
$p(i,t)$	The probability that the system is in a state i at time t
ω_{ji}	The probability that the particle is at site j at time t, given that it was at site i at the previous time
ρ_i	Average density of particle at the lattice site i
j_i	Current passing through the link joining the sites $i-1$ and i
j	Average current in the steady state of the system
$P(N)$	Probability of total number of particle N on the lattice
ρ_1	Density of number of particle in the first lattice site/just in front of the slow particle
ρ_L	Density of number of particle in the L^{th} lattice site
ρ_b	Density of number of particle in the bulk of the lattice
α	Rate of number of particle entering into left most boundary site from the reservoir
β	Rate of number of particle leaving from the right most boundary site to the right reservoir
p	Probability of nonlocal hopping
μ	Hopping probability of slow particle in the periodic TASEP
r	Hopping probability of particle across the slow bond in the periodic TASEP
α_c	The critical point at which the unstable phase transition occurs from LD to MC phase
α^*	The critical point at which transition from ER to LD phase occurs
β_c	The point at which the unstable phase transition occurs from HD to MC phase
p_c	Critical point after that there occurs only ER-HD phase co-existence in the $\alpha-\beta$ parameter space
j_{LD}	Steady state current in the LD phase

j_{HD}	Steady state current in the HD phase
j_{MC}	Steady state current in the MC phase
ρ_s	Density behind the slow particle at the phase transition
ν_b	Velocity of the particle in the bulk of a periodic TASEP with a slow particle
ρ_c	Average density in the CDA model
ω	Ratio of probability of chipping and probability of movement of the whole mass in the CDA model
ρ_A	Average density over the lattice in TASEP with a slowbond
ρ_h	Average density on the high density side of the shock in periodic TASEP with a slowbond
ρ_l	Average density on the low density side of the shock in periodic TASEP with a slowbond
r_s	Deviation of the position of second class particle from its mean position
σ	Standard deviation of second class particle from its mean position(Interface fluctuations)
γ	Exponent of the powerlaw distribution
λ	Constant resetting rate in the exponential distribution
τ	Time interval between two successive resets
$\rho(x,t)$	Density of number of particle in the lattice at position x at time t in a TASEP
$\rho^r(x,t)$	Reset- averaged density in the lattice at position x at time t in a TASEP
τ_0	Smallest time scale of the system causing resetting
ν	Speed of the incoming front of density α in resetting
ν_r	Speed of backward wave front of density $1-\beta$ in resetting
T	The time at which the reverse moving front of density $1-\beta$ reaches the position x on the lattice
$X(t)$	The position of the front edge of the density wavefront travelling backward
$\rho^r_{ss}(x)$	Reset-averaged density at steady state where resetting time has been drawn from powerlaw distribution
$\rho^r_{st}(x)$	Reset-averaged density at steady state where resetting time has been drawn from exponential distribution

Chapter 1

Introduction

The aim of statistical mechanics is to develop a framework to study systems with a large number of degrees of freedom. Instead of calculating the evolution of every degree of freedom, one uses a probabilistic framework to evaluate the average of macroscopic quantities of interest. For systems in thermal equilibrium, where the properties are time-independent and there is no net probability current between any two microstates, there is a well established framework for calculating various thermodynamic quantities of interest. Even though the predictions from equilibrium statistical mechanics provide an excellent approximation for a large class of real systems, the equilibrium state is an idealization, that works well only under certain conditions. Many phenomena in nature such as chemical reactions, turbulence, etc. carry currents of matter and energy, so they are fundamentally out of equilibrium. Out of equilibrium behaviour is seen in diverse physical systems ranging from nano-scale phenomena [1, 2], quantum optics (laser and maser) [3, 4], high energy physics [3,5], radioactive decay [6], soft materials e.g. sedimentation of colloids [7,8], liquid crystals [9, 10], chemical reactions [11] to astrophysics and cosmology [12]. Everyday life phenomena, such as transport processes in biological systems [13, 14], out of equilibrium pattern formation [15], weather forecast [16], turbulence [17, 18], the behaviour of a group of insects [13, 19], birth and death processes [20], the evolution of the stock market [21], and less frequent phenomena e.g. earthquakes [22,23], are all of a nonequilibrium nature.

Despite the importance of nonequilibrium systems, the theoretical foundation is still not as developed as for equilibrium. A generalized framework [24] for nonequilibrium statistical mechanics has not been formulated, and because of the wide range and enormous complexity of systems, neither has a generalized classification scheme yet been found. An interesting class of systems is those where the system settles at large times into nonequilibrium steady states such that the macroscopic physical properties become

time-independent [25]. Different dynamical equations are used to deal with the great variety of nonequilibrium phenomena ranging from radiation transport in stars to metabolic transport in living cell membranes [26]. Typically, one works with a Markov assumption of no memory and writes a master equation connecting the various microstates of the system. This equation can also be connected to a more coarse grained description of the system using a Fokker-Planck equation for a density like variable or a Langevin equation, which describes the motion of a single particle with the effects of its environment modelled by averaging over the microscopic scales [27, 28].

A nonequilibrium steady state though somewhat similar to a stationary state in equilibrium systems has very important differences. They both exhibit time-independence of physical quantities since the probability of finding a system in a particular microstate is a constant in time. On the other hand, the nonequilibrium steady state allows for a net probability current between two connected microstates, while the equilibrium state satisfies the more stringent condition of detailed balance [29] where there is no probability current between any pair of microstates. The probability current is sometimes manifested as a measurable flow in some physical quantities, for example, a conducting rod connecting two heat reservoirs at different temperatures will achieve a nonequilibrium steady state while allowing for continuous heat flow between the reservoirs while it will be in equilibrium if the temperature of the reservoirs is the same, and there won't be a heat flow. The probability current in nonequilibrium systems is a manifestation of the breaking of time-reversal symmetry, while equilibrium systems retain the symmetry.

Contrary to equilibrium systems where the Hamiltonian is used to calculate quantities of interest using the Gibbs-Boltzmann measure, the behaviour in nonequilibrium systems is usually described by specifying the dynamical rule by which the system evolves from one configuration to another. While one can write a master equation for the evolution of the probability of the microstates, it is usually very difficult to solve. One way to approach the problem is to study simple models that are approximations of the real physical situation. An analytic understanding of such models helps us to understand the key features of more complex systems. Another motivation of studying such models is simply to explore the possibilities for the types of phases in nonequilibrium systems and the transitions between them. One such well established model is the TASEP which belongs to the general class of driven diffusive systems (DDS).

As the name indicates, DDS is a class of systems where the constituents undergo a diffusive motion in addition to a directed motion, leading to an effective current flow through the system. In open systems, this current may carry information from boundaries to the

bulk and thus allow the boundary conditions to control the bulk dynamics [30]. The interplay between boundary conditions and bulk transport leads to interesting properties such as first and second order phase transitions even in one dimensional systems [31]. DDS has become an active area of research due to its wide applications such as ribosome motion along RNA [32, 33], motor movement along molecular tracks [34], cars moving on highways [35, 36] and the stochastic motion of molecular motors through cytoskeletal filaments [37].

One of the first models of driven diffusive systems was introduced by Katz, Lebovitz and Spohn [38] to model the dynamics in fast ionic conductors [39]. The model known as the KLS model after its inventors, is a modified version of the well known Ising model. The equilibrium detailed balance of the usual Ising model is broken by dynamics that mimic the effect of an external field. The up spins are mapped to ions and down spins are the vacant sites. An up spin exchanges with a down spin preferentially in the direction of the external field. Unlike the equilibrium case, the spatio-temporal correlations here show a power law behaviour at and above the critical temperature. Another simple model for driven diffusive systems, known as the TASEP, was introduced originally in 1968 to model the kinetics of biopolymerization [40] and henceforth introduced into the mathematical literature by Spitzer [41]. Now it has become an essential part of the study of a wide class of interacting particle systems [42]. Apart from Physics, it is widely used in modelling phenomena across disciplines and length scales - from cell biology [13], insect behaviour, especially ants [43, 44], to traffic on highways [45]. It is one among the few exactly solvable models in DDS. The simplicity of the model allows for the application of rigorous mathematical methods and to arrive at a number of exact results. This, in turn, sheds light into the intricacies of non-equilibrium statistical mechanics. When applied to real physical systems, suitable variation are applied to the dynamics and these variations lead to interesting new possibilities. This model is the basis of our study in this thesis. In section 1.1 below, we provide a detailed description of TASEP in one dimension.

1.1 Totally asymmetric simple exclusion process (TASEP)

TASEP is a simple model of systems with interacting particles belonging to the class of driven diffusive system. It has been shown that the model settles into a nonequilibrium steady state in the limit of large times [46, 47, 48, 49, 50, 51]. In recent years TASEP and its various modifications have been applied to model diverse physical phenomenon such as transport of micro molecules through thin vessels [52], reptation of polymer in a gel [53],

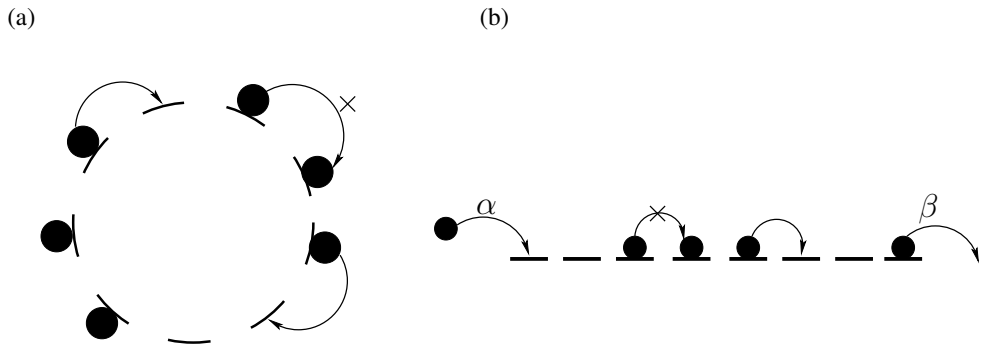

Figure 1.1: (a) The standard TASEP with periodic boundary conditions. The particle number N is conserved. (b) The schematic diagram for TASEP with open boundary conditions. Where α is the injection rate, β is the ejection rate.

hopping conductivity in solid electrolytes [54], surface growth [55] and network analysis [56]. From a theoretical point of view this model provides a platform to study systems out of equilibrium since it is easy to define and to approach analytically, but at the same time has a nontrivial phase structure when the boundaries are open. It has therefore attained a status similar to that of the Ising model in equilibrium statistical mechanics and is seen as a paradigmatic model. In subsections 1.1.1, 1.1.2 and 1.1.3 below, we will first present the basic introduction to TASEP and then the solution for different boundary conditions including the detailed analysis of phase transitions.

1.1.1 Model

We begin with a definition of TASEP on a one dimensional discrete lattice with periodic boundary condition. Sites of the lattice are labelled from 1 to L with site $L+1$ identified as site 1, thus forming a ring. Consider N particles that can move on this lattice. These particles can only move unidirectionally from left to right i.e. site i to site $i+1$. They also have a hardcore exclusion interaction with each other, i.e., if a particle is present on a lattice site, another one cannot move there. The figure 1.1 (a) shows the schematic diagram of TASEP with periodic boundary conditions. At any given time, particles try to move to the nearest neighbour site on their right and the move is successful if the neighbouring site is empty. In this thesis, we will be dealing with stochastic dynamics and therefore the particle moves are random. The model attains a steady state whose properties have been studied using exact analytic methods [57, 58, 59]. We will briefly review the results from these studies in sections 1.1.2 and 1.1.3.

One can similarly define the open boundary version of the TASEP (figure 1.1 (b)). Instead of a ring geometry, we consider the sites 1 and L to be open where particles can enter or exit. We consider site 1 to be the entry site. This is the left-most site and particles attempt to enter this site with a rate of α, the move being successful if site 1 is unoccupied. After entering the lattice, the particles move to the right according to the dynamics described in the previous paragraph. Once a particle reaches the right-most site L, it exits the lattice with a rate of β. The number of particles is not conserved and one can think of the site 1 being connected to an entry reservoir and the site L being connected to an exit reservoir. The system is shown to have different kinds of steady states depending on the entry and exit rates [46, 48].

The configuration or microstate of the system at a given time can be defined in two ways. One can look at the occupation of site i via the variable τ_i ; $\tau_i = 0$ if the site is vacant and $\tau_i = 1$ if it is occupied by a particle. The configuration can then be denoted as the set containing occupancies of all the lattice sites, $\tau = \tau_1, \tau_2, ..., \tau_L$. Another way to specify the configuration of the system is by keeping track of the positions of all the particles. If N is the total number of particles on the lattice (N is fixed in the periodic case but variable in the open boundary case), the state can be defined by the set $x = x_1, x_2, ..., x_N$, where $x_1, x_2, ..., x_N$ are the labels of sites occupied by the particle $1, 2, ..., N$ respectively.

The empty sites in a TASEP are sometimes referred to as holes. The movement of a particle to an empty site can be seen as the exchange of a hole and a particle. An interesting fact regarding holes is that the time evolution of TASEP is symmetric under the particle-hole exchange. Indeed a particle hopping from left to right is equivalent to a hole hopping from right to left. There are various possible updating schemes for the time evolution of a TASEP, such as continuous time, parallel and random sequential [60]. All our work in this thesis has been done using the random sequential updating scheme. In this scheme, one of the L sites is chosen randomly and if a particle is present at the site, it is moved according to the dynamics described above. In case of open boundaries, we consider the system to be having an additional site to the left of site 1, representing the particle reservoir. This site is always taken to be occupied and particles attempt to move out of it and into site 1 with a rate of α. Each such update can be thought of as a micro step and we take one unit of time to consist of L (or $L + 1$ for open systems) such micro steps. A brief description of the analytic solution for TASEP, its phase diagram and the other properties of the system in steady state is given in the subsection 1.1.3.

1.1.2 TASEP with periodic boundary conditions

Figure 1.1(a) shows the schematic diagram of TASEP with periodic boundary conditions. As described above, periodic boundary implies a ring geometry where the sites L and 1 are connected. The total number of particles and therefore the average density is fixed. Using exact analytic calculations, one can show that the TASEP with periodic boundary conditions attains a steady state and its properties can be analytically calculated [57,58,59]. We briefly discuss these results below.

Let $p(i,t)$ be the probability that the system is in a state i at time t. The system makes stochastic transitions between these microstates according to the rules of TASEP dynamics, which are Markovian in nature. The master equation can be written as

$$\frac{\partial p(i,t)}{\partial t} = \sum_j \omega_{ij}\, p(j,t) - \sum_j \omega_{ji}\, p(i,t) \tag{1.1}$$

where ω_{ji} is the probability that a particle move will lead to the system going to a state j at time t, from the state i at the previous time. Only the nearest neighbour moves are allowed, thus $\omega_{ij} \neq 0$ condition is true only for states which are connected to each other via a single particle move by one site.

Steady state implies $\partial p(i,t)/\partial t = 0$. Consider a cluster of particles, i.e. a string of successive sites, all of which are occupied. If there are u such clusters in a configuration, then there are exactly u configurations to which the system can go during the next move, which involves the motion of a single particle from the right end of one of the clusters. Similarly, there are exactly u configurations from which the system can reach the given one via a single particle move. Note that the probabilities ω_{xy} of each of these single particle moves are the same. When we substitute this into the master equation above, and demand a time independent steady state solution, we simply get $p(j) = p(i)$ for all j, i as the solution. Thus all the configurations are equally probable in the steady state. The steady state current can now be calculated and turns out to be the same as the mean field expression: $j = \rho(1-\rho)$ where ρ is the density at the lattice site at steady state [59]. The mean field argument neglects fluctuations, considering an average occupancy for a site. An expression for current can then be constructed by noting that a particle will cross a link between two sites only if the site on the left of a link is occupied and the site on the right is unoccupied. The expression for the current j reflects the fact that when particle densities are low, the increase in density by addition of extra particles will increase the current; on the other hand at high densities, the speed of particles gets impeded by the addition of extra

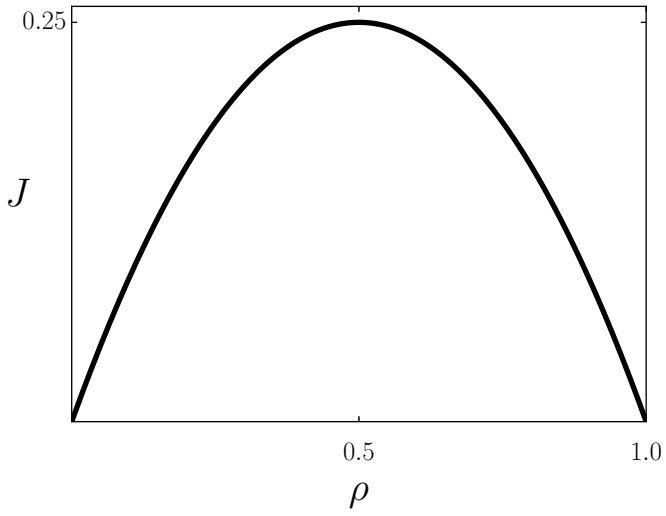

Figure 1.2: Variation of current as a function of density for TASEP.

particles and the current goes down when particle density is increased. This change occurs continuously as a function of the density and there is no phase transition in the system. Figure 1.2 shows the relationship between current and average particle density of particles. It is called the fundamental diagram.

1.1.3 TASEP with open boundaries

Figure 1.1(b) is the schematic diagram for TASEP with open boundary conditions. We consider a one dimensional lattice having L sites. Each site i is either occupied by a particle ($\tau_i = 1$) or is empty ($\tau_i = 0$). The system evolves as follows: at each time step one chooses a site by drawing a random integer from the set $[0, 1, .., L]$ with probability $1/(L + 1)$. If the integer i is between 1 and $L - 1$, and if $\tau_i = 1$, (i,e, we have chosen an occupied site), we move the particle at site i to site $i + 1$ provided site $i + 1$ is empty. There is no move otherwise:

$$\begin{aligned} \tau_i(t+1) &= \tau_i(t)\tau_{i+1}(t), \\ \tau_{i+1}(t+1) &= \tau_{i+1}(t) + [1 - \tau_{i+1}(t)]\,\tau_i(t). \end{aligned} \tag{1.2}$$

If $i = 0$, we have chosen the input reservoir. In this case we move a particle to site 1 with probability α if it is empty. There is no move otherwise:

$$\begin{aligned} \tau_1(t+1) &= 1 \quad \text{with probability} \quad \tau_1(t) + \alpha[1 - \tau_1(t)], \\ \tau_1(t+1) &= 0 \quad \text{with probability} \quad (1-\alpha)[1 - \tau_1(t)]. \end{aligned} \tag{1.3}$$

If $i = L$, we have chosen the exit site. If this site is occupied, we remove the particle with probability β:

$$\begin{aligned} \tau_L(t+1) &= 1 \quad \text{with probability} \quad (1-\beta)\tau_L(t), \\ \tau_L(t+1) &= 0 \quad \text{with probability} \quad 1 - (1-\beta)\tau_L(t). \end{aligned} \tag{1.4}$$

We begin a discussion of the mean field theory approach originally followed in Ref. [46]. While this model has been solved exactly, it is instructive to look at the mean field solution since it will help to understand our approach to other connected models studied in this thesis. The system is expected to achieve a steady state in the limit of large time. In steady state, the average occupation $\langle \tau_i(t) \rangle$ does not change as a function of time. If the occupation at site i $(2 \leq i \leq L-2)$ at time t is $\tau_i(t)$, the occupation at time $t+1$ is given by

$$\tau_i(t+1) = \begin{cases} \tau_i(t) + [1 - \tau_i(t)]\tau_{i-1}(t) & \text{with probability } \frac{1}{L+1}, \\ \tau_i(t)\tau_{i+1}(t) & \text{with probability } \frac{1}{L+1}, \\ \tau_i(t) & \text{with probability } \frac{L-1}{L+1}. \end{cases}$$

Averaging the above equation, one will obtain

$$\langle \tau_i(t+1) \rangle = \langle \tau_i(t) \rangle + \frac{1}{L+1}[\langle \tau_i(t)\tau_{i+1}(t) \rangle - \langle \tau_i(t)\tau_{i-1}(t) \rangle + \langle \tau_{i-1}(t) \rangle - \langle \tau_i(t) \rangle], \tag{1.5}$$

in the steady state average density is time independent and thus

$$\langle \tau_i \rangle - \langle \tau_{i+1}\tau_i \rangle = \langle \tau_{i-1} \rangle - \langle \tau_i \tau_{i-1} \rangle. \tag{1.6}$$

The above equation indicates the conservation of particle current across the lattice in the steady state. Similarly for $i = 1$ and $i = L$

$$\begin{aligned} \langle \tau_1 \rangle - \langle \tau_1 \tau_2 \rangle &= \alpha(1 - \tau_1), \\ \beta \langle \tau_L \rangle &= \langle \tau_{L-1} \rangle - \langle \tau_L \tau_{L-1} \rangle. \end{aligned} \tag{1.7}$$

These are exact steady state equations.

We now use the mean field approximation where correlations are neglected, i.e., $\langle \tau_i \tau_{i+1} \rangle$ is replaced by $\langle \tau_i \rangle \langle \tau_{i+1} \rangle$. We denote $\langle \tau_i \rangle$ by ρ_i. Hence, using the mean field theory, the above equations can be rewritten as:

$$\begin{aligned} \rho_i - \rho_i \rho_{i+1} &= \rho_{i-1} - \rho_{i-1} \rho_i, & (1.8) \\ \rho_1 - \rho_1 \rho_2 &= \alpha(1 - \rho_1), & (1.9) \\ \beta \rho_L &= \rho_{L-1} - \rho_{L-1} \rho_L. & (1.10) \end{aligned}$$

The solutions of these L equations with L unknowns determines the average occupation ρ_i for any finite L. We can rewrite equation (1.8) as simple recursion relation:

$$\rho_{i+1} = 1 - \frac{c}{\rho_i}, \tag{1.11}$$

where c is a constant denoting the current of particle through the lattice. For $c < 1/4$, there are two fixed points for the recursion relation:

$$\rho_{\pm} = \frac{1}{2} \left[1 \pm \sqrt{1 - 4c} \right], \tag{1.12}$$

where ρ_+ is stable and ρ_- is unstable. When $c = 1/4$, there is only one fixed point. When $c > 1/4$, there are no real valued fixed points. We have that ρ_{i+1} is a homographic function of ρ_i

$$\rho_{i+1} = \frac{-\rho_+ \rho_- (\rho_+^i - \rho_-^i) + (\rho_+^{i+1} - \rho_-^{i+1}) \rho_1}{-\rho_+ \rho_- (\rho_+^{i-1} - \rho_-^{i-1}) + (\rho_+^i - \rho_-^i) \rho_1}. \tag{1.13}$$

Clearly ρ_i depends on c and on ρ_1: for $i = L$ this relation can be written as

$$\rho_L = f(c, \rho_1). \tag{1.14}$$

Equation (1.14) and the boundary conditions determines the values of ρ_1, ρ_L and c. From this analysis, we obtain different phases of the given model according to different boundary conditions. Figure 1.3 gives the phase diagram for TASEP.

Phasediagram: 1. *Low density phase:* (Shown in region I of figure 1.3). In this phase, density at site one is set infinitesimally close to the fixed point $\rho_1 = \rho_- + 0^{\pm}$. One sees that the density stays at this value throughout the bulk of the lattice and varies only close to the exit boundary. Using the recursion relation, one can then show that in the

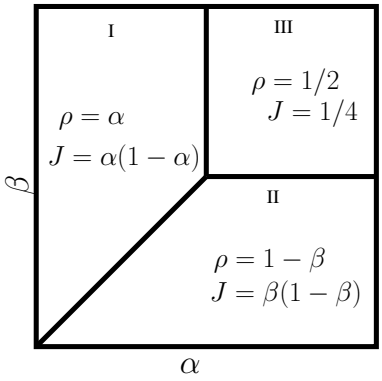

Figure 1.3: Phase diagram of TASEP with open boundaries in the $\alpha - \beta$ plane. Region (I) is the low density (LD) phase, where $\alpha < 1/2$ and $\alpha < \beta$. Region (II) is the high density (HD) phase, where $\beta < 1/2$ and $\beta < \alpha$. Region (III) is the maximal current (MC) phase, where $\alpha > 1/2$ and $\beta > 1/2$.

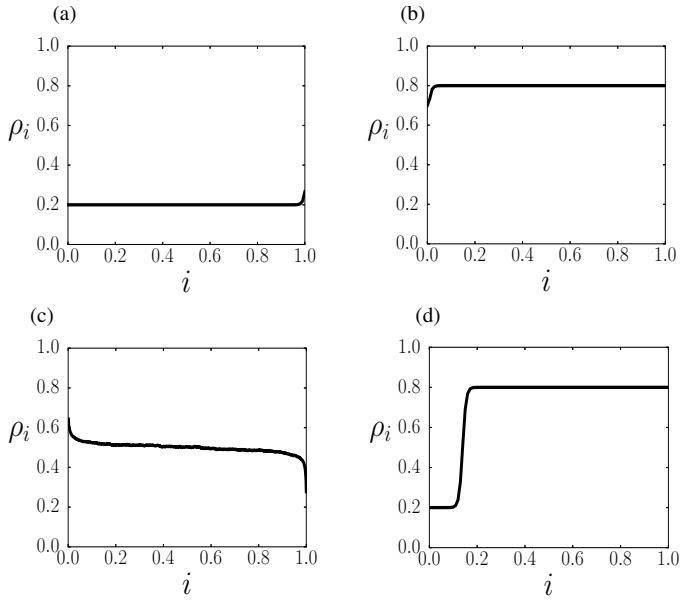

Figure 1.4: Density profile in the various phases. (a) Low density phase, (b) High density phase, (c) Maximal current phase, (d) Co-existence line.

steady state: $\rho_1 = \alpha$ [figure 1.4(a)] and the current in the system is $c = \alpha(1-\alpha)$. The conservation of current implies $\rho_L = \alpha(1-\alpha)/\beta$. One can use equations (1.8), (1.9) and (1.10) to show that this solution exists only if $\alpha \leq 1/2$ and $\alpha < \beta$.

2.*High density phase:* (Shown in region II of figure 1.3). In this phase the density at the exit site is set to the domain of attraction of the stable fixed point $\rho_L = \rho_+ + 0^{\pm}$. One can then show that $\rho_L = 1-\beta$. The current then is $c = \beta(1-\beta)$. While the bulk density is $1-\beta$ [figure 1.4(b)], there is a variation in density near the entry boundary where the density is determined by the constant current condition $\rho_1 = 1 - \frac{\beta(1-\beta)}{\alpha}$. The condition for this phase to occur are $\beta < 1/2$ and $\beta < \alpha$.

3.*Maximal current phase:* (Shown in region III of figure 1.3). Here one considers $\rho_1 \geq 1/2, \rho_L \leq 1/2$. In this phase the system attains the maximal current possible, $c = 1/4$. The density in bulk is half and it changes as we approach the boundaries near $i = 1$ and $i = N$. This solution exists when $\alpha \geq 1/2$ and $\beta \geq 1/2$. The densities at the ends are: $\rho_1 = 1 - \frac{1}{4\alpha}$ and $\rho_L = \frac{1}{4\beta}$. As shown in fig. 1.4(c), the bulk density attains the value $1/2$, while the deviations at the boundary follow a power law with exponent one.

4. *Coexistence line:* The line dividing the high and low density phases, $\alpha = \beta < 1/2$. Here $\rho_1 = \rho_- + 0^+, \rho_L = \rho_+ + 0^-$. The high and low density phases coexist in this region where the recursion starts infinitesimally near to ρ_- and iterates to the stable fixed point ρ_+. One sees a domain wall formation between regions of different density [figure 1.4(d)].

Thus, we obtain three phases depending on the boundary conditions determined by the parameters α and β. The low density and high density phases are separated by a first order phase transition line while there is a continuous phase transition from low density/high density phase to the maximal current phase. We show the phase diagram obtained by the mean-field approximation in figure 1.3. The phase diagram is the same as obtained by exact calculations using the matrix method [49].

The exact solution by matrix method can be used to calculate various quantities including the steady state density distribution as well as two point density-density correlation function [48]. The approach here is to write down the steady state probability of finding the system in a particular state $P_L(\tau_1, \tau_2, ..., \tau_L)$ as

$$P_L(\tau_1, \tau_2, ..., \tau_L) = \frac{f_L(\tau_1, \tau_2, ..., \tau_L)}{\sum_{\tau_1=0,1} \cdots \sum_{\tau_L=0,1} f_L(\tau_1, \tau_2, ..., \tau_L)}, \tag{1.15}$$

where the unnormalized weights can be expressed using matrices:

$$f_L(\tau_1, ..., \tau_L) = \langle W| \prod_{i=1}^{L} (\tau_i D + (1 - \tau_i)E)|V\rangle. \tag{1.16}$$

Here D and E are square matrices and $|V\rangle$ and $\langle W|$ are vectors that satisfy the following relations

$$DE = D + E, \tag{1.17}$$

$$D|V\rangle = \frac{1}{\beta}|V\rangle, \tag{1.18}$$

$$\langle W|E = \frac{1}{\alpha}\langle W|. \tag{1.19}$$

Using these assumptions, one can calculate quantities of interest. From equations 1.18 to 1.19, it is possible to derive the expression for density profile, current as well as the other higher correlation functions without having any particular form of matrices. The calculation of any quantity of interest requires the expression for $\langle W|C^L|V\rangle$ (where $C = D + E$) for arbitrary L and any α and β. Using commutation rules as defined the equations 1.18 and 1.19 one can obtain an expression for $L \geq 1$

$$\langle W|C^L|V\rangle = \sum_{p=1}^{L} \frac{p(2L-1-p)!}{L!(L-p)!} \frac{(1/\beta)^{p+1} - (1/\alpha)^{p+1}}{(1/\beta) - (1/\alpha)}. \tag{1.20}$$

Equations 1.18 and 1.19 can also be used to derive the following equation

$$DC^L = \sum_{p=0}^{n-1} \frac{2p!}{p!(p+1)!} C^{n-p} + \sum_{p=2}^{n+1} \frac{(p-1)(2n-p)!}{n!(n+1-p)!} D^p, \tag{1.21}$$

One then obtains for $i \leq L - 1$, the density profile to be

$$\langle \tau_i \rangle_L = \sum_{p=0}^{n-1} \frac{2p!}{p!(p+1)!} \frac{\langle W|C^{L-1-p}|V\rangle}{\langle W|C^L|V\rangle} + \frac{\langle W|C^{i-1}|V\rangle}{\langle W|C^L|V\rangle} \sum_{p=2}^{n+1} \frac{(p-1)(2n-p)!}{n!(n+1-p)!} \beta^{-p}, \tag{1.22}$$

and for $i = L$ we have

$$\langle \tau_i \rangle_L = \frac{1}{\beta} \frac{\langle W|C^{L-1}|V\rangle}{\langle W|C^L|V\rangle}. \tag{1.23}$$

The current is given by the expression

$$j = \frac{\langle W|C^{i-1}DEC^{L-i-1}|V\rangle}{\langle W|C^{L}|V\rangle} = \frac{\langle W|C^{L-1}|V\rangle}{\langle W|C^{L}|V\rangle}. \tag{1.24}$$

In the $L \to \infty$ limit from the equation 1.24, we obtain the expression for steady state current for various boundary conditions. When the system is in the LD phase the current is $j = \alpha(1-\alpha)$, it is controlled by the entry rate. In the HD phase, the steady state current is controlled by exit rate and is given by $j = \beta(1-\beta)$ and in the MC phase ($\alpha > 1/2$ and$\beta > 1/2$) it is independent of boundaries and attains a constant value $1/4$.

Using the asymptotic expression (1.23), we can also obtain expressions for density away from the boundaries for various phases. For LD phase $\langle\rho_L\rangle_L \simeq \alpha$. For HD phase $\langle\rho_L\rangle_L \simeq 1-\beta$ and in the MC phase, $\langle\rho_L\rangle_L \simeq 1/2$. For the coexistence line, $\langle\rho_L\rangle_L \simeq \alpha + x(1-2\alpha)$. So the density is constant everywhere except at the coexistence line.

The phase diagram of the system, as well as the expression of current through the system, turns out to be the same as that from the mean-field approximation. One of the main predictions different from mean field is the exponent of the power law decay of density in the MC phase, which is found to be $1/2$ in the thermodynamic limit.

Study of TASEP and its variants is an active area of research. We have already seen that TASEP is sensitive to boundary conditions. While in case of open boundaries there are three distinct phases, the system has a unique steady state with a homogeneous density when the boundary condition is periodic. Introduction of disorder in the form of a slow particle or a slow bond in a TASEP with periodic boundaries leads [61, 62, 63] to a significant change in the phase diagram, as we shall discuss later. The inclusion of Langmuir(evaporation/deposition) dynamics, inspired by biological processes [64], changes the phase structure and leads to a rich phase behaviour. Other variations include TASEP with finite resources and blockage at the middle site to mimic transport process with limited resources and a speed bump [65], and TASEP with accelerated and decelerated motion to more effectively capture the behaviour of vehicular transport [66]. TASEP with extended particles was studied as a more realistic model of protein synthesis in biological systems and this system shows a nonlinear relationship between particle current (J) and input rate (α) [67]. The study of the effect of quenched disorder [68] where the rate of movement is random and site dependent reveals the possibility of three distinct regimes depending on disorder parameters. The introduction of a blockage in a system with open boundaries produces a queuing transition [69]. These and many other variations of TASEP have been studied not only to model real systems but also to study the possibilities of steady states

with different kinds of dynamics.

In this thesis, we discuss the effect on TASEP of two different dynamical features - nonlocal hopping and resetting. These features lead to distinct changes in the phase diagram. Nonlocal hopping imitates features of vehicular traffic while the study of TASEP with resetting is inspired by the degradation of mRNA and its subsequent replacement by a new one in the process of protein translation [70]. Further variations within these two dynamics, like the introduction of disorder in a system with nonlocal hopping and the effect of different kinds of resetting time distributions have also been studied. The section 1.2 and1.3 provide a broad overview of the previous work done related to these problems and a brief description of our contributions.

1.2 Nonlocal hopping

One part of our work involves the study of TASEP with the additional feature of nonlocal hopping. The modified dynamics, originally introduced in [71], involves particle motion beyond the usual nearest neighbour sites. Specifically, the dynamics under consideration allows for the particle to jump to the site right before the next occupied site, i.e. cover any gap of empty sites in front of it in one move. These dynamics are in addition to the usual nearest neighbour move and one can stochastically choose either of them by fixing the probabilities of each. There have been previous studies exploring the possibility of particles making long moves, both with the dynamics mentioned above, as well as with other possible moves. Some of these are motivated by real world phenomenon such as traffic on freeways without any speed limit or vehicles moving on wet or icy rods [72, 73], granular flow [74], exploring the role of gravity in static or dynamic sedimentation [75, 76], motion of molecular motors driven by ATP [77] and phase separation in sedimentation of colloids [78].

In a recent study, long range moves were introduced by allowing the particle to jump any distance l with probability $p_l \sim l^{-\sigma-1}$, with jumping over other particles in between being allowed. In this case, the boundary conditions as well as the exponent σ control the phase behaviour of the system. It was found that when $\sigma \leq 1$ there is no phase transition, while for $1 < \sigma < 2$ one sees the usual TASEP phases but with additional features in the density profile [79, 80]. A possible application for this model lies in the transport of DNA regulatory proteins, which attach only to specific sites on the DNA molecule, activating or inhibiting the transcription of genes [81]. A study of the same long range model modified by introducing a defect site or impurity shows a phase transition from a

region of separation to a homogeneous phase [82]. Another modification involves multiple defect sites distributed along the lattice [83] and it is shown here that the phase co-existence does exist in the thermodynamic limit in this system. Another way of introducing long hops are by adding links between non-nearest neighbour sites on a one dimensional lattice. Studies involving such linking in a hierarchical fashion show a simplified phase diagram with the disappearance of the maximal current phase [84].

The effect of nonlocal moves has also been studied on other important models related to TASEP. Symmetric exclusion process (SEP) is a model similar to TASEP with the difference that the particle moves are symmetric and there is no favoured direction. The introduction in SEP of non-local hopping dynamics similar to the one described in the first paragraph of this section leads to a first order phase transition between a fixed density phase and a phase with an empty bulk [85]. Zero range process (ZRP) [86] is a model allowing for the presence of more than one particles at a site. In a ZRP with attractive particles that can also make non-local hops, it was shown that there is a phase transition between a condensate and a homogeneous phase [87]. The parking garage model [88] is a modification of TASEP inspired by queuing phenomena. Here, one considers TASEP with periodic boundary conditions, with the addition of a special reservoir site which acts as a "garage". The dynamics is controlled by two parameters: the total car density and the probability with which a car escapes from the garage. The phase diagram shows two condensate phases where the garage becomes macroscopically occupied. The introduction of nonlocal hops to this model shows a new phase where the bulk of the lattice becomes empty [89].

The model we study is closely related to previous work [71, 89] mentioned above. The system under study consists of particles which can make a long-range jump directly to an empty site right behind the next occupied site, apart from the usual TASEP dynamics involving nearest neighbour motion. The long hops are governed by a parameter p, which is the probability for long hops and the $p = 0$ limit is the usual TASEP. We begin with the study of the combined effect of open boundaries and long hops on the steady state of an open system. Apart from the usual low density (LD), high density (HD) and maximum current (MC) phases, the introduction of a finite p leads to a new possibility - an empty road (ER) phase with particles clearing out faster than they enter. The variation in the phase diagram with p is interesting, with the LD and MC phases vanishing at large values of p while the ER and HD phases divide the parameter space in half. We then look at the combined effect of long hops and static/dynamic impurities. In this study, the boundaries are taken to be periodic for simplicity. We show that the system with a static impurity and with $0 < p < 1$ shows a phase transition from a shock phase characterized by finite densities

on either side of the shock (HD-LD phase) to a phase where the density on one side of the shock is zero (HD-ER phase). We also study the effect of a dynamic impurity, introduced via a slow particle. Here, the system undergoes a phase transition from a homogeneous phase to a shock phase depending on the density, the speed of the slow particle, as well as the probability p. The shock phase dominates the phase diagram at large values of p. All our studies involve numerical simulations which are supported by mean field theory arguments. The mean field approximation works well qualitatively and correctly identifies the possible phases, while the quantitative agreement with numerics varies, depending on parameter values. A detailed description of this work will be provided in the following chapter.

1.3 Resetting

The effect of resetting on dynamical systems is a topic of current interest with many recent studies (see [90] for a recent review). The word resetting in this context means sudden, large dynamical moves in addition to the usual continuum dynamics of the system. One of the favoured examples used to invoke such sudden dynamics is the search problem involving a lost pet. Such a search will involve a slow random scan of a given area followed by quick checks to see if the pet has returned home by its own. There are many real life situations where such dynamics capture the system behaviour. It finds applications in diverse fields like computer networks (to find an element in a sorted and pivoted array) [91], ecology [92], microbiology [93] and biochemistry [94]. One of the very first studies of such a process involved its application to stochastic multiplicative processes where the system develops a stationary power law distribution of the relevant variable [95] when resetting dynamics are introduced. In the context of search problems, resetting models a quick return to the original state which may optimize the time of the search for lost pets or the searching of food by foraging animals [96]. Resetting dynamics also finds application in several microbiological processes such as cleavage during recovery from backtrack during RNA polymerization [97], destruction of mRNA during the process of translation [70, 98] and sudden decrease in microbe population during a catastrophe [99]. It has been used to model the motion of E. Coli bacteria which alternate between ballistic moves (runs) with random changes of direction (tumbles) in order to reach regions with a high concentration of a chemo-attractant (chemotactic search) [100]. The resetting in a birth-death process [90] may model a return to an initial small population after reaching an absorbing state, or random catastrophes that suddenly decrease the population, and in either case,

there are interesting stationary state properties. Such dynamics have also been studied in the context of stochastic thermodynamics and in systems where quantum effects become important [101].

Single particle diffusion is one of the simplest and most interesting models where the effect of resetting can be studied and analysed. Consider a diffusing particle in one dimension which starts at a given point. The probability distribution for this particle will be an ever expanding Gaussian in the absence of resetting. If this particle is stochastically reset with a constant rate r to its original position, one sees a non equilibrium stationary state with non Gaussian fluctuations [102]. It was also shown that the mean time to find a stationary target by a diffusive searcher is finite and has a minimum value at an optimal resetting rate. These results were extended to arbitrary spatial dimension [103]. The optimal resetting induced by resetting was explored with several generalisations including resetting to a random position, and with a space dependent reset rate [104]. Another study involved diffusion with resetting to a position from the past, chosen according to a memory kernel [105]. Varying the memory kernel leads to different possible behaviours ranging from the standard diffusive to anomalous ultra slow growth. Introducing a partially absorbing target along with the resetting dynamics leads to the survival probability of the searcher decreasing exponentially with time, and the mean time to absorption increasing by an additive term [106]. The possibility of a one dimensional random walker reset to the maximum of already visited positions shows a ballistic behaviour for the average position [107]. One way of generalising the resetting rate is to make it time dependent which was again explored from the point of view of an optimal search strategy [108]. Other studies involving diffusion and resetting include the effect of reflecting boundary conditions [109] as well as resetting with finite return speed [110].

Besides single particle diffusion, the effect of resetting in other dynamics has also been studied. Optimal parameters for a search process undergo a first order phase transition as a function of initial position when the underlying dynamics involves choosing jump sizes from a heavy-tailed Levy stable jump distribution, as well as resetting with a constant rate [111]. Application of resetting in the continuous time random walk with drift leads to a power law tail for the density [112]. Other examples include, e.g. the connection between home range search and resetting [113], the interplay between population dynamics and resetting [114], branching processes and resetting [115] and resetting of the scaled Brownian motion with a time-dependent diffusion coefficient [116].

The dynamical feature of resetting has also been studied in quantum systems. One such work involves the study of the effect of a reset that projects the system to its initial

state [101]. The effect of reset on quantum and classical Markovian dynamics shows an acceleration in relaxation to a steady state [117]. The effect of repeated measurements on quantum random walks has been explored in [118, 119]. The resetting process has also been studied from a stochastic thermodynamics point of view and entropy production [120] as well as work fluctuations have been calculated and deviations from Jarzynski's equality have been demonstrated [121].

Most of the studies mentioned above involve systems with non-interacting particles. Interparticle interactions can be very important in many real systems and in this thesis, we study an example of such a system. A well known example of an interacting particle system is the Ising model, and a recent study involving stochastic resetting in Ising model reveals that it drives the system into non-equilibrium steady state through the rapid quenching of temperature and magnetic field and a rich phase diagram is obtained when temperature and resetting rate are varied [122]. Our work model is related to previous studies on the effect of resetting on fluctuating interfaces [123]. Here, it has been shown that interfaces governed by the Kardar-Parisi-Zhang (KPZ) and the Edwards-Wilkinson (EW) equation show a nonequilibrium steady state with non-Gaussian fluctuations under the effect of resetting to the initial flat state at a constant rate. While a constant rate implies an exponential distribution of the inter-reset times, it is worth exploring other possibilities for the inter-reset time, like the power law distribution, which indicates long term memory effects [124]. Indeed the power law distribution leads to a change in behaviour of the system as a function of the power law exponent, as can be seen from a study of the effect of resetting on diffusion [125], as well as on fluctuating interfaces [126].

In this thesis, we have studied the effect of resetting on a system undergoing the TASEP in one dimension with open boundaries. The system undergoes stochastic resetting to the initial, empty state at time intervals that are drawn from a given probability distribution. We consider two possibilities for this distribution, a power law with the exponent γ, and an exponential distribution corresponding to a constant rate of resetting λ. It should be remembered that the microscopic models corresponding to the KPZ equation for an evolving interface can be mapped exactly to a TASEP, with density variables in the exclusion model corresponding to the slope in the interface evolution language. The crucial difference in the current study and the previous ones involving EW and KPZ systems is the presence of open boundaries in our case. As seen before, open boundaries lead to a very different phase structure from the periodic boundary case and there are three possible phases of the system. We study the effect of resetting on all three phases.

We will describe our work in more details in the following chapters. The rest of the

thesis is arranged as follows:

Chapter 2 In this chapter, we describe our work on a model of particles with hard-core interactions which are allowed to make long-hops. We consider the open boundary version of the problem, where the non-local hops lead to a change in the phase diagram. We also consider the periodic boundary case, where the presence of dynamic/static impurities leads to interesting behaviour, including phase transitions.

Chapter 3 In this chapter, we describe our work on the effect of resetting on a TASEP with open boundaries. We explore this effect on all three phases of the TASEP and also explore two different possibilities for the distribution of times between successive resets.

Chapter 4 We concludes the thesis with this chapter with a summary and brief remarks on our work as well as a list of open problems for further research.

Chapter 2

Effects of boundaries and impurities on a one dimensional driven diffusive system

In this chapter we discuss the effect of nonlocal hops on the steady state properties of a one dimensional system, where particles interact with each other via a hard-core repulsion. In the recent past, many studies have focused on dynamics that allow for nonlocal motion via large jumps. A previous study [79] involves particles that can hop to an arbitrary distance l, with the probability of hopping decaying as a power law, $p_l \sim 1/l^{\sigma+1}$. It was shown that the phase diagram resembles that of a TASEP for $\sigma > 1$ but for $\sigma < 1$ there is no phase transition. One way of generating long hops is by introducing links between distant sites. These links may be hierarchical [84] or random [127] and lead to significant changes in the steady state properties of the system. Another work studies the phase transition caused by the competing tendencies of declustering via nonlocal hops and clustering promoted by inter-particle attraction [87].

The model we study is closely related to previous work [71, 89] where the system under study consists of particles that can make a long-range jump directly to an empty site right behind the next occupied site, apart from the usual TASEP dynamics involving nearest neighbour motion. The nonlocal hop mimics the sudden acceleration by a car when there is a large gap available on the road in front. A similar model but with symmetric dynamics [85] of the particles was later studied and both studies saw the emergence of a new phase - the empty road (ER) phase with zero bulk density which was explained using a cluster analysis. With periodic boundary conditions and conserved particle numbers, the dynamics of these models can be mapped exactly to the chipping-diffusion-aggregation models (henceforth CDA models) [128, 129, 130, 131, 132]. The CDA models consider a lattice that allows occupancy of multiple particles at the same site. The dynamics allow for particle motion via the movement of a whole mass cluster to the next site (corresponding to

nonlocal hops in our model) or by the "chipping" of one particle from a given cluster (maps to nearest neighbour motion in our model). In these models, the empty road phase shows up as an aggregate phase with the empty lattice stretch translating to an infinite aggregate.

Our study considers the asymmetric version of the nonlocal hop models mentioned in the previous paragraph and explores the effect of two dynamical features on the steady state properties of this system: open boundaries (entry as well as exit), and impurities - static and dynamic. Below, we provide a brief description of the content and organisation of our work.

In section 2.1 of this chapter, we study a one-dimensional system with open boundaries such that particles enter at one end and leave at the other. The particles move unidirectionally on the lattice and interact via hard-core repulsion, like in TASEP. The particles can either attempt a move to the nearest neighbour with probability $1-p$ or make a long-range hop to the empty site before the next occupied site with a probability p. We thus have three parameters - particle entry rate α, exit rate β and the hop rate p governing the dynamics. The interplay of entry-exit rates as well as the competition between the local and nonlocal hops leads to interesting behaviour and we construct a complete steady state picture of this system via the phase diagram. Our numerical study, supported by a mean field theory, shows that the system has four possible phases at low values of p: three phases similar to the TASEP and an additional phase where the particle density vanishes in the bulk. As p is increased, and long-range hops dominate the dynamics, the number of possible states decreases to two such that the system is either controlled by the long-range hops, or by the exit boundary. The novelty of our work lies in the complete characterisation of an open system with long-range hops and in showing that the output boundary exerts a significant influence on determining the steady state of the system.

In section 2.2, we consider a system with the same dynamics as above, but with periodic boundary conditions and a fixed number of particles. We study the effect of a dynamic impurity on this system by introducing a slow-moving particle that makes only local hops with a rate μ. The parameters here are p, μ and the particle density ρ. We map out the phase diagram of the system and see that it exists in either of the two phases: a homogeneous density phase where the effect of the slow particle is localised, and a shock phase where the system separates into two regions of different density across the slow particle. The $p \to 0$ limit of our model has been studied before [51,62] and the results show a separation of the parameter space into two halves divided by the line $\mu = 1-\rho$, thus indicating that there is a phase transition for every finite density. The introduction of nonlocal hops via p enhances the shock formation tendency and we find that for low values of density,

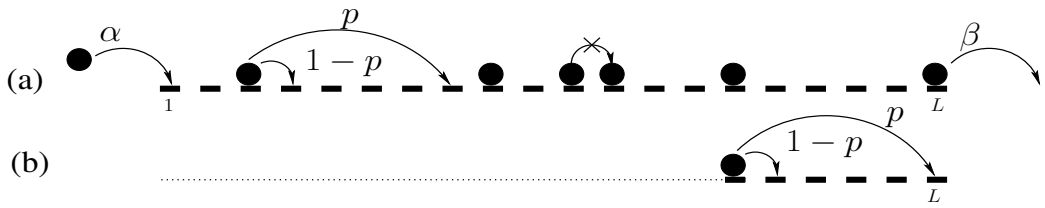

Figure 2.1: (a) Schematic diagram for the dynamics of our model with open boundaries. Particles enter the left boundary with rate α and exit from the right boundary with rate β. The rate for nonlocal hopping is p and local hopping is $1 - p$. (b) If all sites to the right of the chosen particle are unoccupied, it hops to the last site L.

the system always exists in a shock phase without undergoing a phase transition. Our model with a slow particle can be exactly mapped to the CDA model with a slow site. We translate our condition for the phase transition to a shock phase into the condition for a phase transition to an infinite aggregate phase in the CDA model.

In section 2.3, we consider the model with periodic boundary conditions as described above, but the impurity in the system is of a static nature. A special slow site is introduced in the system such that a particle at this site can only move out via a local hop with a rate r. In the regular TASEP ($p \to 0$ limit), the problem of a static impurity has been studied with much interest since initial studies threw up conflicting results on the presence of a phase transition as a function of the parameter r [61, 69, 133, 134]. More recent results suggest that there is no phase transition and the system always exists in a shock phase [135, 136]. The introduction of nonlocal hops via the parameter p leads to interesting results and we see a phase transition in our system - albeit to a different kind of state. As expected, we see that increasing the value of p enhances the tendency of shock formation and therefore the system always shows two different regions : the region behind the slow site having a high density and the region in front having a low density. As we increase the value of p, we see that the density in front of the slow particle decreases continuously to zero and remains at zero for all higher values of p. The zero density portion is much like the empty road phase of our study with open boundaries, with a similar mechanism flushing out particles quicker than they arrive.

The consideration of open boundaries, as well as static and dynamic impurities, helps us in constructing a broad view of the effect of nonlocal hops in one dimensional driven systems and throws up some interesting results.

2.1 Open boundaries

2.1.1 Model

We consider particles moving on a one-dimensional lattice of size L as shown in figure 2.1. The particles interact via hard-core repulsion, implying that a particle cannot move to a site that is already occupied and therefore a given site cannot accommodate more than one particle. The particles always move unidirectionally (left to right in figure 2.1) with the following rules: (i) particles attempt to enter the leftmost site with a rate α, the attempt is successful if the leftmost site is empty, (ii) particles leave out of the rightmost site with a rate β and (iii) a randomly chosen particle on the lattice attempts to hop to its nearest neighbour site with a rate $1 - p$ or make a long hop to the next unoccupied site preceding an occupied one with a rate p. Either of these attempts is successful only if there is at least one unoccupied site to the right of the chosen particle. If all sites to the right of a particle are unoccupied, it jumps to the rightmost site L. We thus have three parameters: α, β and p governing the particle dynamics, each of which can take any value in the interval $[0, 1]$.

2.1.2 Numerical results and phase diagram

We performed Monte Carlo simulation of the model described above using random sequential updating. One move corresponds to selecting a particle on the lattice or a particle in the reservoir at the entry end and then trying to move it using the dynamics defined above. We define one time step to be $L + 1$ such random updates such that in a unit time, particles at all sites, including the reservoir, will have attempted a move once. We performed long time averages of the quantities of interest after ensuring that the system is in a time-independent steady state. We covered all possible regions of the $\alpha - \beta - p$ parameter space. The phase diagram has been presented as a projection on the $\alpha - \beta$ plane for various values of p. Our numerical approach was to scan the $\alpha - \beta$ plane at a gap of 0.05 for α and β, for a given p. The p values were themselves varied by 0.1 from 0 to 1. Further, after the identification of the gap containing a phase boundary, more detailed data was taken in that particular parameter range, an example of which can be seen in figure 2.4.

For $p = 0$, our model reduces to TASEP which can be seen in figure 2.2(a) where the system has three possible phases. When the entry rate of the particle is lower than the exit rate ($\alpha < \beta$ and $\alpha < 0.5$), the system is in an entry boundary controlled phase with a bulk density of α. This is the low density (LD) phase. When the exit rate is smaller than the entry rate ($\beta < \alpha$ and $\beta < 0.5$), the flow is controlled by the exit boundary and one enters

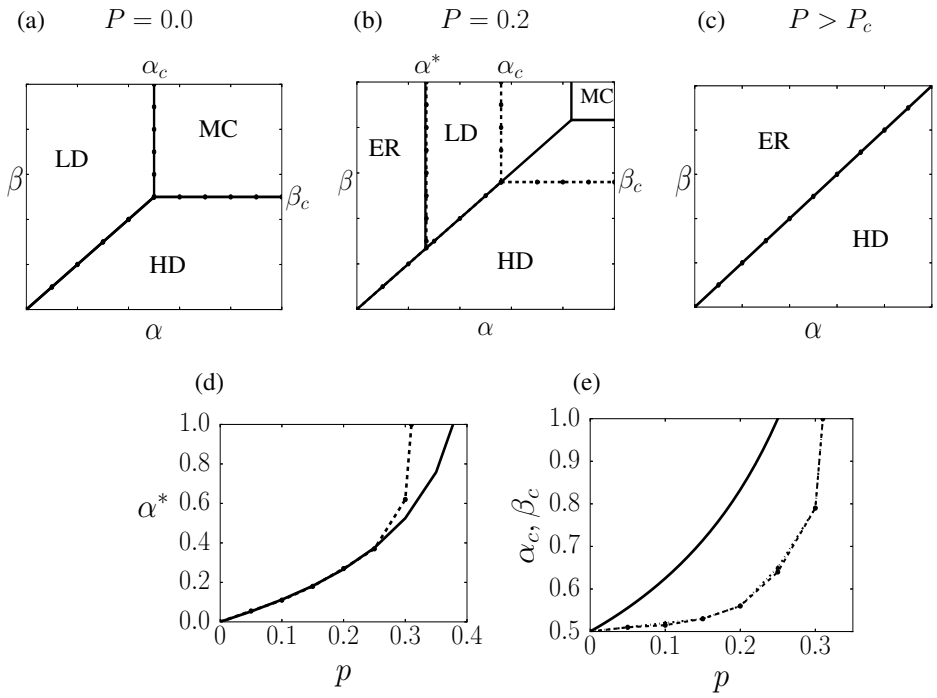

Figure 2.2: (a)-(c) Phase diagram projected in the α-β plane for different values of the nonlocal hopping rate p. Here LD, HD, MC and ER correspond to the low density phase, high density phase, maximal current phase and empty road phase respectively. The solid lines are from the mean field analysis while the dashed lines indicate boundaries determined through simulations. (d) The variation in α^* with p. α^* is the value of α at which the LD to ER phase transition occurs. The dashed line shows the Monte Carlo simulation results while the solid line indicates the output from mean field. (e) The dependence of α_c and β_c on p. The transition from LD to MC and HD to MC occurs at α_c and β_c respectively. Dotted and dashed lines indicate the results from MC simulation for α_c and β_c respectively. The solid line indicates the mean field result.

the high density (HD) phase with a bulk density of $1 - \beta$. When both the exit and entry rates are high ($\alpha, \beta > 0.5$) the system enters into a phase where the density at the center is no longer governed by the boundaries and is fixed at $1/2$ irrespective of α and β. This phase is called the maximal current phase since the current in this phase is $1/4$, which is the maximum possible current.

As the probability for long-range hops p is increased, we see a marked change in the phase behaviour. For non-zero values of p, we find that the system can have four different kinds of phases in steady state. We have shown various slices of the three-dimensional phase diagram, figure 2.2, in the $\alpha - \beta$ plane, each for a constant p. The four phases are named as the low density (LD) phase, high density (HD) phase, maximal current (MC)

phase and the empty road (ER) phase. In the LD phase, the bulk density of the particles is controlled by the injection rate α and in the HD phase, it is controlled by the ejection rate β similar to the TASEP at $p = 0$. In the MC phase, the particle density is independent of α and β but the current, unlike TASEP, can be more than $1/4$. The ER phase, where the particle density approaches zero, is a unique phase generated solely by the nonlocal hopping effect. In the following, we describe the variation in the phase diagram as projected on the $\alpha - \beta$ plane as we vary p.

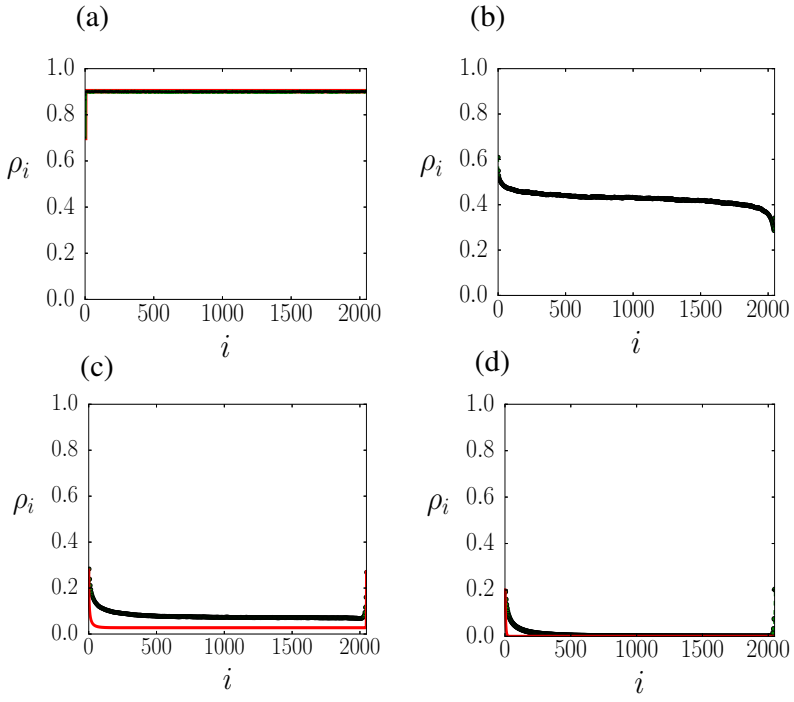

Figure 2.3: Density profile as a function of the distance along the lattice. (a) $\alpha = 0.3$, $\beta = 0.1$, $p = 0.2$. The system is in the HD phase. (b) $\alpha = 0.7$, $\beta = 0.8$, and $p = 0.2$ (MC phase). The profile is obtained numerically using Monte Carlo simulation. (c) $\alpha = 0.3$, $\beta = 0.8$ and $p = 0.2$ (LD phase). (d) $\alpha = 0.2, \beta = 0.8$ and $p = 0.2$. The system is in ER phase. Monte Carlo simulation data is shown in green and mean field theory result in red solid line and system size $L = 2048$.

(i) For $0 < p < p_c$: The system shows the four phases: LD, HD, MC and ER as mentioned previously. Figure 2.2(b) shows a representative phase diagram of the system for this range of p values. The value of p_c as determined in our simulations is $p_c \approx 0.3$. A discussion of the various possible phases of the system is given below.

(a) $\alpha > \beta$ and $\beta < \beta_c$ (HD phase): In this case, the input rate is higher than the exit rate which creates a jam at the exit leading to high density in the bulk. The density in the bulk

and the current in this HD phase are thus controlled by the exit rate β and is independent of α. It is found that the density ρ_b in the bulk is equal to the density ρ_L at the right boundary site $i = L$, i.e. $\rho_b = \rho_L$ as seen in figure 2.3(a).

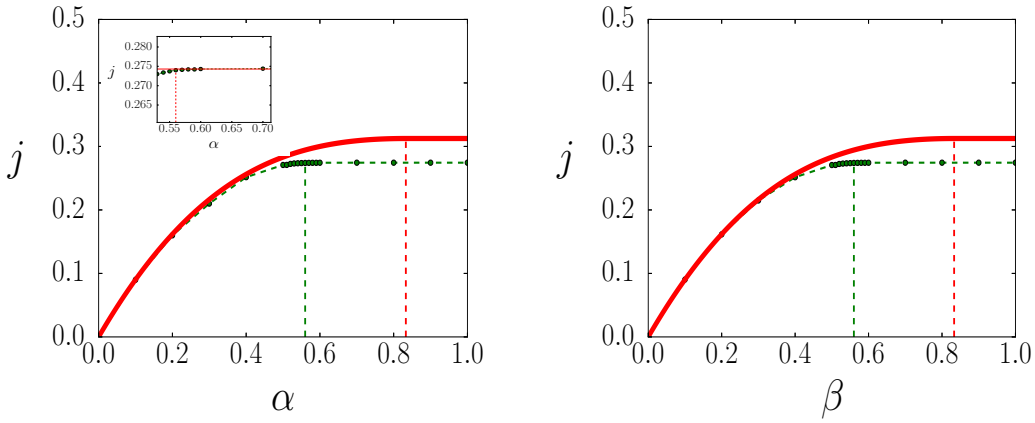

Figure 2.4: (a) Current as a function of α for $\beta = 0.8$ and $p = 0.2$. The initial increase corresponds to the ER/LD phase and the constant portion at higher α shows a transition to the MC phase. The Monte Carlo simulation data shown in the green dashed line shows a transition at $\alpha_c \approx 0.56$ while the mean field result in red line shows a transition at $\alpha_c = 0.83$. The inset shows an enlarged portion of the Monte Carlo data with the green dots indicating the data. The horizontal red line shows the constant value of current in the MC phase while the vertical red line shows the transition point at which this constant value is achieved. (b) Current as a function of β for $\alpha = 0.8$ and $p = 0.2$. The initial increase corresponds to the HD phase and the constant portion at higher β shows a transition to the MC phase. The Monte Carlo simulation data in green dashed line shows a transition at $\beta_c \approx 0.56$ while the mean field result in red line shows a transition at $\beta_c = 0.833$.

(b) $\alpha > \alpha_c$, $\beta > \beta_c$ (MC phase): Consider the $p = 0$ case where we have the regular TASEP dynamics. Here we know that α_c, $\beta_c = 0.5$, such that for α, $\beta > 0.5$, we have a maximal current (MC) phase where the current for all values of α and β has the maximum possible value of $1/4$. As p is increased, we see a phase with similar characteristics as the MC phase of TASEP - the value of the current is the maximum possible and remains a constant throughout the phase. Figure 2.4 show the variation in current with α and β. We can see from the figures that as the system enters the MC phase, the current reaches its maximum value and becomes independent of α and β. The point at which the current becomes constant is taken as the crossover value from LD/HD to MC phase. This is a continuous transition and the boundaries between the phases are defined by the lines $\alpha = \alpha_c$ and $\beta = \beta_c$ in the phase diagram [figure 2.2(b)]. Numerically, we see that $\alpha_c = \beta_c = 0.5$ for $p = 0$, as expected. As p is increased, we observe that $\alpha_c \approx \beta_c$ and their values increase

as a function of p. Figure 2.3(b) shows the average particle density on the lattice in the MC phase obtained numerically.

(c) For $\beta > \alpha$ and $\alpha^* < \alpha < \alpha_c$ (LD phase): In the regime $\alpha < \beta$ and $\alpha < \alpha_c$, one expects, similar to TASEP, the emergence of a phase with a low density since the bulk behaviour is governed by the lower input rate of particles. As p is increased, we indeed see such a phase, but only in the range $\alpha_c > \alpha > \alpha^*$. In this region of phase space, we see a phase with a finite but low density, similar to TASEP. We note that bulk density here is lower than α and the bulk is separated from the input boundary by a boundary layer. This is in contrast to the TASEP, where the bulk density is equal to the input rate α and the bulk extends right up to the input boundary. We can see the density profile in this phase in figure 2.3(c) where the density in the bulk can be seen to be lower than α which is the value at $p = 0$. As expected for an input boundary controlled phase, for a given p, this density is a function only of the input rate α and not of β. The low density leads to an increase in the range of the long hops thus facilitating a further decrease in the density. There is then a competition between the input rate and the long-range hops in this range of parameters which leads to a different phase for small values of α.

(d) For $\beta > \alpha$ and $\alpha < \alpha^*$ (ER phase): The density in the bulk is a decreasing function of α in the LD phase and goes to zero at $\alpha = \alpha^*$. The system has a bulk density of zero for all $\alpha < \alpha^*$, see figure 2.3(d). This implies a transition to a new kind of phase having an empty bulk - the empty road (ER) phase. The continuous transition between the LD and ER phase can be seen in figure 2.5 where the probability $P(N)$ of finding a total number of particles N is plotted. We can see that $P(N)$ develops a distinct cusp with a finite value at $N = 0$ for $\alpha < \alpha^*$. As expected, the value of α^* increases with an increase in p [figure 2.2(d)], since it is the nonlocal hops that are helping to clear out the particles quickly, leading to an empty bulk. The line $\alpha = \beta$ ($\alpha < \alpha_c$, $\beta < \beta_c$) separates the HD phase from the LD and ER phases. The LD to HD and ER to HD transitions are first order and the sudden change in the probability density distribution $P(N)$ of the total number of particles can be seen in figure 2.6.

(ii) For $p > p_c$: As mentioned above, the values of α_c and β_c increase as p is increased, indicating that the MC phase shrinks as the probability of nonlocal hops is increased. We observe that as p crosses the value 0.3, both α_c and β_c take the value 1 and there is a sharp transition with the MC phase vanishing. We also see that for the LD phase, the value of α^* increases with p and again the LD phase vanishes at the same value of $p \approx 0.3$. We thus have only two phases for all $p > 0.3$. The nonlocal hops therefore completely dominate the dynamics in the $\alpha < \beta$ region and this whole region now becomes an ER phase with zero

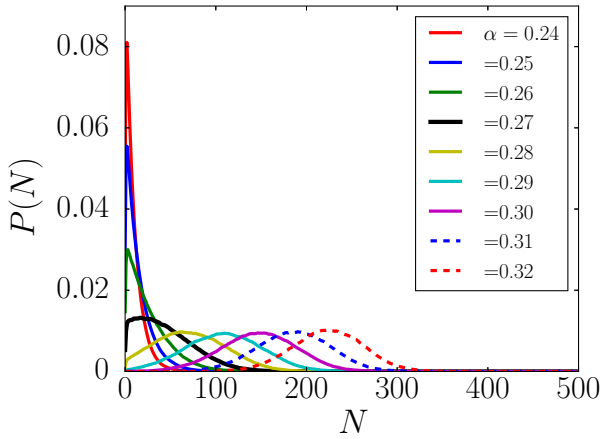

Figure 2.5: Probability distribution, $P(N)$, of the total number of particles on the lattice N for $\beta = 0.8$, $p = 0.2$ and α varying from 0.24 to 0.32. We can see that the phase transition from ER phase to LD phase happens at $\alpha \approx 0.27$. The data was obtained numerically using Monte Carlo simulation. System size $L = 2048$.

bulk density. The rest of the phase space comprises the HD phase. Figure 2.2(c) shows the line separating these phases.

In our numerical work above, we see that the LD and MC phases vanish simultaneously at $p \approx 0.3$. As we shall see below, our mean field analysis shows all the phases discussed above, but predicts that ER and MC phases vanish at different values of p, which is in contradiction to the result above. Our results however are in good agreement with previous numerical work [71] which essentially studies the $\beta = 1$ limit of our model. We ascribe the difference in theory and numerics to the long hop dynamics, which ensure that the occupancy of a site is correlated to that of another site far away.

2.1.3 Mean Field approach

We have tried a mean field approach, neglecting correlations. The dynamics of long-range hops is expected to introduce correlations, nonetheless, our theory explains reasonably well the various phases and their characteristics as seen in the numerics. We define the average density at a lattice site i to be ρ_i. Consider the current passing through the link joining the sites $i-1$ and i:

$$j_i = (1-p)\rho_{i-1}(1-\rho_i) + p\left[1 - \prod_{k=1}^{i-1}(1-\rho_k)\right](1-\rho_i). \tag{2.1}$$

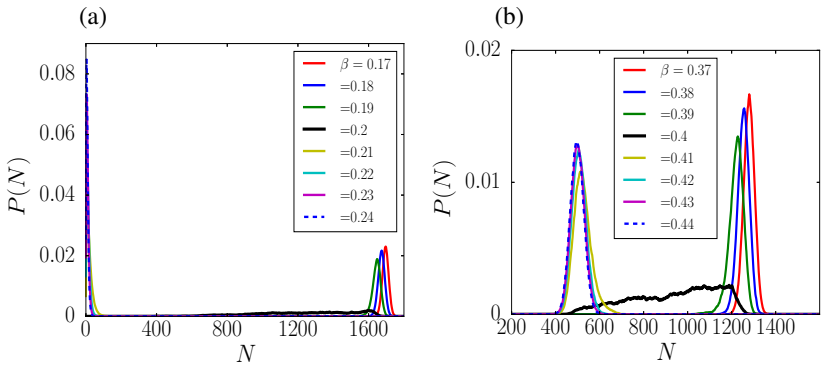

Figure 2.6: (a) $P(N)$ versus N when the system moves from the ER to HD phase. The parameters are $\alpha = 0.2$, $p = 0.2$ and β varying from 0.17 to 0.24. The value of β at which the phase transition occurs is $\beta_c \approx 0.2$. (b) The variation in the probability distribution $P(N)$ of the total number of particles N on the lattice when the system moves from LD to HD phase. The parameters are $\alpha = 0.4, p = 0.2$ and β varying from 0.37 to 0.44. The value of β at which the phase transition occurs is $\beta_c \approx 0.4$. The system size in both figures is $L = 2048$.

The first term comes from the local motion of particles into site i due to hopping from the nearest neighbour site $i-1$. The second term stands for nonlocal hopping events where particles may hop into the site i or surpass it. For such a nonlocal hop to happen, there should be at least one particle in the lattice on one of the sites preceding site i. The probability that there is at least one such particle is accounted for by the $1 - \prod_{k=1}^{i-1}(1-\rho_k)$ part of the second term. When the system achieves a steady state, the current through all links will be equal. We also note that in the steady state, if the system has a finite density in the bulk, we have $\prod_{k=1}^{i-1}(1-\rho_k) = 0$ since the probability of having all empty sites before a given site in the bulk will approach zero in the thermodynamic limit. We then have, far from the input boundary:

$$j_i = (1-p)\rho_{i-1}(1-\rho_i) + p(1-\rho_i). \tag{2.2}$$

We expect that the effect of the boundary has decayed deep in the bulk of the system and therefore the bulk has a constant density ρ_b which will be the fixed point of the above equation. We can see that $j = 1/[4(1-p)]$ is the maximum possible value of the current by using the condition $\frac{dj}{d\rho_b} = 0$ with $j = (1-p)\rho_b(1-\rho_b) + p(1-\rho_b)$. When current is at this maximum value, there is only one fixed point for the system given by

$$\rho_b = \frac{1-2p}{2(1-p)}. \tag{2.3}$$

We see that, for $j < 1/[4(1-p)]$, there may be two possible fixed points:

$$\rho_{b\pm} = \frac{(1-2p) \pm \sqrt{(1-2p)^2 - 4(1-p)(j-p)}}{2(1-p)}, \tag{2.4}$$

and for $j > 1/[4(1-p)]$, there are no fixed points. This analysis can be seen graphically in figure 2.7.

We now try to analyse the phases and the transitions between them caused by the effect of boundary conditions. Consider figures 2.7(a) and 2.7(b) where a fixed point can be seen at high densities. This corresponds to the HD phase where the output boundary controls

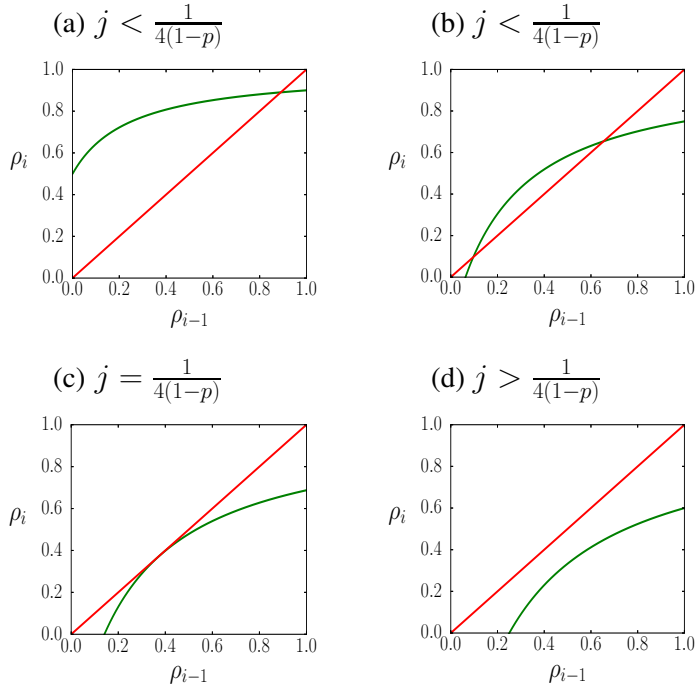

Figure 2.7: Fixed point analysis for various values of j. For $j < 1/4(1-p)$ there are two possibilities: (a) shows two possible fixed points corresponding to ER phase (zero density) and HD phase while (b) shows two fixed points corresponding to the LD and HD phases. Figure (c) is for $j = 1/[4(1-p)]$ and there is only one fixed point corresponding to the MC phase. (d) shows that for $j > 1/4(1-p)$ there are no fixed points.

the flow of the particles. The current out of the exit site $i = L$ is given by $j_L = \rho_L \beta$ while the current into this site is given by the expression $j_{L-1} = (1-p)\rho_{L-1}(1-\rho_L) + p(1-\rho_L)$ where ρ_L is the density at the exit site and ρ_{L-1} is the density at the site preceding it. In the steady state, we have $j_L = j_{L-1} = j_b$ where j_b is the current in the bulk: $j_b = (1-p)\rho_b(1-\rho_b) + p(1-\rho_b)$. This equality of current permits the solution $\rho_{L-1} = \rho_L = \rho_b$

where ρ_b satisfies

$$\rho_b\beta \quad = (1-p)\rho_b(1-\rho_b) + p(1-\rho_b), \tag{2.5}$$

which gives us

$$\rho_b \quad = \frac{1-2p-\beta+\sqrt{(1-2p-\beta)^2+4p(1-p)}}{2(1-p)}. \tag{2.6}$$

Using the above equation and equation (2.1), we evaluate the density on the lattice, which matches well with our Monte Carlo data as can be seen in figure 2.3(a).

Consider now the ER and LD phases where the density of the particles is low and the input boundary is in control. Figure 2.7(b) shows a fixed point at a lower density corresponding to the LD phase while figure 2.7(a) indicates that the bulk density going to zero may be a solution. Again, to evaluate the current and bulk density in these phases, we need to evaluate the density at the input boundary which controls this phase. In steady state, the current into the first site is $j_1 = \alpha\,(1-\rho_1)$ while the current out of it is $\rho_1\,(1-\rho_2)$, thus $\alpha\,(1-\rho_1) = \rho_1\,(1-\rho_2)$. Now consider the lattice site 2. Equating current into and out of this site gives $(1-p)\rho_1(1-\rho_2) = \rho_2(1-\rho_3)$. The density at the second site ρ_2 can then be approximated as $\rho_2 = (1-p)\rho_1$ by assuming a low density and ignoring the quadratic terms. Using this approximation, we can write for ρ_1, the equation

$$(1-p)\rho_1^2 - \rho_1(1+\alpha) + \alpha = 0, \tag{2.7}$$

the solution of this equation is

$$\rho_1 = \frac{(1+\alpha)-\sqrt{(1+\alpha)^2-4\alpha(1-p)}}{2(1-p)}. \tag{2.8}$$

Again, one can calculate the density distribution on the lattice using equation (2.1). The match with numerics, as seen in figure 2.3(c), in this case, is not as good as in the HD case.

Let us now try to look at the various phase transitions. The current in the bulk is given by equation (2.5) while the density is given by equation (2.6). These equations admit the solution $\rho = 0$ when $j = p$, thus giving us an ER phase. This can be seen visually in figure 2.8 where a zero bulk density is seen at a finite value of j. At lower values of j, you can only have a high density solution or a negative density solution, which is unphysical and simply implies that the system cannot support a non-zero, positive density. Contrast this to the usual TASEP where the density is zero only when the current is nil. The reason

we can have a finite current while having a zero density is that the current consists solely of long-range jumps in which the particle hops across the site without contributing to the density at the site in the bulk. These long-range hops are taking the particle from the input end directly to the output boundary. The value of nonlocal hopping α^* at which the transition from LD to ER phase occurs can be inferred from the condition $j = p$:

$$\alpha^*(1 - \rho_1) = p. \tag{2.9}$$

Substituting the value of ρ_1 from equation (2.8), we get

$$\sqrt{(1+\alpha^*)^2 - 4\alpha^*(1-p)} = (1+\alpha^*) - 2(1 - \frac{p}{\alpha^*})(1-p). \tag{2.10}$$

Squaring on both sides and then multiplying by $(\alpha^*)^2$ gives us a linear equation in α since the quadratic terms cancel out, and we finally get

$$\alpha^* = \frac{p(1-p)}{1-2p}. \tag{2.11}$$

The variation of α^* with p is plotted in figure 2.2(d) and shows a good match with the numerics. This mean field value overestimates α^* at higher values of p and does not capture the sudden transition to the ER phase at $p = 0.3$.

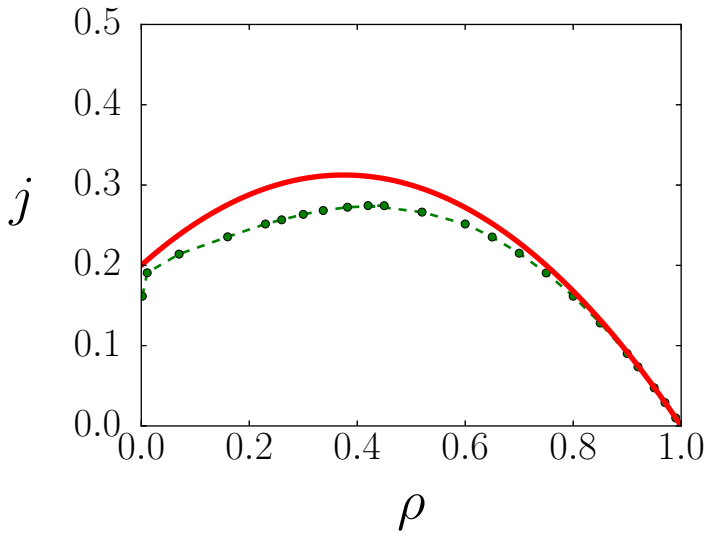

Figure 2.8: Variation in current j with bulk density ρ for $p = 0.2$. MC simulations are shown in green with a dashed line while MF calculations are shown by a red solid line.

Consider now the transition between the entry controlled LD/ER phases, to the exit controlled HD phase. Equating the current on two sides $j_{\rm LD} = j_{\rm HD}$ gives

$$\alpha(1-\rho_1) = \rho_b\beta. \tag{2.12}$$

Substituting the expressions of ρ_1 and ρ_b from equations (2.8) and (2.6) in equation (2.12) above, we see that the line $\alpha = \beta$ separates these phases, in excellent agreement with the numerics. We have seen that at high values of the input and output rates the system goes to a state in which the current stays at its maximum value, irrespective of the change in α or β. This phase is the MC phase corresponding to the single fixed point in figure 2.7(c). We again equate the currents in the different phases to get the condition for transition to the MC phase. The transition from LD to MC phase would happen when we increase the input rate beyond a critical value α_c which can be obtained from the condition $j_{\rm LD} = j_{\rm MC}$. We then have

$$\alpha_c(1-\rho_1) = \frac{1}{4(1-p)}. \tag{2.13}$$

Substituting the expression for ρ_1 from equation (2.8), we obtain

$$\alpha_c = \frac{1}{2(1-2p)}. \tag{2.14}$$

Similarly, to evaluate the condition for the HD-MC phase transition, we use $j_{\rm HD} = j_{\rm MC}$ to obtain the expression for β_c

$$\rho_b\beta_c = \frac{1}{4(1-p)}. \tag{2.15}$$

Substituting for ρ_b from equation (2.6) gives us

$$\sqrt{(1-2p-\beta_c)^2 + 4p(1-p)} = \frac{1}{2\beta_c} - (1-2p-\beta_c),$$

which, after taking squares on both sides gives us the quadratic equation

$$(2p-1)^2\beta_c^2 + (2p-1)\beta_c + \frac{1}{4} = 0. \tag{2.16}$$

The root of this equation is degenerate, and we get

$$\beta_c = \frac{1}{2(1-2p)}. \tag{2.17}$$

We thus see that $\alpha_c = \beta_c$ and we have an MC phase in the regime $\alpha, \beta > \alpha_c$. The

value of α_c at $p = 0$ is 0.5. The variation in α_c and β_c as a function of p is plotted in figure 2.2(e). The matching with numerics here is not satisfactory, with the mean field underestimating the extent of the MC phase. The mean field predicts a vanishing of the MC phase at $p = 0.25$ whereas we see from numerics that it persists for even higher values of p and shows a sudden transition to the ER phase for $p \approx 0.3$, similar to the LD to ER transition.

We now have a complete description of the effect of open boundaries on the phase behaviour of our system. In the next sections, we are going to study another important dynamical feature that leads to new kinds of behaviour in steady states - the presence of impurities in the system. Even a single impurity or defect can have a significant macroscopic effect, leading to new phases in driven diffusive systems. These defects could be of a static (particle-type) or dynamic (site-type) nature. We study the effects of a dynamic defect in section 2.2 below, followed by a study of the static defect in section 2.3.

2.2 Dynamic defect: Slow particle

Let us consider the case of particle-type defect where apart from the regular particles that move according to the dynamics defined in section 2.1, we also have a slower particle. To focus only on the effect of the defect, we use periodic boundary conditions here. The defect particle resembles a slowly moving car in traffic. We expect that under certain conditions, this slower particle may cause a separation of densities with a higher density region behind it and a lower density region in front, similar to a traffic jam. We define below, the model in detail and then our results from numerical simulations and mean field analysis.

2.2.1 Model

Consider a periodic lattice with L sites, having N number of particles following the long hop dynamics, in addition to a slowly moving particle. So the density of the normal particles is $\rho = \frac{N}{L}$. The boundaries are periodic and no new particle can enter or leave. The dynamics of our model, as shown in figure 2.9, are: (i) as before, a normal particle attempts to move to its nearest neighbour site on the right with rate $(1 - p)$ or to the site just preceding the next occupied site to the right with a rate p, (ii) the slow particle attempts to move to the nearest neighbour site to the right with a rate μ. The system behaviour is controlled by two parameters μ and p. The effect of a slower particle on the TASEP has been studied in earlier work [51, 63]. The model there is more general, allowing for an overtaking of the

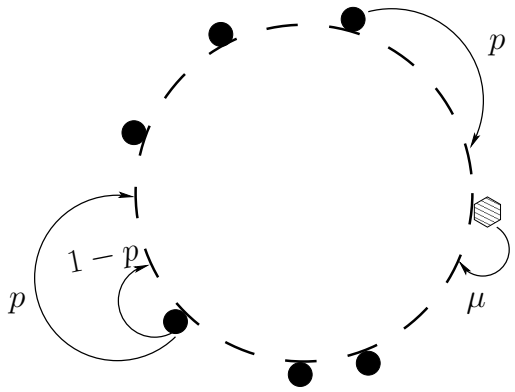

Figure 2.9: Schematic diagram of dynamics on a periodic lattice with a slow particle. The circles indicate normal particles, which undergo local hopping with a rate $1 - p$ and nonlocal hopping with a rate p. The hexagon indicates the slow particle which can make a local hop with a rate μ.

slower particle by normal particles with a rate β, which our study discounts ($\beta = 0$). Note that in the case of TASEP, the parameter governing the slow particle is named α instead of μ used by us. We have changed the nomenclature to avoid confusion with the entry parameter α in the previous section. The introduction of nonlocal hopping via parameter p in our case leads to interesting results since it increases the tendency of clustering caused by the slower particle.

2.2.2 Numerical results

We performed Monte Carlo simulations spanning the entire range for the parameters μ and p, and for various lattice sizes and densities. As before, we calculated the quantities of interest after the system has reached steady state. To measure the clustering caused by the slower particle, we evaluate the average density as seen from a frame moving with the slower particle. As we change μ for a given value of ρ and p, we see a change in phase. At high values of μ, we have a phase in which the effect of the impurity is local: the density along the lattice is a constant, apart from a kink around the defect (see figures 2.10 (a)(II) and 2.10(b)(II). As we slow down the defect particle by decreasing μ, we see that a macroscopic shock is formed in the system. A region of density higher than the average is formed behind the defect particle, while a region of zero density forms just ahead of it (see

figure 2.10(a)(I) and 2.10(b)(I).

The transition between a homogeneous phase and a shock phase as described above can also be seen as a function of the average density ρ of the system while p and μ are held constant. A decrease in the density allows the normal particles to move faster and create a jam behind the slow particle, at the same time opening up a region of lower density in front of it. At higher densities, we have the homogeneous phase with a kink in density near the slower particle. As we decrease the density beyond a certain value, the system goes into the shock phase with a high density region behind the slow particle and a zero density region in front of it. As we decrease the average density further, the value of density in the "jam" behind the particle remains the same. The decrease in average density leads to the decrease in the length of the high density region behind the slow particle with a corresponding increase in the length of the zero density region in front (see figure 2.11).

We are working with periodic boundary conditions and therefore the low and high density regions on either side of the slow particle will meet each other at an interface where a shock between these regions is formed. It interests us to characterise the fluctuations of this shock interface. To do this, we make use of a second-class particle [50] which has dynamics such that it acts as a normal particle with respect to empty spaces but acts as an empty space as far as other particles are concerned. Thus, when a second-class particle is introduced in a TASEP, it is designed to move forward by one step if the site in front is empty but exchanges place with a normal particle and move back by one step if a normal particle attempts to move to its position. These dynamics ensure that such a second-class particle always likes to sit at the interface of a high density and a low density region. Its location, therefore, can be taken as the location of the shock front. Our system has an additional long-hop dynamics for the particles. The only addition to the dynamical rules then is that if a normal particle attempts to move to the position of a second-class particle, whether by local or nonlocal hops, the move occurs with the second-class particle moving one step backwards while the normal particle moves to the position vacated by it. This rule again ensures that a second-class particle sits at the interface with normal particles always in front of it and empty sites behind it.

The width of the shock front is calculated using the deviation of the position of the second-class particle (r_s) from its mean: $\sigma = \sqrt{\langle r_s^2 \rangle - \langle r_s \rangle^2}$. We start with a random initial state and after reaching the steady state, we numerically evaluate this quantity for various system sizes, L, keeping the density constant. We see that the width of the shock front scales with system size L as $L^{1/2}$ irrespective of the value of density and α (see figure 2.12). This is the same behaviour as seen in the normal TASEP without long-range

hops [63]. In our model, no particles surpass the slow one and therefore the second class particle is essentially following the fluctuations of the last particle in the shock front.

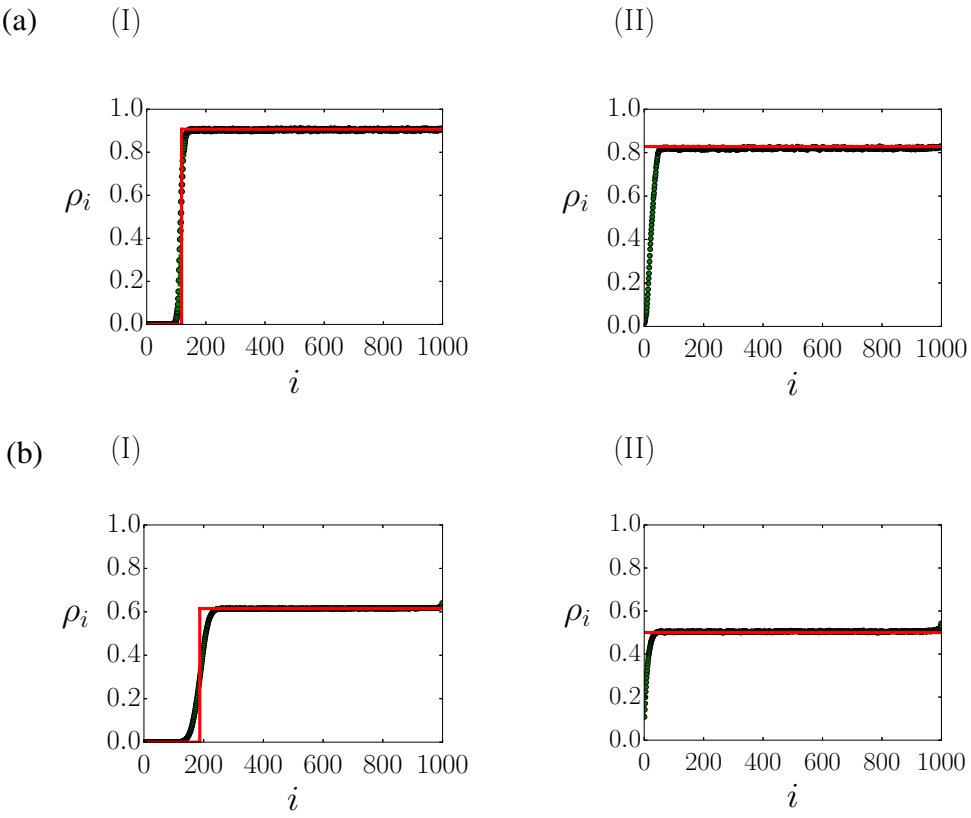

Figure 2.10: The density profile as seen in the frame of the slow particle, i represents the distance as measured in front of the slow particle. We show this profile in the shock phase and homogeneous phase for two different values of average density ρ. Figure (a) : $\rho = 0.8$, $p = 0.8$, $L = 1000$, with (a)(I) $\mu = 0.1$, and (a)(II) $\mu = 0.2$. Figure (b) : $\rho = 0.5, p = 0.2, L = 1000$ with (b)(I) $\mu = 0.4$ and (b)(II) $\mu = 0.6$. The data from Monte Carlo simulation is shown in green and the red lines are from mean field analysis.

2.2.3 Mean field analysis

It is expected that the slow particle may cause a jam behind it and this jam moves with the same speed as that of the slow particle. We may thus expect that the mean density at a site will vary periodically in time instead of being constant. Whether or not such a shock form depends on the speed of the slow particle and therefore, to understand the transition between a homogeneous and a shock phase, we look at a mean field description of the velocity of the particles on the lattice. Increasing the density restricts the speed while

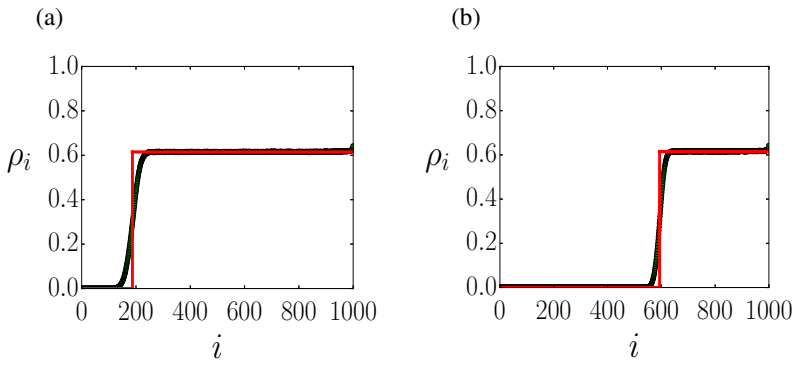

Figure 2.11: The density profile as seen in the frame of the slow particle, i represents the distance as measured in front of the slow particle. Here, we show the change in the density profile on the lattice as a function of average density, keeping other parameters the same. Here $\mu = 0.4, p = 0.2, L = 1000$. Average density: (a) $\rho = 0.5$ and (b) $\rho = 0.25$. The Monte Carlo simulation data is shown in green while the mean field result is shown in red.

an increase in p increases the average speed of a normal particle. The speed of the slow particle is controlled by μ. The transition between a homogeneous phase and a shock phase happens when the slower particle is not able to match the speed of the normal particles either because density is low or μ is low or the value of p is high. Since the system is in a steady state, the velocity of particles in the bulk, behind the slow particle, is the same as the velocity of the slow particle,

$$\mu(1-\rho_1) = (1-p)(1-\rho) + \frac{p(1-\rho)}{\rho}. \tag{2.18}$$

The right side of this equation gives the velocity v_b in the bulk using the expression $v_b = j/\rho$ where j is the current as given in equation (2.2), density ρ being a constant in the bulk. Here ρ_1 is the density just in front of the slow particle. We consider the criterion for shock formation as $\rho_1 = 0$, i.e. a region of zero density just opens up in front of the slow particle. We thus get the condition:

$$\mu = \frac{(1-p)\rho(1-\rho) + p(1-\rho)}{\rho}, \tag{2.19}$$

which describes a two dimensional surface in the three dimensional parameter space of μ, p and ρ. This surface separates a shock phase from a homogeneous phase. Figure 2.14 shows the phase transition on the $\mu - \rho$ plane for different values of p, which shows a good agreement with the data. The density behind the slow particle at the phase transition can

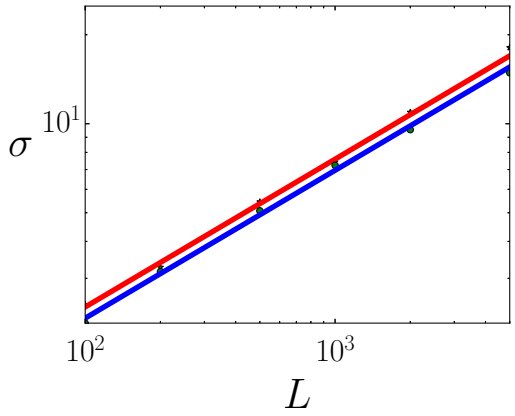

Figure 2.12: Interface fluctuations for $\mu = 0.1$ and $p = 0.2$ as a function of the system size L. The green stars are numerical data obtained for $\rho = 0.5$, whereas the green dots are the data points for $\rho = 0.4$. The solid lines (red, blue) are fits to $L^{1/2}$.

be calculated by solving equation (2.19):

$$\rho_s = \frac{(1-2p-\mu) + \sqrt{(2p+\mu-1)^2 + 4p(1-p)}}{2(1-p)}. \tag{2.20}$$

In the shock phase, the density behind the slow particle is essentially controlled by the speed of the particle which is μ, since it is not restricted by the presence of other particles on the neighbouring site. We then expect that in the shock phase, the value of density in the region behind the slower particle is independent of the average density and will always have the value ρ_s. This prediction is in agreement with the numerics (see figure 2.11).

As mentioned before, the periodic boundary version of our nonlocal hop dynamics can be mapped exactly to the chipping-diffusion-aggregation (CDA) models studied earlier [128, 130]. Figure 2.13 shows a schematic diagram of this mapping for our slow particle dynamics. The movement of the whole mass present at one site to the nearest neighbour site corresponds to the long-range hop in our case while the chipping of one particle corresponds to the local move. It can easily be seen that the slow particle in our case is translated to a slow site in the CDA model. The particles on the slow site of the equivalent CDA model can only move out of it via chipping with rate μ. The shock formation in our model thus corresponds to the formation of an infinite aggregate, i.e. an aggregate whose size is proportional to the total number of particles. Our result above thus also gives the condition for the phase transition to the aggregate phase in the CDA model with totally asymmetric

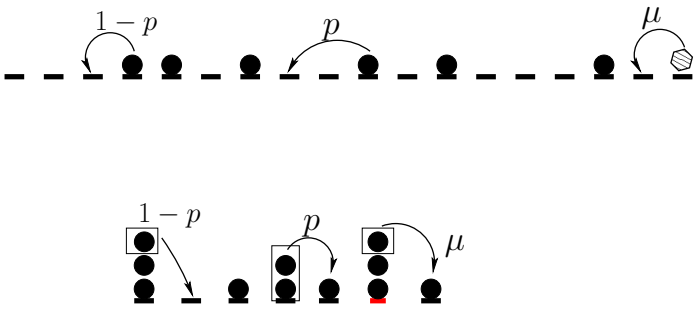

Figure 2.13: The mapping of a particular configuration of our model with a slow particle to the corresponding configuration in the CDA model. Our slow particle translates to a slow site while our non-local hop translates to the movement of the whole cluster in the CDA model. The slow site is shown in red colour.

dynamics and a slow site:

$$\mu = \frac{\rho_c(w + \rho_c + 1)}{(w + 1)(\rho_c + 1)}. \tag{2.21}$$

Here w is the ratio of the probability of chipping (equivalent to local hops in our model) and the probability of the movement of the whole mass (nonlocal hops in our model), $w = (1 - p)/p$ and ρ_c is the average density in the CDA model, which is connected to density in our case as: $\rho = 1/(1 + \rho_c)$. Note that the open boundary versions of our model and the CDA model do not have a proper mapping to each other since fluctuating particle number in one case would imply a fluctuating lattice size in the other.

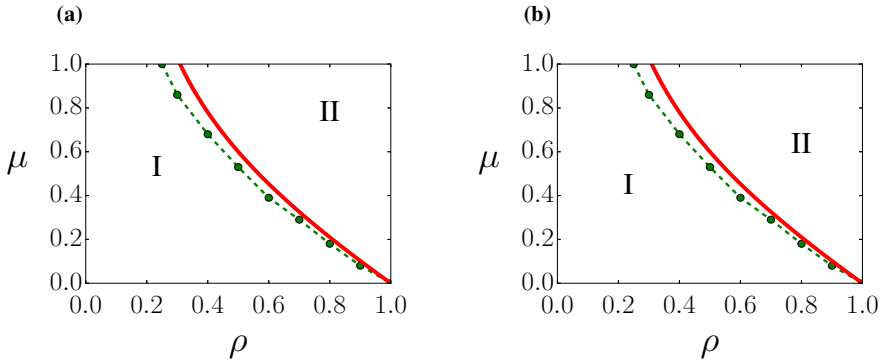

Figure 2.14: The phase transition from shock phase (region I) to homogenous phase (region II) drawn in the $\rho - \mu$ plane for (a) $p = 0.2$ and for (b) $p = 0.8$. The green dashed line shows results from numerical simulations while the red line is obtained using mean field analysis.

2.3 Static defect: Slow bond

Another problem of interest in nonequilibrium systems is the effect of a lattice defect or static impurity on the system. A system that has been well studied in this regard is the TASEP with a single impurity or blockage [61, 69, 134, 135, 136]. Here one considers a TASEP on a periodic lattice where one of the sites is slower than the rest. A particle attempts to move out with a rate one at all other sites except the slow site, which it leaves at a rate r (< 1). The initial work using mean-field [61] was in contradiction with numerical simulations [69]. While the mean field argument predicted that any value of $r < 1$ is sufficient to produce a macroscopic shock or a 'traffic jam' state, the numerical simulations suggested that there is a finite value of r (≈ 0.8) below which one sees a shock phase while for $r > r_c$ there is no real separation of the system into two densities, rather a power law, long-range decay of density towards the average behind the slow site. More recent studies using rigorous arguments [135] as well as more precise numerical work [136] indicate that $r_c = 1$ is the transition point.

2.3.1 Model

To study the effect of such a slow site in our model with long hops, we again consider a periodic one-dimensional lattice of size L with a slow site located at the site numbered L. Any particle present at the slow site can only move to the nearest neighbour (site numbered one) with a rate r. The dynamics on the rest of the lattice are the same as before, except for the long-range hops over the slow site, which are not allowed. A long-range hop by the last particle before site L does not cross site L but terminates at it. A schematic diagram of these dynamics can be seen in figure 2.15 Unlike the previous sections , we begin with reporting results from the mean field analysis instead of the numerical work. The reason for this change is that the mean field results are needed to be used as a guide for choosing density values, as shall become clear later.

2.3.2 Mean field results

The steady state density at all sites except site 1 and site L can be described by equation (2.1) and in the bulk one expects the equation (2.2) to hold. To solve the system, we make a simplifying assumption, similar to [133]. We assume that there are two different density values across the slow site, which extend to the bulk. At the slow site and its left, we expect a higher density, ρ_h, due to the traffic jam while the density on its right is lower, represented

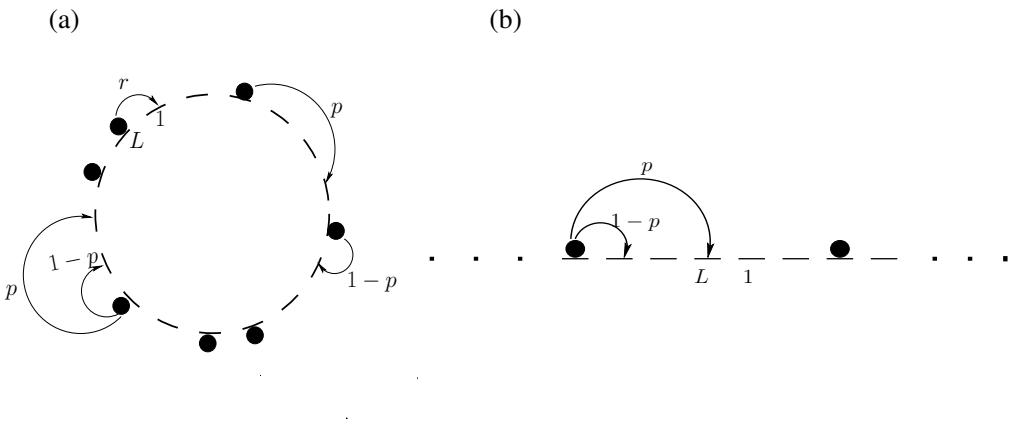

Figure 2.15: Dynamics in our model with periodic boundary and one slow site. (a) Normal dynamics at all other sites: local hops with rate $1-p$ and nonlocal hops with rate p. At the slow site, we can only have local hops with rate r. (b) Nonlocal hops cannot cross the site L, they terminate at L.

by ρ_l. We again use the fact that in the steady state, the current across any link between two sites is the same across the lattice. Thus the current inside the bulk of the high density region is the same as the current in the low density region.

Equating the current across the link between the site L (slow site) and the next site (site 1) and the current across any link deep inside the low density region, we have

$$r\rho_h(1-\rho_l) = (1-p)\rho_l(1-\rho_l) + p(1-\rho_l), \tag{2.22}$$

which gives us

$$\rho_l = \frac{r\rho_h - p}{1-p}. \tag{2.23}$$

Similarly as above, we can equate the current in the high density region to get:

$$r\rho_h(1-\rho_l) = (1-p)\rho_h(1-\rho_h) + p(1-\rho_h). \tag{2.24}$$

Combining the two, we will get the value of ρ_h by solving a quadratic equation as:

$$\rho_h = \frac{(1-2p)(1-p) - r + \sqrt{[(1-2p)(1-p)-r)^2 + 4((1-p)^2 - r^2]\,p(1-p)}}{2\left[(1-p)^2 - r^2\right]}. \tag{2.25}$$

Looking at these expressions, we see that as p increases for a given value of r, the value of

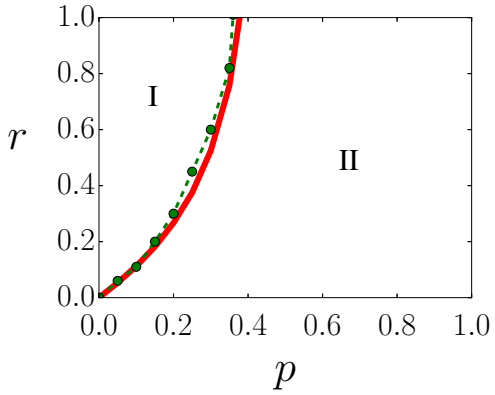

Figure 2.16: The continuous transition from LD-HD (I) phase to ER-HD (II) phase in the $r - p$ plane. The green, dashed line shows data obtained from numerical simulation. The red line is obtained from the mean field analysis.

ρ_L decreases till it touches zero and remains there for all larger values of p. Thus, similar to the TASEP with open boundaries, we have a situation where the input from the slow site cannot catch up with the removal of particles via long hops and part of the system goes into an empty road state. The condition for transition to this HD-ER state can be obtained by substituting $\rho_L = 0$ in equation (2.23) and then using the expression for ρ_h from equation (2.25). This leads us to:

$$r = \frac{p(1-p)}{1-2p}, \tag{2.26}$$

which is the expression for the phase boundary between the HD-ER and HD-LD phases. It should be noted that while the value of average density on the lattice plays no role in the analysis above, we should choose this value carefully such that the number of particles on the lattice is not more than a number that can accommodate the two phases properly. In other words, we should ensure that the product of the average density with the system size should not be greater than the product of the predicted density on high density side with the system size.

2.3.3 Numerical results

Before simulating, we have to fix the value of the average density ρ_A on the lattice. ρ_A has to be chosen such that it is smaller than the predicted value of the density on the high

density side of the shock, ρ_h. Thus, we first calculate the density ρ_h for a given value of r and p using equation (2.25) and then choose ρ_A to be any value smaller than ρ_h. We look at

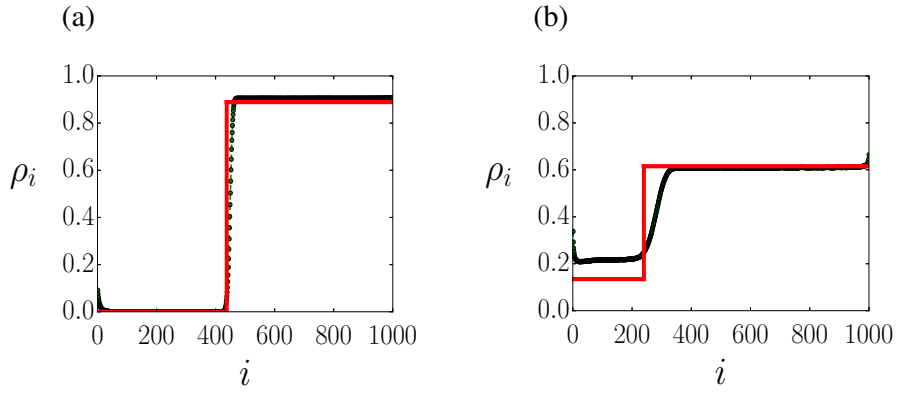

Figure 2.17: Density profile obtained in the two phases as we vary r when $p = 0.2, \rho_A = 0.5$. (a) The system is in an ER-HD phase when $r = 0.1$, and (b) in LD-HD phase when $r = 0.5$. The Monte Carlo simulation results are shown in green while red line shows results from mean field analysis.

the density distribution on the lattice as a function of position in the steady state. As seen in the regular TASEP, we see the formation of regions of low density (ρ_l) and high density (ρ_h) across the slow site. We also see, as established for the regular TASEP, that a shock region is present for all values of $r < 1$. The parameter p increases the speed of the particles thus causing them to cluster more easily. Due to this reason, our analysis did not suffer from the subtle problems in numerical work which make the determination of a shock phase more difficult in the case of regular TASEP. However, the variation of parameters p or r that govern the dynamics in our case, shows us an interesting phase transition, as predicted by the mean field theory above. As we increase p for a given value of r, the density ρ_l on the low density side decreases and becomes zero beyond a particular value of p. Equivalently, we can see the same transition by keeping p as constant and varying r (see figure 2.17). We thus have a phase transition from a phase with finite densities in both regions (HD-LD phase) to a phase where the density is always zero on the low density side (HD-ER phase). The variation of densities as we change p can be seen in figure 2.18. These results show a good agreement with mean field prediction in the section above, which can be seen in figure 2.16.

Another quantity of interest is the fluctuations of the shock front between the low density and high density side. We again use a second class particle, as described in the slow particle problem, to track the fluctuations. In the regular TASEP, it has been shown [133]

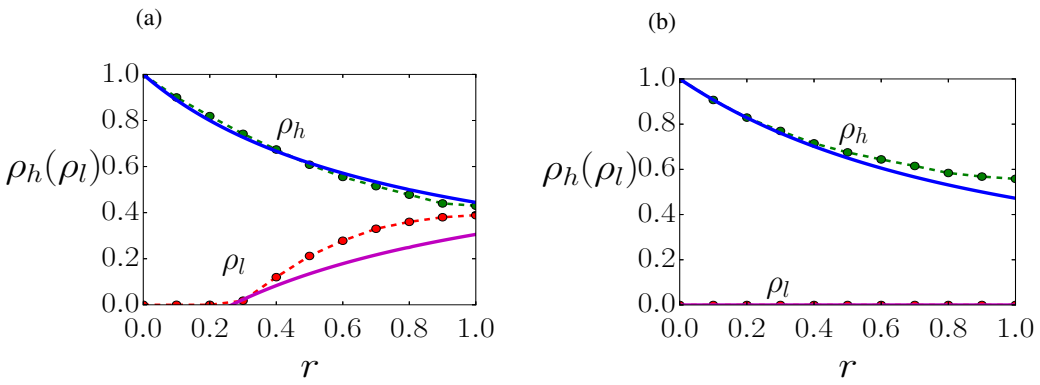

Figure 2.18: (a) Density versus r for the case p=0.2. The density ρ_l vanishes for low values of r signaling a transition from the LD-HD phase at high values of r to ER-HD phase at low values of r. $r \approx 0.2$ is the point of phase transition here. The average density ρ_A is taken as 0.5 for data corresponding to $r = 0.6$ and smaller. For $r = 0.7, 0.8, 0.9, 1.0$, ρ_A is 0.4. (b) At higher values of p ($p = 0.8$ in this case), the LD-HD phase completely vanishes and only the ER-HD phase exists. The average densities are taken as follows: $[r = 0.1, \rho_A = 0.5]$, $[r = 0.2, \rho_A = 0.4]$, $[r = 0.3, 0.4, \rho_A = 0.3]$, $[r = 0.5, \rho_A = 0.25]$, $[r = 0.6, 0.7, \rho_A = 0.2]$, $[r = 0.8, 0.9, \rho_A = 0.15]$, $[r = 1.0, \rho_A = 0.1]$. The mean field values are obtained from equation 2.24. In both figures, green and red with dashed lines show results from Monte Carlo simulations while blue and violet solid lines show results from mean field calculations.

that the variation of fluctuations with system size depends on the average density on the lattice; the fluctuations scale as $L^{1/3}$ for density $1/2$ and $L^{1/2}$ for all other densities. The different behaviour at density $1/2$ is ascribed to particle-hole symmetry in this case leading to the density fluctuations only having dynamical randomness as their origin. Our dynamics do not have the particle-hole symmetry. We thus expect that our system will show the same behaviour at all parameter values. This is indeed the case, and we find that the fluctuations behave as $L^{1/2}$ similar to the normal TASEP with a slow site and with a density different from $1/2$ (see figure 2.19). The nature of fluctuations does not change across the phase transition and we see the same behaviour of fluctuations in both the phases. In these simulations, r and p are chosen such that the value of density in the high density part is higher than the average density, for reasons explained before.

We have also tried a slightly different version of dynamics to see how robust our results are. In this version, the dynamics out of the slow site are different from the model above while the rest of the dynamics remain the same. We consider that a particle moving out of a slow site can make local as well as nonlocal hops, both with a rate scaled by the same factor r: local hops with rate $r(1-p)$ and nonlocal hops with rate rp where $0 \leq r \leq 1$. As

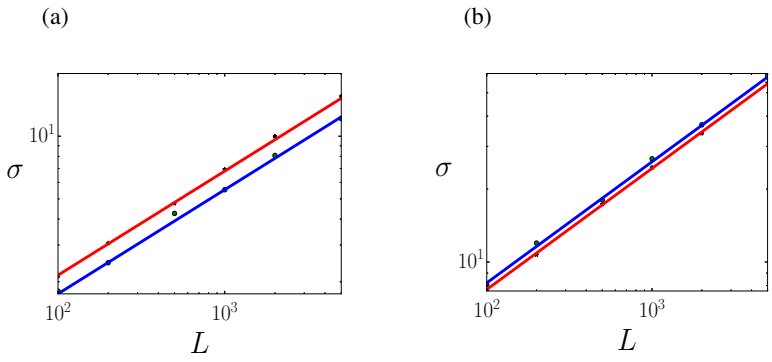

Figure 2.19: Interface fluctuations as a function of system size L. $p = 0.2$ for both figures. Figure (a): $r = 0.1$, system is in the ER-HD phase. Figure (b): $r = 0.5$, system is in LD-HD phase. In both the figures, green stars are numerical data obtained for $\rho_A = 0.5$ and the green dots are the data points for $\rho_A = 0.4$. The solid lines (red, blue) show fits to $L^{1/2}$.

before, all long hops of the particle just before the slow site, terminate at it. One can easily see that the mean field description of this model is the same as the one we described above. Numerically, we again see a phase separation across the slow site. We also see a transition to a phase with zero density on the low density site (HD-LD to HD-ER transition) as seen above. So qualitatively, the results from these models are very similar.

To summarise, we have studied the effects of long range hops on the TASEP with open as well as periodic boundaries. The long hops lead to a significant change in the phase behaviour of the TASEP for the open boundary system, with the ER and HD phases dominating the phase diagram at higher values of p, the parameter governing long hops. We also studied the effect of a combination of long range hops and disorder (static and dynamic) in a TASEP with periodic boundaries and our study again shows that changing p changes the steady state behaviour and also leads to the formation of a new phase in the case of a static defect.

Chapter 3

Totally Asymmetric exclusion process with resetting

In this chapter, we describe our work on the one-dimensional TASEP with open boundaries having the additional dynamical feature of stochastic resetting to the initial, empty state. The system evolves according to the TASEP dynamics with particles entering the input side with rate α and leaving the other side with rate β. The system has the additional dynamical feature of resetting wherein it is brought back to its initial state of empty lattice at random intervals τ. These intervals are drawn from probability distributions, for which we consider two possibilities - a power law $\sim \tau^{-(1+\gamma)}$ with $\gamma > 0$ and an exponential distribution $\lambda e^{-\lambda\tau}$. We use approximate expressions for the time evolution of density on the lattice for a normal TASEP to calculate the reset-averaged density as a function of time. We also perform numerical simulations results which show good agreement with our analytic expressions.

A related problem was addressed previously in the context of protein production during the mRNA translation process [70,98]. While TASEP is a simple model for mRNA translation, the resetting dynamics was introduced to model the degradation of the mRNA and its subsequent replacement by a new one. Here, a constant rate of degradation was assumed - implying an exponential distribution of inter-reset times. The quantity of interest here was the average of particle density over resetting distribution in the limit $t \to \infty$, which can be interpreted as the ensemble average of density of ribosomes loaded over the mRNA. This average can be measured experimentally. The model provided an explanation for the decay of the average ribosome density along the length of the mRNA as seen in the experiments.

In this work, we calculate the full time dependent distribution of the particle density in a TASEP with open boundaries, such that the system is reset stochastically to its initial, empty state with inter-reset times drawn from either exponential or power law distributions.

Our motivation for studying these models are more general than the particular example of protein production by the mRNA-ribosome complex, where only the $t \to \infty$ limit of the exponential reset distribution was considered. As we have mentioned in the introduction chapter, TASEP is a paradigm in nonequilibrium statistical mechanics due to its simple dynamics that nonetheless lead to a nontrivial phase structure in the case of open boundaries [137]. It is one of the few models where steady state properties can be calculated analytically exactly. Apart from the considerable interest from a purely theoretical point of view, the model and its many variations have found applications in diverse problems like mRNA-translation [138, 139, 140] movement of motor proteins inside cells [67, 141], vehicular traffic [66] and motion of ants [43, 44].

In our model, the TASEP is reset at intervals drawn from exponential and power law distributions. Both these distributions are again ubiquitous in many natural and man made phenomenon. While power law gaps between event times show up in many places where the activity is known to happen in bursts, e.g. earthquakes [142, 143], coronal mass ejections from sun [144], neuron firings [145], successive crashes in stock exchange [146], fluorescence decay in nanocrystals and biomolecules [147, 148]; the exponential gap between successive events is seen in many systems where the underlying rate of the event is constant and the process is memoryless - e.g. radioactive decay [149], job service times in queuing theory [150] the time between two communications by the same person [151,152]. The broad range of scales and settings in the above examples show that the problem under study is of general interest and may in the future reflect upon interesting phenomena. The steady state of the TASEP, as well as the approach to it as a function of time, are governed by the input and output rates α and β respectively. The particle density on the lattice evolves in a different fashion for each of the three possible phases and we explore the effect of resetting for each of them. The different inter-reset distributions themselves also lead to very different behaviours. The system always settles to a steady state for the exponential distribution but for the power law distribution, the appearance of a steady state distribution depends on the exponent γ. The average time between resets is infinite when $\gamma < 1$ and this leads to the system not achieving a steady state, while for $\gamma > 1$, the system achieves a time-independent state at large times.

The chapter is arranged as follows. We begin with a description of our model and provide an idea of the calculations in Section (3.1). Before studying the effect of resetting on the system, we need to know how the density evolves in time, starting with an empty lattice, in the usual TASEP with open boundaries. An approximate analytical description of this time evolution is provided in section (3.2), along with the numerical results from Monte-

Carlo simulations. In section (3.3), we calculate the time-dependent density distribution taking into account resetting events that happen according to a power law distribution. We compare this to the results from our Monte-Carlo simulations. In section (3.4), we carry out the same exercise, taking the resetting distribution to be an exponential one.

3.1 Model and theory

We consider a TASEP in one dimension with a lattice of length L where particles can enter the lattice at the left boundary at a rate α and exit at the right boundary with a rate β. The particles interact via hard-core repulsion, i.e. a particle cannot move to a site which is already occupied by another one. At any moment in time, a given particle on the lattice site i attempts to move to site $i+1$ with a rate one. The sites on the lattice are labelled by numbers 1 to L from left to right. We consider the lattice to be initially empty. The density of particles on the lattice, ρ, evolves as the particles start entering the lattice from the left boundary and move towards the right. In addition to these regular TASEP dynamics, we have the resetting dynamics as follows. The system is reset stochastically to its initial, empty state after having evolved for a time τ. We consider two possibilities for the time intervals between the resets: they could be drawn from a power law distribution, or assuming a constant rate of resets in which case the distribution is exponential. The quantity we are interested in exploring is the density of particles on the lattice as a function of time and position, averaged over the resetting distribution. We denote this density by $\rho^r(x,t)$, while $\rho(x,t)$ will stand for the density on the lattice as in a regular TASEP, without the resetting dynamics.

Let us first consider the case of power law distribution where the time between two resets is chosen from the distribution:

$$\phi(\tau) = \frac{\gamma}{\tau_0(\tau/\tau_0)^{1+\gamma}};\ \tau \in [\tau_0, \infty),\ \gamma > 0, \tag{3.1}$$

where τ_0 is a cut-off that enables normalization of the distribution and can be interpreted as the smallest time scale of the underlying system causing the resetting. For the power law distribution in equation (3.1) above, we can calculate the reset-averaged density as

$$\rho^r(x,t) = \int_0^t \rho(x,\tau)\ f_\gamma(t, t-\tau) d\tau. \tag{3.2}$$

Here $\rho(x,t)$ is the distribution of density along the lattice at time t, beginning with an

empty lattice at time $t = 0$, as would happen in a regular TASEP. The above equation then describes a system which has been evolving for a time τ since the previous reset and the integration considers all possible values of τ. The probability that this reset happened at time $t - \tau$, with the inter-reset time governed by equation (3.1), is given by $f_\gamma(t, t-\tau)$. This probability density $f_\gamma(t, t-\tau)$ can be seen as a product of the probability of two events - having a reset at a time $t - \tau$, and having no reset after that for a time τ [125]. The expression can be calculated in the large time limit ($t >> \tau_0$) and comes out to be different for the cases $\gamma > 1$ and $\gamma < 1$. For $\gamma < 1$, we get

$$f_{\gamma<1}\left(t, t-\tau\right) = \frac{\sin\left(\pi\gamma\right)}{\pi}\tau^{-\gamma}\left(t-\tau\right)^{\gamma-1}, \tag{3.3}$$

while for $\gamma > 1$, we have

$$f_{\gamma>1,\tau\geq\tau_0}(t, t-\tau) = \frac{1}{\tau_0}\left(\frac{\gamma-1}{\gamma}\right)\left(\frac{\tau}{\tau_0}\right)^{-\gamma}, \tag{3.4}$$

which comes with the normalization condition:

$$\int_0^{\tau_0} d\tau f_{\gamma>1,\tau<\tau_0}(t, t-\tau) = 1 - \int_{\tau_0}^{t} d\tau f_{\gamma>1,\tau\geq\tau_0}(t, t-\tau). \tag{3.5}$$

The details for the derivation of equations (3.3) and (3.4) have been provided in the appendix A.

If the resets take place with a constant rate λ, the expression is simpler than the above power law case and $\rho^r(x,t)$ can be calculated as [123]

$$\rho^r(x,t) = \int_0^t \rho(x,\tau)\lambda e^{-\lambda\tau} d\tau + e^{-\lambda t}\rho(x,t). \tag{3.6}$$

The resetting here can be seen as the renewal process and the distribution of the time of the previous reset is the age process. The second term on the RHS comes from the possibility that no resets happen in time t. The limit $t \to \infty$ of the above expression for resetting-averaged density is used to model the processes of translation of mRNA during protein production [98], where one interprets this expression as an average over a large ensemble of mRNA (lattices), each of which is undergoing the translation process (TASEP) with ribosomes (particles with hard-core interactions) entering on one side and exiting on the other. The process of resetting models the random degeneration of an mRNA and its subsequent replacement by a fresh, unloaded one. Such random degradation is known to happen in real

systems [70, 153]. The reset averaged density $\rho^r(x,t)$ is calculated from above expressions can be used to calculate other quantities of interest. In the context of protein production, a relevant and experimentally measurable quantity is the average number of ribosomes sitting on mRNA. The effect of reset on this quantity can easily be calculated by integrating the $\rho^r(x,t)$ over the lattice, as can be seen in previous work [70,98]. One can also calculate the total current flowing through a TASEP, which can be quantified by the number of particles entering the system [137]. Within our approximation for the time evolution of density, we can calculate this quantity by accounting for the increase in density as well as the particles leaving at the other end per unit time.

3.2 Evolution of density in a TASEP

Before calculating the density $\rho^r(x,t)$ averaged over resetting events, as in equations (3.2) and (3.6), we need to know $\rho(x,t)$, which is the time dependent density with regular TASEP dynamics, beginning with an empty lattice. In this section we describe the evolution of this density for various parameter ranges of the input/output parameters.

It is well known that in the long time limit, the TASEP settles into one of three possible steady states depending on the values of α and β [46, 48, 50]. When $\alpha < \beta$ and $\alpha < 0.5$, the system is in a low density (LD) phase, where the bulk density is governed by the input boundary and takes a value of α. On the other hand, when $\beta < \alpha$ ($\beta < 0.5$), the system is in a high density (HD) phase, where the restricting action of output boundary controls the phase and the density in the bulk has the value $1-\beta$. When both α and β have values higher than 0.5, the system goes into the maximal current (MC) phase, where the bulk density is half, irrespective of parameter values and the density shows a long range decay from the boundaries towards the bulk. The value of current in this phase is $1/4$, which is the maximum possible value for the system. While the above paragraph describes the steady state behaviour of the system, the time dependence of the density is also dependent on the entry and exit rates and therefore shows different behaviours for each of the three phases. Indeed, within the HD phase, there are two different possibilities for the development of the density distribution $\rho(x,t)$ on the lattice, as we will see. We will describe below the approximate expressions for $\rho(x,t)$ that we have used for further calculations. We will compare our approximation with numerical data, which we have obtained using Monte-Carlo simulations, the method for which we will describe at the end of the section.

Many steady state properties of TASEP can be studied analytically exactly using the matrix method [49] apart from the mean field approach. The time evolution of the TASEP

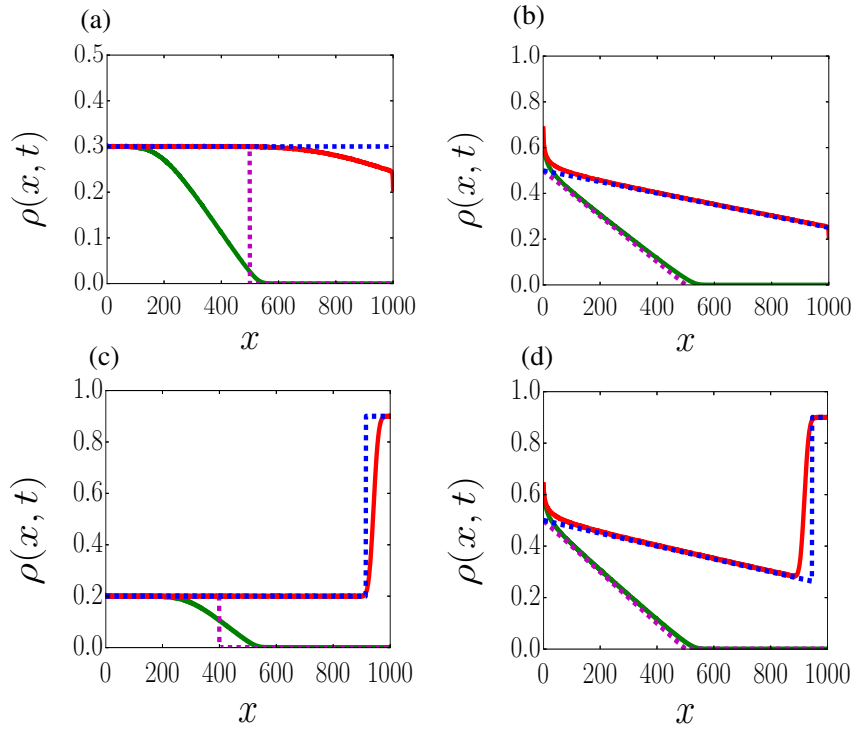

Figure 3.1: Time dependent density profile of TASEP in the various parameter regimes. Here dotted lines stand for analytical results and solid lines stand for numerical results. Green solid line and the magenta dotted line stand for t=500, the red solid line and the blue dotted line stand for t=2000. The parameter values are as follows: (a) $\alpha = 0.3, \beta = 0.9$ [analytic result from equation (3.8)], (b) $\alpha = 0.8, \beta = 0.9$ [analytic result from equation (3.10)], (c) $\alpha = 0.2, \beta = 0.1$ [analytic result from equation (3.11)] and (d) $\alpha = 0.7, \beta = 0.1$ [analytic result from equation (3.13)]. $L = 1000$ for all figures.

density profile within the mean field can be captured by the hydrodynamic equation [154]

$$\frac{\partial \rho(x,t)}{\partial t} = -(1-2\rho)\frac{\partial \rho}{\partial x} + \frac{1}{2}\frac{\partial^2 \rho}{\partial x^2}, \tag{3.7}$$

which is the Burgers equation for a fluid. While this equation can be formally solved for eigenvalues, capturing the time dependence of density, getting a closed-form expression that can be used for our purposes is only possible in the limit of large times [57]. Another way of understanding the dynamics in TASEP is provided by the domain wall theory [154, 155,156,157], which describes the density change in terms of the evolution of a shock front between two density domains imposed by the input and output boundaries. Our calculations require the system behaviour at all times, beginning with an empty lattice, where the density

front starts evolving from the input end towards the output end. The output boundary comes into play only once the particles start reaching it. For our purposes, we make a simple approximation for the time dependence of the density evolution, as done previously [98]. In the calculations below, we consider a coarse grained description of the system where the space co-ordinate x varies continuously with $0 \leq x \leq L$.

We begin with the LD phase, where $\alpha < \beta$ and $\alpha < 0.5$. We know that the density equilibrates with the input reservoir at the value α and the current is $\alpha(1-\alpha)$ in the steady state. The density evolution here can be taken to be a front or a shock wave of density α that moves with a velocity of $1-\alpha$. One can neglect the small, exponential change in the density at the exit boundary and thus write the density in this phase as

$$\rho(x,t) = \begin{cases} 0 & \text{if } 0 < t \leq \frac{x}{v}, \\ \alpha & \text{if } \frac{x}{v} < t, \end{cases} \tag{3.8}$$

where the speed v is $1-\alpha$ and the maximum value of x is the lattice size L. The expression above can also be written as $\rho(x,t) = \alpha H(t - \frac{x}{v})$, where $H(y)$ is Heaviside step function

$$H(y) = \begin{cases} 0 & y < 0, \\ 1 & y \geq 0. \end{cases} \tag{3.9}$$

A comparison of the approximation in the above equation (3.8) with numerical data from Monte-Carlo simulations is shown in figure 3.1(a). We notice that unlike our sharp front, the actual density gradually declines from α to zero.

We discuss the MC case next, where $\alpha, \beta > 0.5$. The kinematic wave associated with the movement of a patch of density α does not propagate into the system when $\alpha > 0.5$ [57]. Instead, we observe from our simulations that the density quickly decays towards the value half, after which it evolves like a rarefaction wave type solution which fits well to the following form:

$$\rho(x,t) = \begin{cases} 0 & \text{if } 0 < t < x, \\ \frac{1}{2}\left(1 - \frac{x}{t}\right) & \text{if } t \geq x. \end{cases} \tag{3.10}$$

Note that the above solution is consistent with the maximal current value of $1/4$ and satisfies equation (3.7) with a boundary fixed at density half. We can also express the above expression in the form $\rho(x,t) = \frac{1}{2}\left(1 - \frac{x}{t}\right) H(t-x)$. We know that the steady state solution in the MC case is a power law decay towards the density half, from both ends of the lattice. We therefore expect our approximation to get progressively worse as time grows

larger. Figure 3.1(b) shows a comparison of this approximation with numerical results at smaller times, where it appears to agree well with the numerics.

We finally consider the HD case, where $\beta < \alpha$, $\beta < 0.5$ and the exit boundary controls the steady state behaviour of the system by blocking the outflow. To describe the time-dependent behaviour of the density, we will consider the two distinct possibilities, $\alpha < 0.5$ and $\alpha > 0.5$, while $\beta < \alpha$. As the system evolves towards the steady state, the density starts evolving from the input boundary end and the output boundary does not come into the picture till particles start reaching it. In the initial phase, where none of the particles has reached the exit boundary, the system density evolves only based on the input rate α and thus shows the LD phase like behaviour for $\alpha < 0.5$ and a behaviour same as the MC phase for $\alpha > 0.5$.

Once the incoming particles arrive at the exit boundary, the slow rate of exit leads to an accumulation of particles. This clustering leads to a reverse front of density $1 - \beta$ that travels from the exit end towards the entry end. The density on the lattice is then divided into two portions with the input side still being governed by the entry front and the other side by the exit end. Eventually, the reverse front reaches the entry end and we get a steady state situation with no more change in the average density of the particles on the lattice. Thus, when $\alpha < 0.5$, we have

$$\rho(x,t) = \begin{cases} 0 & \text{if } 0 < t \leq \frac{x}{v}, \\ \alpha & \text{if } \frac{x}{v} < t < \frac{L}{v} + \frac{L-x}{v_r}, \\ 1-\beta & \text{if } t > \frac{L}{v} + \frac{L-x}{v_r}, \end{cases} \tag{3.11}$$

where $v = 1 - \alpha$ is the speed of the incoming front of density α. The speed of the backward front of density $1 - \beta$ is given by $v_r = \frac{\alpha(1-\alpha)-\beta(1-\beta)}{1-\alpha-\beta}$. This can be inferred from the change in the total number of particles on the lattice per unit time, which is given by $\alpha(1-\alpha)-\beta(1-\beta)$ and the fact that the reverse density wave is moving across a previously imposed density of α from the input end [see figure 3.1(c)]. This is again, the same velocity as predicted by the domain wall picture [154]. The above equation can also be written in terms of the Heaviside function as

$$\rho(x,t) = \alpha \left[H\left(t - \frac{x}{v}\right) - H\left(t - \left\{\frac{L}{v} + \frac{L-x}{v_r}\right\}\right)\right] + (1-\beta)\, H\left(t - \left\{\frac{L}{v} + \frac{L-x}{v_r}\right\}\right). \tag{3.12}$$

In the case of $\alpha > 0.5$, the input boundary dynamics is similar to the MC case and we

have for the density:

$$\rho(x,t) = \begin{cases} 0 & \text{if } 0 < t \leq x, \\ \frac{1}{2}(1 - \frac{x}{t}) & \text{if } x < t \leq T, \\ 1 - \beta & \text{if } t > T, \end{cases} \tag{3.13}$$

where T is the time at which the reverse moving front of density $1-\beta$ reaches the position x on the lattice. In terms of a Heaviside function, we can write the above expression as $\rho(x,t) = \frac{1}{2}(1-\frac{x}{t})(H(t-x) - H(t-T)) + (1-\beta)H(t-T)$. We can calculate T as follows. Consider the change in number of particles per unit time, after the reverse front has started

$$\frac{1}{4} - \beta\,(1-\beta) = v_R(t)\left[(1-\beta) - \frac{1}{2}\left(1 - \frac{X(t)}{t}\right)\right] + \frac{X(t)^2}{4t^2}, \tag{3.14}$$

where $X(t)$ is the position of the front edge of the density wavefront travelling backward and $v_R(t)$ is the velocity of the wavefront. The LHS gives the change in the number of particles on the lattice by accounting for the entry and exit of particles from the respective boundaries. The first two terms on the RHS account for the increase in the density due to the backwards moving front, which has a density of $(1-\beta)$ and is moving across the already present density $\frac{1}{2}(1-\frac{x}{t})$.

The third term accounts for the increase in the number of particles on the left side of the density front. Unlike the previous case of $\alpha < 1/2$, here the density on the left of $X(t)$ is itself evolving. The change in density $\rho(x,t)$ at a point x to the left of X(t) is given by:

$$\frac{\partial}{\partial t}\rho(x,t) = \frac{\partial}{\partial t}\left[\frac{1}{2}\left(1 - \frac{x}{t}\right)\right] = \frac{x}{2t^2}, \tag{3.15}$$

therefore, the change in total number N_p in the whole region preceding the returning density front is given by integrating the above expression:

$$\frac{dN_p}{dt} = \int_0^X \frac{x}{2t^2}dx = \frac{X^2}{4t^2}, \tag{3.16}$$

which is the third term on the right hand side of equation (3.14). The position of the front and the velocity of the front are connected as:

$$X = L - \int_L^t v_R dt'. \tag{3.17}$$

It can be recast into the expression $\frac{dX}{dt} = -v_R$ which, along with the equation (3.14), give us

$$\frac{dX}{dt} = \frac{\frac{1}{4} - \beta(1-\beta) - \frac{X^2}{4t^2}}{\beta - \frac{1}{2} - \frac{X}{2t}}, \tag{3.18}$$

which can be solved to give

$$X(t) = t(2\beta - 1) + c\sqrt{t}. \tag{3.19}$$

Substituting the boundary condition $X = L$ when $t = L$, we get $c = 2(1-\beta)\sqrt{L}$, and thus

$$X(t) = t(2\beta - 1) + 2(1-\beta)\sqrt{tL}, \tag{3.20}$$

using this equation, we express the time T at which the front $X(t)$ reaches a position x as

$$T^2(2\beta-1)^2 - T\left[2x\,(2\beta-1) + 4L\,(1-\beta)^2\right] + x^2 = 0, \tag{3.21}$$

which has the solution

$$T = \frac{2x(2\beta-1) + 4L(1-\beta)^2 + \sqrt{\left[-2x(2\beta-1) - 4L(1-\beta)^2\right]^2 - 4x^2(2\beta-1)^2}}{2(2\beta-1)^2}. \tag{3.22}$$

See figure 3.1(d) for the approximate density profile derived above.

We now have the expressions for the evolution of density in a TASEP in all the parameter ranges. In figures 3.1(a)-(d), our approximate expressions above have been compared with numerical data. We obtained this data using Monte-Carlo simulations, where the TASEP dynamics are simulated as follows. At a given time, a site is chosen with equal probability from amongst the L lattice sites and a reservoir site. If the chosen site is the reservoir site, an attempt is made to add a particle to site number one, with probability α. The move is successful if there is no particle already sitting on site one. If the chosen site is the rightmost site (L) and a particle is present at that site, then it is removed from the lattice with a probability β. If any other site i apart from these two is chosen and if it is occupied with a particle, that particle attempts to move towards the site on its right (i+1) with a probability one. The move is successful if the site on the right is empty. $L+1$ such steps constitute a single unit of time. The resetting dynamics, which is discussed in sections 3.3 and 3.4, is simulated in the following manner. At the beginning of the dynamics, when all lattice sites are unoccupied, we draw a number from the concerned distribution (power law distribution in equation (3.1) or the exponential distribution $\lambda e^{-\lambda t}$) which corresponds to

the time at which the dynamics will be reset. After running the TASEP dynamics for this amount of time, we reset the configuration to an empty state. The simulation is run until the total time reaches the desired number t. The density on the lattice at this moment in time is recorded. We then perform an average of this density over multiple realizations.

3.3 Effect of power law resetting

As mentioned before, we want to calculate the density distribution $\rho^r(x,t)$ on the lattice at a given time, averaged over all the possibilities of resetting, beginning with an empty lattice at time $t = 0$. This can be done using equation (3.2), with the input for density without resetting, $\rho(x,t)$, coming from the results in section 3.2. The probability that the gap between given time t and the previous reset is τ is given by the equations (3.3) and (3.4), for times $t >> \tau_0$. This distribution has a different behaviour depending on whether the exponent γ is greater than or smaller than one. We will describe below the results for all the three phases of LD, HD and MC, taking into account both the cases $\gamma > 1$ and $\gamma < 1$.

3.3.1 LD phase

Using equations (3.2), (3.8) and (3.4), we have for $\gamma > 1$

$$\begin{aligned}
\rho^r(x,t) &= \int_0^t \rho(x,\tau) f_{\gamma>1}(t,t-\tau)d\tau \\
&= \int_0^{\tau_0} \rho(x,\tau) f_{\gamma>1,\tau\leq\tau_0}(t,t-\tau)d\tau + \int_{\tau_0}^t \rho(x,\tau) f_{\gamma>1,\tau\geq\tau_0}(t,t-\tau)d\tau \\
&= \frac{\alpha\tau_0^{\gamma-1}(\gamma-1)H\left(t-\frac{x}{v}\right)}{\gamma}\int_{\frac{x}{v}}^t \left(\frac{\tau}{\tau_0}\right)^{-\gamma} d\tau + \rho(x,\tau_0)\left[1-\int_{\tau_0}^t f_{\gamma>1,\tau\geq\tau_0}(t,t-\tau)d\tau\right].
\end{aligned}$$

The above integral can be simplified as

$$\rho^r(x,t) = \frac{\alpha\tau_0^{\gamma-1}}{\gamma}\left[\left(\frac{x}{v}\right)^{1-\gamma} - t^{1-\gamma}\right] H\left(t-\frac{x}{v}\right) + \frac{\alpha}{\gamma}\left[\gamma - 1 + \left(\frac{t}{\tau_0}\right)^{1-\gamma}\right] H\left(\tau_0 - \frac{x}{v}\right) \quad (3.23)$$

The Heaviside function in the first expression on the RHS indicates that at any given time t, the front cannot reach a distance beyond the point vt in space, while the $H(\tau_0 - \frac{x}{v})$ in the second expression on RHS merely expresses the contribution due to resetting at the cut-off time ($\tau_0 = 1$). Figure 3.2(a) shows the comparison of numerical data obtained from Monte-Carlo simulations to our analytic expression above. The fit is good in the bulk of

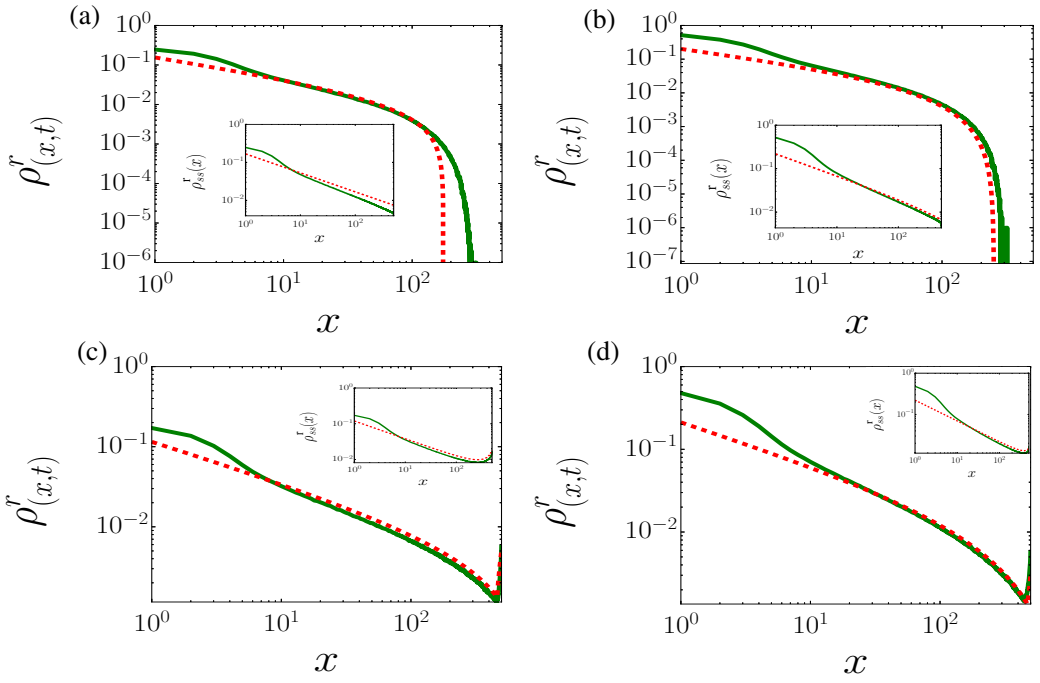

Figure 3.2: Density profile when the time interval between resettings is drawn from the power law distribution. Here the dotted lines stand for analytical results and the solid lines stand for numerical results. The parameters are as follows: $\gamma = 1.5$ and lattice size $L = 500$ for all figures. (a) $\alpha = 0.3$, $\beta = 0.9$, $t = 250$ [analytic result from equation (3.23)], in (b) $\alpha = 0.8, \beta = 0.9$, $t = 250$ [analytic result from equation (3.25)], in (c) $\alpha = 0.2$, $\beta = 0.1$, $t = 1000$ [analytic result from equation (3.27)] and in (d) $\alpha = 0.7$, $\beta = 0.1$, $t = 1000$ [analytic result from equation (3.29)]. The inset in each figure contains the density profile for $t = 10000$, with the rest of the parameter values same as the corresponding main figure.

the graph. Our approximation assumes that the density front is always sharp with a value α but we see that the real front decays gradually towards zero density as seen in figure 3.1(a), and the sharpness of the front changes with time. This effect leads to the deviation in the initial and end portions of the graph. As time $t \to \infty$, the system reaches a steady state since the average time gap between two resets is finite and this dictates a time independent average behaviour. We indeed see that in this limit, in the bulk of the lattice, far from the boundaries, we have $\rho^r_{ss}(x) = \frac{\alpha}{\gamma}\left(\frac{x}{v\tau_0}\right)^{1-\gamma}$, where the subscript "ss" stands for steady state. The inset in figure 3.2(a) shows the comparison with this limiting expression with the simulations at large times and the agreement is good.

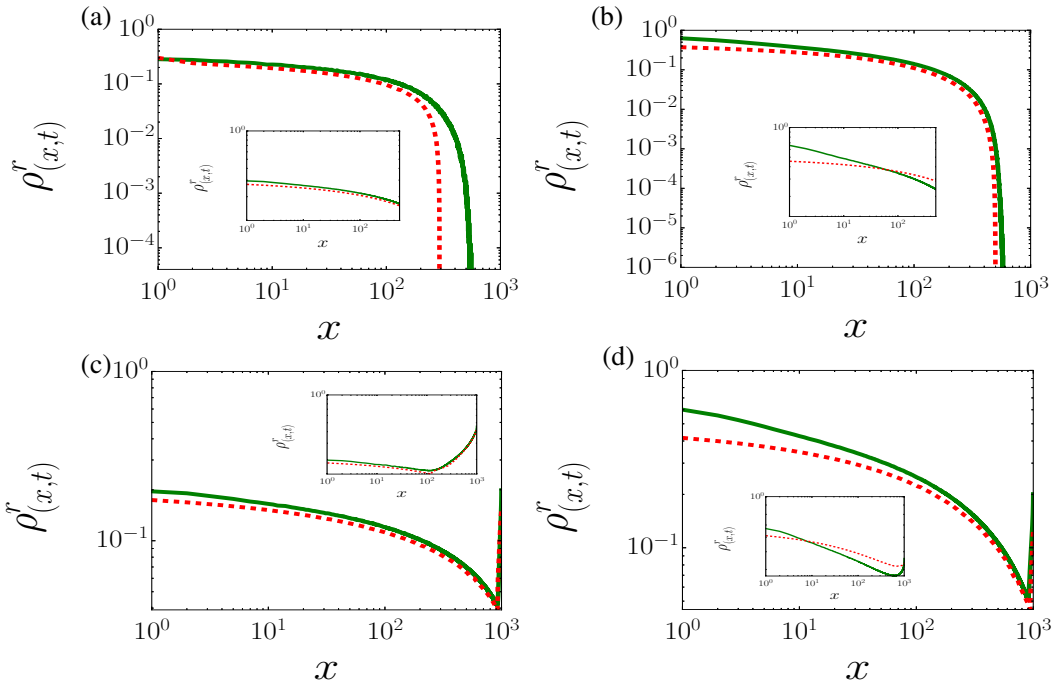

Figure 3.3: Density profile when the time interval between resettings is drawn from the power law distribution. Here the dotted lines stand for analytical results and the solid lines stand for numerical results. The parameter values are as follows: $\gamma = 0.75$ and lattice size $L = 1000$ for all figures. In (a) $\alpha = 0.3$, $\beta = 0.9$, $t = 500$ [analytic result from equation (3.24)], in (b) $\alpha = 0.8$, $\beta = 0.9$, $t = 500$ [analytic result from equation (3.26)], in (c) $\alpha = 0.2$, $\beta = 0.1$, $t = 2000$ [analytic result from equation (3.28)] and in (d) $\alpha = 0.7$, $\beta = 0.1$, $t = 2000$ [analytic result from equation (3.30)]. The inset in each figure contains the density profile for $t = 10000$, with the rest of the parameter values same as the corresponding main figure.

We similarly calculate for the case $\gamma < 1$ using equations (3.2), (3.8) and (3.3)

$$\rho^r(x,t) = \alpha \left[1 - \frac{\sin(\gamma\pi)}{\pi} B\left(\frac{x}{vt}; 1-\gamma, \gamma\right)\right] H(vt - x), \tag{3.24}$$

where $B(y; a, b)$ is the incomplete Beta function defined by

$$B(y; a, b) = \int_0^y x^{a-1}(1-x)^{b-1} dx.$$

For $\gamma < 1$, the first moment of the distribution of inter-reset times diverges. This implies that on an average, there is an infinite time between two resets - this is reflected in the

expression of density (3.24) above where we can see that x scales as t and we do not have a time-independent steady state. Nonetheless, we can make an approximation, of finite system size L and $t >> L$ such that for any point x in the bulk of the system, we have $\frac{x}{t} << 1$. In this limit, using the expansion of incomplete Beta function at small argument, we have

$$\rho^r(x,t) \approx \alpha \left[1 - \frac{\sin(\gamma\pi)}{\pi(1-\gamma)} \left(\frac{x}{vt}\right)^{1-\gamma}\right].$$

Figure 3.3(a) shows a comparison of the analytic results from equation (3.24) and numerical simulation of the model. The agreement is good except at the right front for reasons explained before. The inset in this figure shows a comparison of the numerical data with the expression in the $\frac{x}{t} << 1$ limit above, which again agrees well.

3.3.2 MC phase

We use equations (3.2), (3.10) and (3.4) to get for $\gamma > 1$

$$\begin{aligned}\rho^r(x,t) &= \frac{(\gamma-1)\tau_0^{\gamma-1}}{2\gamma}\left[\frac{1}{(1-\gamma)}\left(t^{-\gamma+1} - x^{-\gamma+1}\right) + \frac{x}{\gamma}\left(t^{-\gamma} - x^{-\gamma}\right)\right] H(t-x) \\ &+ \frac{1}{2}\left(1 - \frac{x}{\tau_0}\right)\left[\frac{\gamma-1}{\gamma} + \frac{1}{\gamma}\left(\frac{t}{\tau_0}\right)^{1-\gamma}\right] H(\tau_0 - x), \end{aligned} \tag{3.25}$$

where again the first Heaviside function on RHS indicates that the edge of the density front can not move beyond the point $x = t$ while the second one comes from the contribution of resets at the smallest time. In the limit of $t \to \infty$, we get the following expression away from the boundaries

$$\rho^r_{ss}(x) = \frac{1}{2\gamma^2}\left[\frac{x}{\tau_0}\right]^{1-\gamma}.$$

Figure 3.2(b) shows the density profile obtained using numerical simulation compared to equation (3.25), while the inset shows the corresponding comparison between numerical data at large times and the steady state expression above. Except at the edges, the fitting to the approximate expression is good.

For $\gamma < 1$, we use equations (3.2), (3.10) and (3.3) to get

$$\rho^r(x,t) = \frac{1}{2}\left[1 - \frac{\sin(\gamma\pi)}{\pi}\left\{B\left(\frac{x}{t}; 1-\gamma, \gamma\right) + \frac{x}{\gamma t}\left(\frac{t}{x} - 1\right)^{\gamma}\right\}\right] H(t-x), \tag{3.26}$$

where we have used the result

$$\int y^{-m-1}(1-y)^{m-1}dy = -\frac{(1-y)^m y^{-m}}{m} + c,$$

with $m > 0$ and $0 < y < 1$. In our case, $y \equiv \frac{x}{t}$ and $m \equiv \gamma$. Again, as the LD case above, we do not have a time-independent steady state density but can make an approximation for a given small x at large times:

$$\rho^r(x,t) \approx \frac{1}{2}\left[1 - \frac{\sin\gamma\pi}{\pi(1-\gamma)}\left(\frac{x}{t}\right)^{1-\gamma}\right].$$

Figure 3.3(b) shows the density profile obtained using numerical simulation and using equation (3.26) while the inset shows the same comparison at larger times. We see that our approximation for density as taken in equation (3.10) works well at smaller times but does not fare very well at large times. The power law decay of density towards the value $1/2$, which is a distinguishing character of the density in the MC phase is not captured in our analytic expression and hence at large times it does not work well in the case of $\gamma < 1$, where the average time between resets is unbounded and hence the large time behaviour of power law decay dominates.

3.3.3 HD phase

As described in section (3.2), when the system is in the HD phase with $\beta < \alpha$ and $\beta < 0.5$, we have two possibilities for the dynamics of the TASEP density evolution depending on whether $\alpha < 0.5$ or $\alpha > 0.5$. The front from the input boundary side evolves similar to the LD case when $\alpha < 0.5$ and it is similar to the MC case when $\alpha > 0.5$. After this incoming front hits the exit boundary, another front of density $1-\beta$ starts off in the reverse direction towards the input end. The system, therefore, gets divided into two zones, the zone on the left or input end where the reverse front has not reached, and the zone on the right where the front has reached. When this front reaches all the way to the input boundary, the TASEP achieves a steady state. Therefore, When we calculate the effect of resetting in this phase, we have to distinguish the two possibilities of $\alpha < 0.5$ and $\alpha > 0.5$.

We begin with the case $\alpha < 0.5$. We know that initially a front of density α moves from the input end towards the exit boundary. When $t < \frac{L}{v}$ where $(v = 1-\alpha)$, the front has not reached the exit end and therefore there is nothing to distinguish this system from the LD behaviour. We then get exactly the same result as in equation (3.23) for $\gamma > 1$ and equation (3.24) for $\gamma < 1$. After the forward wave has reached the exit end at time $\frac{L}{v}$, a

reverse wavefront of density $1-\beta$ starts to move towards the entry boundary. We can then use equations (3.2), (3.11) and equation (3.4) for $\gamma > 1$ to obtain the expression for $t > \frac{L}{v}$.

$$\begin{aligned}\rho^r(x,t) &= \frac{\tau_0^{\gamma-1}}{\gamma}(1-\beta-\alpha)\left[\left(\frac{L}{v}+\frac{L-x}{v_r}\right)^{1-\gamma} - t^{1-\gamma}\right] H\left(t-\frac{L}{v}-\frac{L-x}{v_r}\right) \\ &+ \frac{\tau_0^{\gamma-1}}{\gamma}\alpha\left[\left(\frac{x}{v}\right)^{1-\gamma} - t^{1-\gamma}\right] + \frac{\alpha}{\gamma}\left[\gamma - 1 + \left(\frac{t}{\tau_0}\right)^{1-\gamma}\right] H\left(\tau_0 - \frac{x}{v}\right). \quad (3.27)\end{aligned}$$

In the steady state, we have the expression

$$\rho^r_{ss}(x) = \frac{\alpha}{\gamma}\left(\frac{x}{v\tau_0}\right)^{1-\gamma} + \frac{(1-\beta-\alpha)}{\gamma}\left(\frac{L}{v\tau_0}+\frac{L-x}{v_r\tau_0}\right)^{1-\gamma}.$$

We see that decay on both sides of the lattice is governed by the exponent $1-\gamma$. Figure 3.2(c) shows the density profile obtained using numerical simulations compared to the expression in equation (3.27). The matching is very good, except for a small region at the input boundary. Similarly, the matching is good in the inset of this figure which shows a comparison of numerics at large times with the expression for $\rho^r_{ss}(x)$ above.

We now consider the case of $\alpha < 0.5$ and $\gamma < 1$ and use equations (3.2), (3.11) and (3.3) for the calculation. As already mentioned, equation (3.24) gives us the behaviour for times smaller than L/v. For $t > L/v$, we get the expression

$$\begin{aligned}\rho^r(x,t) &= (1-\beta-\alpha)\left[1 - \frac{\sin\pi\gamma}{\pi}B\left(\frac{L}{vt}+\frac{L-x}{v_r t}; 1-\gamma, \gamma\right)\right] H\left(t-\frac{L}{v}-\frac{L-x}{v_r}\right) \\ &+\alpha\left[1 - \frac{\sin\pi\gamma}{\pi}B\left(\frac{x}{vt}; 1-\gamma, \gamma\right)\right], \quad (3.28)\end{aligned}$$

where $v = 1-\alpha$, $v_r = \frac{\alpha(1-\alpha)-\beta(1-\beta)}{1-\alpha-\beta}$. As in the various cases above, there is no steady state, since $\gamma < 1$, but we can see that for a point x at a finite distance from the input end, at $t >> x$, the averaged density is given by

$$\rho^r(x,t) \approx \alpha\left[1 - \frac{\sin\pi\gamma}{\pi(1-\gamma)}\left(\frac{x}{vt}\right)^{1-\gamma}\right] + (1-\beta-\alpha)\left[1 - \frac{\sin\pi\gamma}{\pi(1-\gamma)}\left(\frac{L}{vt}+\frac{L-x}{v_r t}\right)^{1-\gamma}\right].$$

Figure 3.3(c) shows the density profile obtained using numerical simulation compared to the expression in equation (3.28), which captures well the initial decrease and then the subsequent increase in the density due to the returning wavefront. The approximate expression in the $t >> x$ limit is plotted in the inset along with the numerical data and again shows a

good match.

We now consider the case of input rate α being greater than half. As we saw in section 3.2, the density evolution from the input end can be approximated by the function $\frac{1}{2}(1-\frac{x}{t})$. The exit boundary is not reached before the time $t = L$ and therefore for times $t < L$, the expressions will be exactly the same as the MC case and we will get the same expression as in equation (3.25) for $\gamma > 1$ and equation (3.26) for $\gamma < 1$. Once the particles start reaching the boundary at $t = L$, a reverse front of density $1-\beta$ starts in the direction of the input boundary. For $\gamma > 1$, $\alpha > 0.5$, equations (3.2), (3.4) and (3.13) give us the following result for $t > L$

$$\begin{aligned}\rho^r(x,t) &= \frac{\tau_0^{\gamma-1}\gamma-1}{\gamma}\left[\frac{1-\beta-\frac{1}{2}}{\gamma-1}\left(T^{1-\gamma}-t^{1-\gamma}\right)-\frac{x}{2\gamma}\left(t^{-\gamma}-T^{-\gamma}\right)\right]H(t-T)\\ &+\frac{\tau_0^{\gamma-1}\gamma-1}{2\gamma}\left[\frac{1}{\gamma-1}\left(x^{1-\gamma}-t^{1-\gamma}\right)+\frac{x}{\gamma}\left(t^{-\gamma}-x^{-\gamma}\right)\right]\\ &+\frac{1}{2\gamma}\left(1-\frac{x}{\tau_0}\right)\left[\gamma-1+\left(\frac{t}{\tau_0}\right)^{-\gamma+1}\right]H(\tau_0-x), \qquad (3.29)\end{aligned}$$

where T, given by equation (3.22), is the time at which the returning front of density $1-\beta$ reaches the space point x. In the long time, steady state limit, we have the expression

$$\rho^r_{ss}(x) = \frac{1}{2\gamma^2}\left(\frac{x}{\tau_0}\right)^{1-\gamma}+\frac{\gamma-1}{2\gamma^2}\left(\frac{x}{\tau_0}\right)\left(\frac{T}{\tau_0}\right)^{-\gamma}+\frac{1-\beta-\frac{1}{2}}{\gamma}\left(\frac{T}{\tau_0}\right)^{1-\gamma}.$$

Figure 3.2(d) shows the comparison of numerics to the expression in equation (3.29) where the matching is good except for at the entry boundary. Same is the case at large times [inset of figure 3.2(d)] where the numerics match well with the expression for ρ^r_{ss} above. Comparing the various cases for $\gamma > 1$ [figures 3.2(a)-(d)], we see that the mismatch between numerics and analytical expression at the entry end is higher for $\alpha > 0.5$ [figures 3.2(b) and 3.2(d)] than for $\alpha < 0.5$ [figures 3.2(a) and 3.2(b)]. This is because our linear approximation for $\alpha > 0.5$, where the density actually decays as a power law towards the value half does not work as well as the approximation of a constant density wave front for $\alpha < 0.5$, where the actual decay is exponentially fast.

When the power law exponent $\gamma < 1$ and $\alpha > 0.5$, we use equations(3.2), (3.13) and

(3.3) to derive the expression for the averaged density for $t > L$. We obtain

$$\begin{aligned}\rho^r(x,t) &= \frac{1}{2}\left[1 - \frac{\sin\pi\gamma}{\pi}B\left(\frac{x}{t};1-\gamma,\gamma\right) - \frac{\sin\pi\gamma}{\pi\gamma}\frac{x}{t}\left(\frac{t}{x}-1\right)^{\gamma}\right] \\ &+ \left[\left(1-\beta-\frac{1}{2}\right)\left(1 - \frac{\sin\pi\gamma}{\pi}B\left(\frac{T}{t};1-\gamma,\gamma\right)\right)\right. \\ &\left.+\frac{1}{2}\frac{\sin\pi\gamma}{\pi\gamma}\frac{T}{t}\left(\frac{t}{T}-1\right)^{\gamma}\right]H(t-T). \qquad (3.30)\end{aligned}$$

Again, while we do not have a steady state here, we can expand the Beta function in the $\frac{x}{t} << 1$ limit to see the leading behaviour:

$$\rho^r(x,t) \approx \frac{1}{2}\left[1 - \frac{\sin\pi\gamma}{\pi\gamma(1-\gamma)}\left(\frac{x}{t}\right)^{1-\gamma}\right] + (1-\beta-\frac{1}{2})\left[1 - \frac{(1-3\gamma)\sin\pi\gamma}{2\gamma(1-\gamma)\pi}\left(\frac{T}{t}\right)^{1-\gamma}\right].$$

Figure 3.3(d) shows the comparison between the analytic expression (3.30) at small and large (inset) times. In this case the matching is not satisfactory, again because the approximate expression (3.13) does not work well at large times. At larger times, the system settles into a state with a density decaying towards the value half as a power law, unlike our linear approximation.

3.4 Effect of resetting with a constant rate λ

We now consider the case where the time between two resets is given by the exponential distribution $\lambda e^{-\lambda t}$ where λ represents the constant rate of resetting. We are interested in the density averaged over the resetting distribution $\rho^r(x,t)$ which, as mentioned in section 3.1, is given by equation (3.6). As for the power law case above, we begin our discussion with the LD phase, then the MC phase and finally we look at the HD phase, where a returning density front from the exit boundary determines the density on the lattice.

3.4.1 LD phase

In the LD case, where $\alpha < 0.5$ and $\alpha < \beta$, we use equations (3.6) and (3.8) to obtain

$$\begin{aligned}\rho^r(x,t) &= \int_0^t \alpha H\left(\tau - \frac{x}{v}\right)\lambda e^{-\lambda\tau}d\tau + e^{-\lambda t}\alpha H\left(t-\frac{x}{v}\right) \qquad (3.31)\\ &= \alpha e^{-\lambda\frac{x}{v}}H\left(t-\frac{x}{v}\right). \qquad (3.32)\end{aligned}$$

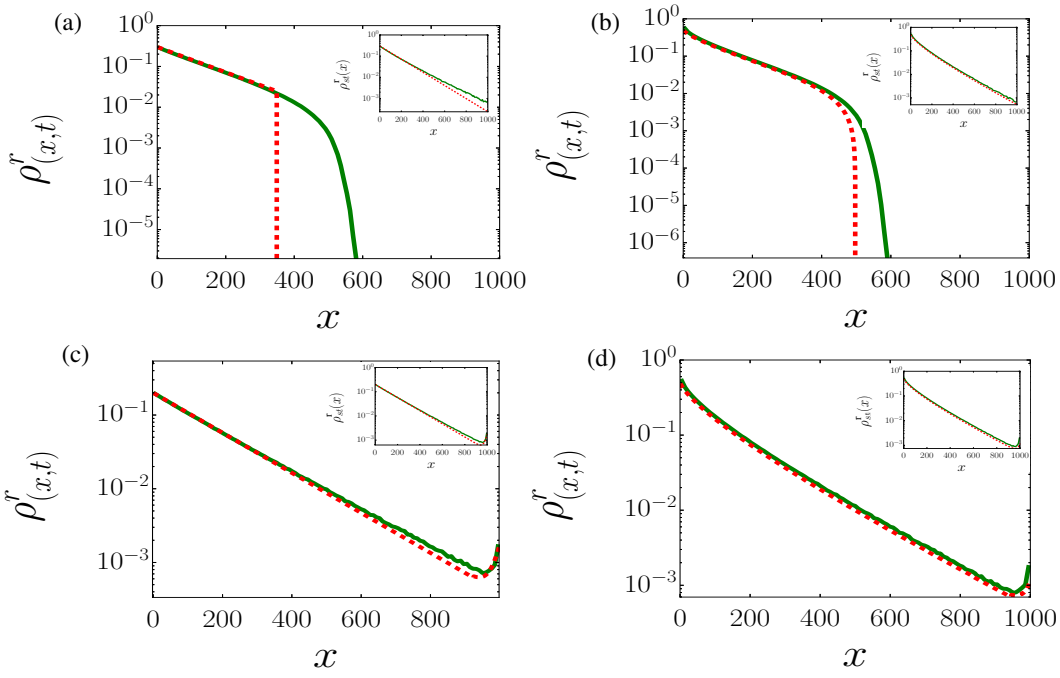

Figure 3.4: Density profile when the time interval between resettings is drawn from an exponential distribution. Here the dotted lines stand for analytical results and the solid lines stand for numerical results. The parameter values are as follows: $\lambda = 0.005$ and Lattice size $L = 1000$ for all figures. (a) $\alpha = 0.3$, $\beta = 0.9, t = 500$ [analytic result from equation (3.32)], in figure (b) $\alpha = 0.8$, $\beta = 0.9, t = 500$ [analytic result from equation (3.34)], in (c) $\alpha = 0.2$, $\beta = 0.1, t = 2000$ [analytic result from equation (3.36)] and in (d) $\alpha = 0.7$, $\beta = 0.1$, $t = 2000$ [analytic result from equation (3.38)]. The inset in each figure contains the density profile for $t = 10000$, with the rest of the parameter values same as the corresponding main figure.

In the limit $t \to \infty$, we have the steady state result $\rho^r_{st}(x) = \alpha e^{-\lambda \frac{x}{v}}$. Figure 3.4(a) shows the numerical simulation result and the analytical expression from equation (3.32). The analytical and numerical results show excellent matching till $t = \frac{x}{v}$, where our approximation has a sharp boundary for the density front, unlike the gradual decay seen in numerics. Density decays exponentially till this point. The same mismatch shows up at large x in the inset of figure 3.4(a), which shows the comparison at large times, between the numerics and the steady state expression above.

3.4.2 MC phase

For the MC case, where $\alpha, \beta > 0.5$, we use equations (3.6) and (3.10) to get

$$\rho^r(x,t) = \int_0^t \left(1 - \frac{x}{\tau}\right) \frac{\lambda e^{-\lambda\tau}}{2} H(\tau - x) d\tau + \frac{e^{-\lambda t}}{2} \left(1 - \frac{x}{t}\right) H(t - x), \tag{3.33}$$

which gives us

$$\rho^r(x,t) = \left[\frac{1}{2}\left(e^{-\lambda x} - \frac{x}{t}e^{-\lambda t}\right) - \frac{x\lambda}{2}\left\{\Gamma(0,\lambda x) - \Gamma(0,\lambda t)\right\}\right] H(t-x), \tag{3.34}$$

where

$$\Gamma(s,x) = \int_x^\infty t^{s-1}e^{-t}dt,$$

is the incomplete gamma function. In the steady state limit $t \to \infty$, we get

$$\rho^r_{st}(x) = \frac{1}{2}\left[e^{-\lambda x} - x\lambda\Gamma(0,\lambda x)\right].$$

Figure 3.4(b) shows the numerical simulation result and the analytical expression from equation (3.34). While the effect of our approximation shows up at large x, the matching with the analytic expression is good in the bulk of the graph. The matching is good also at large times with the steady state expression, as can be seen in the inset of the figure.

3.4.3 HD phase

As before, in the HD case we have two possibilities - $\alpha < 0.5$ or $\alpha > 0.5$. For $\alpha < 0.5$, the system behaves similar to the LD case for times $t < \frac{L}{v}$ and the behaviour will be governed by equation (3.32). For $t > \frac{L}{v}$, we get from equations (3.6) and (3.11):

$$\begin{aligned}\rho^r(x,t) &= \alpha \int_0^t \lambda e^{-\lambda\tau} H\left(\tau - \frac{x}{v}\right) d\tau + (1-\beta-\alpha)\int_0^t \lambda e^{-\lambda\tau} H\left(\tau - \frac{L}{v} - \frac{L-x}{v_r}\right) d\tau \\ &\quad + e^{-\lambda t}\left[\alpha H\left(t - \frac{x}{v}\right) + (1-\beta-\alpha) H\left(\tau - \frac{L}{v} - \frac{L-x}{v_r}\right)\right],\end{aligned} \tag{3.35}$$

which gives us

$$\rho^r(x,t) = \alpha e^{-\lambda\frac{x}{v}} + (1-\beta-\alpha)e^{-\lambda\left(\frac{L}{v} + \frac{L-x}{v_r}\right)} H\left(t - \frac{L}{v} - \frac{L-x}{v_r}\right). \tag{3.36}$$

In the steady state limit $t \to \infty$, we get the expression

$$\rho^r_{st}(x) = \alpha e^{-\frac{\lambda x}{v}} + (1-\beta-\alpha)e^{-\lambda\left(\frac{L}{v}+\frac{L-x}{v_r}\right)}.$$

This expression matches well with the numerical data for large times as seen in the inset of figure 3.4(c). The main figure 3.4(c) compares the expression in equation (3.36) above with the density profile obtained using numerical simulation and captures both the initial decay and the final rise in the density well. The mismatch at large values of x points to the limitation of our approximation, as before.

When $\alpha > 0.5$, for times $t < L$ we see the same behaviour as MC phase, equation (3.34). For $t > L$, from equations (3.6) and (3.13) we have

$$\begin{aligned}\rho^r(x,t) &= \frac{1}{2}\int_0^t \left(1-\frac{x}{\tau}\right) H(\tau-x)\lambda e^{-\lambda\tau}d\tau + \left(1-\beta-\frac{1}{2}\right)\int_0^t H(\tau-T)\lambda e^{-\lambda\tau}d\tau \\ &\quad + \frac{x}{2}\int_0^t \frac{\lambda}{\tau}H(\tau-T)e^{-\lambda\tau}d\tau, \end{aligned} \tag{3.37}$$

which gives us

$$\begin{aligned}\rho^r(x,t) &= \left[\left(1-\beta-\frac{1}{2}\right)e^{-\lambda T} + \frac{x}{2t}e^{-\lambda t} + \frac{\lambda x}{2}\left(\Gamma(0,\lambda T)-\Gamma\left(0,\lambda t\right)\right)\right] H(t-T) \\ &\quad + \frac{1}{2}\left[e^{-\lambda x} - e^{-\lambda t}\frac{x}{t} - \lambda x\Gamma(0,\lambda x) - \Gamma(0,\lambda t)\right], \end{aligned} \tag{3.38}$$

and in the steady state, we have

$$\rho^r_{st}(x) \approx \frac{1}{2}\left[e^{-\lambda x} - \lambda x\left(\Gamma(0,\lambda x)-\Gamma\left(0,\lambda T\right)\right] + \left(1-\beta-\frac{1}{2}\right)e^{-\lambda T}.$$

Figure 3.4(d) shows the density profile obtained using numerical simulation, as well as from the expression in equation (3.38) above. The inset shows data at large times compared to ρ^r_{ss} above and we see a very good agreement.

To summarise, in this chapter we have studied the effect of sudden, random resets to the empty lattice state on the TASEP with open boundaries. We have considered two possibilities for the probability distribution of the inter-reset time: power law and exponential. We derive expressions for the time evolution of particle density, averaged over resetting, for all three phases of the TASEP. We compare these analytic calculations with results from numerical simulations. The system is seen to always achieve a steady state for the exponential distribution of inter-resets times, while in the power law case, the exponent γ

determines whether or not the system achieves a steady state at large times. The behaviour in the HD phase is found to be interesting for both distributions, with the reset-averaged density showing peaks at both the entry and the exit ends.

Chapter 4

Conclusion

In this thesis, we have described our work on the effects of two different kinds of dynamical features - non-local hopping and resetting - on steady states in nonequilibrium systems. The underlying model which we have used to understand these effects is the well known TASEP. The effect of nonlocal hops was studied in the presence of open boundaries and in a system with periodic boundaries and defects. The effect of resetting to the initial, empty state was studied on the TASEP with open boundaries for all the three possible phases. The summary of these studies is given below.

4.1 Effect of nonlocal hopping

We have studied the various possibilities arising in a system where particles are allowed to make long hops in addition to local dynamics of the usual TASEP. The long or non-local hops allow the particle to move all the way to the next unoccupied site before an occupied site. The basic version of this model was studied earlier [71] and the appearance of a new possible phase - the ER phase was reported.

4.1.1 Effects of boundaries

We have done a complete analysis of this model in the presence of open boundaries and identified the phases numerically as well as through approximate mean field theory. The three parameters governing the system behaviour are the input rate α, exit rate β and the rate of nonlocal hopping p. We determine the full phase diagram numerically as well as using mean field theory and see four phases, the usual LD, HD and MC phases, as well as a phase where the bulk is empty - the ER phase.

We see an interesting variation in the phase diagram as p is changed. We find that the

two dominant phases of the system are the HD phase, where the congestion at the output boundary controls the density in the bulk, and the ER phase, where the large jumps clear the lattice quickly, leading to zero bulk density. As the rate p of nonlocal hopping is increased, the volume of the phase space occupied by these phases grows at the cost of the other two - the LD and the MC phases. Interestingly, numerics show that both these phases suddenly disappear at the value $p \approx 0.3$. Thus for $p > 0.3$, the system has only two possible steady states; it is either empty in the bulk (ER phase) due to the particles leaving the lattice via long hops soon after entry, or the exit boundary jams the system leading to a high density (HD phase).

Our mean field analysis though good at predicting the results qualitatively and at some places quantitatively, does not work very well at determining the bulk density accurately in the LD and MC phases, as also the boundaries between these two phases. Mean field arguments predict that the LD and MC phases disappear at different values of p but numerics suggest that they move out simultaneously. It may be noted that the input boundary is extremely important in this region of the phase diagram and the long-range hops lead to a quick decay of density as we move away from the input. The correlations brought in by these long hops are then important and neglecting them, as a mean field approach does, lead to inaccuracies.

4.1.2 Effects of impurity

In the next part of this work, we explored the effect of static and dynamic impurity on our system. Here we work with periodic boundary conditions so that the only effects observed are due to a combination of the long hops and the impurity dynamics.

We began with studying the effect of a single slow particle which can only perform local hops to the nearest site at a rate μ. In the usual TASEP dynamics without the long hops, it is seen that depending on the average density and μ, the system can exist in two phases: a homogeneous density phase - where the effect of the slow particle is local, and a shock phase - in which a macroscopic region of low density forms in front of the slow particle. The transition between the two phases across the line $\mu = 1 - \rho$ can be understood in terms of the speed of the particles. At high densities, it is the density that controls the average speed of the particles while at lower densities, the speed pf the slower particle restricts the motion and causes the formation of a shock front.

The long hop dynamics introduced via the parameter p is expected to enhance the clustering tendency since the particles just in front of the slow particle, can move away more

quickly. This is indeed seen in our simulations and we show that unlike for the regular TASEP, where both the shock phase and the homogeneous phase exist for every given density, the introduction of long hops leads to the clustered phase being the only possible phase at low densities for any finite value of p. We map out the phase diagram for the system as a function of μ, p and density. Our mean field approach, based on the velocity argument outlined above gives a good match to the numerical predictions.

Our model with a slow particle maps exactly to the CDA model [128] with a slow site. Our calculation for the transition to a shock phase directly translates to the criterion for the formation of an infinite mass aggregate in the CDA model. Our study thus sheds light on the effect of static impurity in such diffusion-aggregation systems - a problem that has not been studied previously.

The final part of the work focuses on the effect of a static impurity. We consider a slow site in a periodic lattice whose effect is to reduce the departure rate by a factor $r < 1$. The problem of such a slow site on a lattice with the usual TASEP dynamics has generated much interest due to the conflicting claims on the existence of a phase transition between a homogeneous phase and a shock phase. It has now been established that the system exists only in a shock phase for all values of $r < 1$.

Our study shows that the introduction of a nonlocal hop leads to a more interesting phase structure than the usual TASEP. As expected, we find that the density profile shows a shock structure with a low density in front of the slow site and a high density behind it. Interestingly, as we increase p for a given r (or decrease r for a given p), the density in front of the slow site decreases until it becomes zero and then continues to be zero for all higher values of p. The low density side of the shock structure thus characterises a continuous phase transition from an HD-LD phase to an HD-ER phase. Our simple mean field argument captures this transition. We see that the mean field prediction for the phase diagram agrees with our numerics.

To summarise, we have studied various aspects of a one-dimensional lattice model of particles that interact via hard-core interactions and that can make long-range hops in addition to the usual local, widely studied, nearest neighbour moves. We mapped the complete phase diagram of this system for open boundary conditions. We also studied the effect of static and dynamic impurity on this system and saw that nonlocal hopping leads to interesting new features. The periodic boundary versions of this model can be mapped to a CDA model with asymmetric dynamics and our study with a slow particle therefore also describes a phase transition in the CDA model. Apart from numerical work, we set up simple mean field arguments which correctly capture the phase structure of the systems

under study qualitatively, but not always quantitatively. We ascribe this mismatch to the correlations induced in the system because of long-range hopping dynamics. We would like to study the nature of correlations further in future work. Another problem that can be explored is the effect of non-local hops in a symmetric exclusion process with open boundaries and asymmetric boundary conditions.

4.2 Stochastic resetting in TASEP

We have explored the effects of stochastic resetting to an initial, empty state on the TASEP which is a model of much theoretical interest as well as applicability in varied systems. A previous study modelled the effect of degradation of mRNA on protein production using the exponential distribution of inter-reset times in the time-independent steady state limit [98]. In this study, we have considered two possible distributions of times between successive resets - power law with exponent γ and exponential distribution governed by the parameter λ and we report the full time-dependent distribution of reset-averaged density. Given the importance of TASEP as a paradigm in non-equilibrium systems, our work here may prove to be of wider interest.

Using approximate expressions for the evolution of density on a TASEP with open boundaries, we have been able to calculate the reset-averaged density distributions in the three possible phases of the original system. We compare these analytic results with our numerical results from Monte Carlo simulations on the lattice model and see that the two match well.

In the case of resetting with a power law distribution, one sees a sudden change in behaviour when γ crosses one. When γ is less than one, we see that the expression for density depends on the ratio x/t and therefore does not have a steady state limit. This can be explained from the fact that for $\gamma < 1$, the inter-reset distribution will have a diverging value of the mean while for $\gamma > 1$, the same distribution has a finite mean. Thus for $\gamma > 1$, we see a time-independent distribution as $t \to \infty$. The TASEP with open boundaries has three possible steady states, depending on the boundary conditions. In the presence of resetting, the three phases show distinct behaviour, as expected, but the resetting distribution also imposes some common features on the average density. We see that for $\gamma > 1$, the leading behaviour of density at large times, for both the LD and MC phases is a power law decay with the exponent $1 - \gamma$.

The behaviour becomes more interesting in the HD case. While there is nothing to differentiate the system from an LD or MC phase before particles start experiencing the

output boundary, once the particles experience the jamming effect due to low output rates, we see that a reverse front of higher density starts from the exit side towards the entry end. The interplay of the incoming and backward moving fronts with the resetting dynamics leads to the density showing two maxima, on either end of the lattice. The decay on both the sides is again a power law with $\gamma - 1$ being the exponent. When $\gamma < 1$, we see that the density is a function of x/t and there is no long time steady state behaviour. The leading behaviour at small x/t is of the form $a - b(\frac{x}{t})^{1-\gamma}$ in the LD and MC phases, while it is more complex in the HD case - with two maxima again at the input and output ends.

The results for the exponential distribution of inter-reset times are simpler and the system always has a well defined steady state limit. In the steady state, one sees an exponential decay of the reset-averaged density along the length of the lattice in the LD phase. The exponential decay, albeit with a different length scale is again the behaviour at large distances for the MC phase. In the HD phase, similar to the behaviour for the power law resetting described above, one sees two maxima at the input and exit boundaries with a minimum in between. The change in density along either boundary is exponential again.

While we have summarised the broad features of density as seen in TASEP with open boundaries in the presence of resets, it is the detailed expressions that may be of interest when applied to a particular system of interest. Our study is the first one involving the effect of resets on a system undergoing boundary driven phase transitions. We see that while there is some similarity in the behaviour of density across phases due to the resetting dynamics, the phase boundaries are still critical and can lead to surprising steady state features like two density maxima at either end of the lattice in the HD phase.

We expect that problems related to the effect of sudden, large changes in the dynamics of nonequilibrium systems with coupled degrees of freedom will be explored further as their applicability to more real life systems emerge. Our study on TASEP - which is a cornerstone of the nonequilibrium model systems - is an important initial step in this direction. A particular system where we would like to look at the effects of resetting is the study of particles driven by KPZ and EW surfaces [158, 159], where the usual steady state shows a strong clustering of the particles as they settle closer to the "valleys" of the surface. A sudden return to a homogeneous initial condition may lead to the formation of multiple smaller clusters that break and re-form repeatedly.

Bibliography

[1] B. Baretzky, M. Baró, G. Grabovetskaya, J. Gubicza, M. Ivanov, Y. Kolobov, T. Langdon, J. Lendvai, A. Lipnitskii, A. Mazilkin, A. Nazarov, J. Nogués, I. Ovidko, S. Protasova, G. Raab, Á. Révész, N. Skiba, J. Sort, M. Starink, B. Straumal, S. Suriñach, T. Ungár, and A. Zhilyaev, "Fundamentals of interface phenomena in advanced bulk nanoscale materials," *Reviews on Advanced Materials Science*, vol. 9, pp. 45–108, apr 2005.

[2] V. S. Khrapai, S. Ludwig, J. P. Kotthaus, H. P. Tranitz, and W. Wegscheider, "Nonequilibrium phenomena in adjacent electrically isolated nanostructures," *Physica E Low-Dimensional Systems and Nanostructures*, vol. 40, no. 5, pp. 995–998, Mar. 2008.

[3] E. B. Davies, "Markovian master equations," *Communications in Mathematical Physics*, vol. 39, no. 2, pp. 91–110, Jun 1974.

[4] R. Zwanzig, *Nonequilibrium statistical mechanics*. Oxford University Press, 2001.

[5] M. Levy, "Universal variational functionals of electron densities, first-order density matrices, and natural spin-orbitals and solution of the v-representability problem," *Proceedings of the National Academy of Sciences*, vol. 76, no. 12, pp. 6062–6065, 1979.

[6] D. C. Mattis, *Statistical Mechanics Made Simple*. World Scientific, 2003.

[7] C. P. Royall, J. Dzubiella, M. Schmidt, and A. van Blaaderen, "Nonequilibrium sedimentation of colloids on the particle scale," *Physical Review Letters*, vol. 98, p. 188304, May 2007.

[8] M. Schmidt, C. P. Royall, A. van Blaaderen, and J. Dzubiella, "Non-equilibrium sedimentation of colloids: confocal microscopy and brownian dynamics simulations," *Journal of Physics: Condensed Matter*, vol. 20, no. 49, p. 494222, nov 2008.

[9] L. Giomi, M. C. Marchetti, and T. B. Liverpool, "Complex spontaneous flows and concentration banding in active polar films," *Physical Review Letters*, vol. 101, p. 198101, Nov 2008.

[10] A. Ahmadi, T. B. Liverpool, and M. C. Marchetti, "Nematic and polar order in active filament solutions," *Physical Review E*, vol. 72, p. 060901, Dec 2005.

[11] J. Keizer, *Statistical thermodynamics of nonequilibrium processes*. Springer Science & Business Media, 2012.

[12] S. Dodelson and M. S. Turner, "Nonequilibrium neutrino statistical mechanics in the expanding universe," *Physical Review D*, vol. 46, pp. 3372–3387, Oct 1992.

[13] D. Chowdhury, A. Schadschneider, and K. Nishinari, "Physics of transport and traffic phenomena in biology: from molecular motors and cells to organisms," *Physics of Life Reviews*, vol. 2, no. 4, pp. 318 – 352, 2005.

[14] A. Awazu, "Complex transport phenomena in a simple lattice gas system," *Physica A: Statistical Mechanics and its Applications*, vol. 373, pp. 425 – 432, 2007.

[15] M. C. Cross and P. C. Hohenberg, "Pattern formation outside of equilibrium," *Review of Moden Physics*, vol. 65, pp. 851–1112, Jul 1993.

[16] T. N. Palmer, "Predicting uncertainty in forecasts of weather and climate," *Reports on Progress in Physics*, vol. 63, no. 2, pp. 71–116, jan 2000.

[17] H. Hinrichsen, "Non-equilibrium critical phenomena and phase transitions into absorbing states," *Advances in Physics*, vol. 49, no. 7, pp. 815–958, 2000.

[18] P. Bak, K. Chen, and C. Tang, "A forest-fire model and some thoughts on turbulence," *Physics Letters A*, vol. 147, no. 5, pp. 297 – 300, 1990.

[19] D. Chowdhury, A. Schadschneider, and K. Nishinari, "Traffic phenomena in biology: From molecular motors to organisms," in *Traffic and Granular Flow'05*, A. Schadschneider, T. Pöschel, R. Kühne, M. Schreckenberg, and D. E. Wolf, Eds. Berlin, Heidelberg: Springer Berlin Heidelberg, 2007, pp. 223–238.

[20] M. Plischke and B. Bergersen, *Equilibrium Statistical Physics*, 3rd ed. World scientific, 2006.

[21] A. Chatterjee, B. K. Chakrabarti, and R. B. Stinchcombe, "Master equation for a kinetic model of a trading market and its analytic solution," *Physical Review E*, vol. 72, p. 026126, Aug 2005.

[22] D. S. Fisher, K. Dahmen, S. Ramanathan, and Y. Ben-Zion, "Statistics of earthquakes in simple models of heterogeneous faults," *Physical Review Letters*, vol. 78, pp. 4885–4888, Jun 1997.

[23] D. S. Fisher, "Collective transport in random media: from superconductors to earthquakes," *Physics Reports*, vol. 301, no. 1, pp. 113 – 150, 1998.

[24] N. G. Van Kampen, *Stochastic processes in physics and chemistry*. Elsevier, 1992, vol. 1.

[25] B. Schmittmann and R. Zia, "Statistical mechanics of driven diffusive systems," in *Statistical Mechanics of Driven Diffusive System*, ser. Phase Transitions and Critical Phenomena, B. Schmittmann and R. Zia, Eds. Academic Press, 1995, vol. 17, pp. 3 – 214.

[26] J. L. Lebowitz and E. W. Montroll, "Nonequilibrium phenomena. ii - from stochastics to hydrodynamics." Elsevier Science Pub. Co., 1984.

[27] H. Risken, *Fokker-planck equation*. Springer, 1996, vol. 18.

[28] W. Coffey and Y. Kalmykov, *The Langevin Equation: With Applications to Stochastic Problems in Physics, Chemistry and Electrical Engineering, 3rd Edition*, 09 2012.

[29] V. Vliet and M. Carolyn, "Equilibrium and non-equilibrium statistical mechanics." World scientific, 2008.

[30] J. Krug, "Boundary-induced phase transitions in driven diffusive systems," *Physical Review Letters*, vol. 67, pp. 1882–1885, Sep 1991.

[31] M. R. Evans, Y. Kafri, H. M. Koduvely, and D. Mukamel, "Phase separation in one-dimensional driven diffusive systems," *Physical Review Letters*, vol. 80, pp. 425–429, Jan 1998.

[32] T. Chou, K. Mallick, and R. K. P. Zia, "Non-equilibrium statistical mechanics: from a paradigmatic model to biological transport," *Reports on Progress in Physics*, vol. 74, no. 11, p. 116601, oct 2011.

[33] T. Chou and G. Lakatos, "Clustered bottlenecks in mrna translation and protein synthesis," *Physical Review Letters*, vol. 93, p. 198101, Nov 2004.

[34] C. Appert-Rolland, M. Ebbinghaus, and L. Santen, "Intracellular transport driven by cytoskeletal motors: General mechanisms and defects," *Physics Reports*, vol. 593, pp. 1 – 59, 2015, intracellular transport driven by cytoskeletal motors: General mechanisms and defects.

[35] H. J. Hilhorst and C. Appert-Rolland, "A multi-lane TASEP model for crossing pedestrian traffic flows," *Journal of Statistical Mechanics: Theory and Experiment*, vol. 2012, no. 06, p. P06009, jun 2012.

[36] J. Cividini and C. Appert-Rolland, "Wake-mediated interaction between driven particles crossing a perpendicular flow," *Journal of Statistical Mechanics: Theory and Experiment*, vol. 2013, no. 07, p. P07015, jul 2013.

[37] R. Lipowsky, S. Klumpp, and T. M. Nieuwenhuizen, "Random walks of cytoskeletal motors in open and closed compartments," *Physical Review Letters*, vol. 87, p. 108101, Aug 2001.

[38] S. Katz, J. L. Lebowitz, and H. Spohn, "Phase transitions in stationary nonequilibrium states of model lattice systems," *Physical Review B*, vol. 28, pp. 1655–1658, Aug 1983.

[39] W. Dieterich, P. Fulde, and I. Peschel, "Theoretical models for superionic conductors," *Advances in Physics*, vol. 29, no. 3, pp. 527–605, 1980.

[40] C. T. MacDonald, J. H. Gibbs, and A. C. Pipkin, "Kinetics of biopolymerization on nucleic acid templates," *Biopolymers*, vol. 6, no. 1, pp. 1–25, 1968.

[41] F. Spitzer, "Interaction of markov processes," *Advances in Mathematics*, vol. 5, no. 2, pp. 246 – 290, 1970.

[42] T. M. Liggett, *Interacting particle systems*. Springer Science & Business Media, 2012, vol. 276.

[43] A. Lemouari and M. Benmohamed, "Trace emergence of ants' traffic flow, based upon exclusion process," *International Journal of Mathematical and Computational Sciences*, vol. 2, no. 7, pp. 507 – 513, 2008.

[44] A. John, A. Schadschneider, D. Chowdhury, and K. Nishinari, "Trafficlike collective movement of ants on trails: Absence of a jammed phase," *Physical Review Letters*, vol. 102, p. 108001, Mar 2009.

[45] A. Schadschneider, "Statistical physics of traffic flow," *Physica A: Statistical Mechanics and its Applications*, vol. 285, no. 1, pp. 101 – 120, 2000.

[46] B. Derrida, E. Domany, and D. Mukamel, "An exact solution of a one-dimensional asymmetric exclusion model with open boundaries," *Journal of Statistical Physics*, vol. 69, no. 3-4, pp. 667–687, 1992.

[47] G. Schütz and E. Domany, "Phase transitions in an exactly soluble one-dimensional exclusion process," *Journal of statistical physics*, vol. 72, no. 1, pp. 277–296, 1993.

[48] B. Derrida and M. Evans, "Exact correlation functions in an asymmetric exclusion model with open boundaries," *Journal de Physique I*, vol. 3, no. 2, pp. 311–322, 1993.

[49] B. Derrida, M. R. Evans, V. Hakim, and V. Pasquier, "Exact solution of a 1d asymmetric exclusion model using a matrix formulation," *Journal of Physics A: Mathematical and General*, vol. 26, no. 7, p. 1493, 1993.

[50] B. Derrida, S. A. Janowsky, J. L. Lebowitz, and E. R. Speer, "Exact solution of the totally asymmetric simple exclusion process: shock profiles," *Journal of statistical physics*, vol. 73, no. 5-6, pp. 813–842, 1993.

[51] B. Derrida and M. Evans, "Bethe ansatz solution for a defect particle in the asymmetric exclusion process," *Journal of Physics A: Mathematical and General*, vol. 32, no. 26, p. 4833, 1999.

[52] S. Klumpp and R. Lipowsky, "Traffic of molecular motors through tube-like compartments," *Journal of Statistical Physics*, vol. 113, pp. 233–268, 01 2003.

[53] J. M. J. van Leeuwen * and A. DrzewiÅĎski, "Boundary effects for weakly driven polymers," *Molecular Physics*, vol. 103, no. 21-23, pp. 3091–3102, 2005.

[54] S. H. Jacobson, M. A. Ratner, and A. Nitzan, "Motion mechanisms in framework solid electrolytes: Correlated hopping and liquidlike diffusion," *The Journal of Chemical Physics*, vol. 78, no. 6, pp. 4154–4161, 1983.

[55] A. Hernández-Machado, H. Guo, J. L. Mozos, and D. Jasnow, "Interfacial growth in driven diffusive systems," *Physical Review A*, vol. 39, pp. 4783–4788, May 1989.

[56] A. I. Curatolo, M. R. Evans, Y. Kafri, and J. Tailleur, "Multilane driven diffusive systems," *Journal of Physics A: Mathematical and Theoretical*, vol. 49, no. 9, p. 095601, jan 2016.

[57] R. A. Blythe and M. R. Evans, "Nonequilibrium steady states of matrix-product form: a solver's guide," *Journal of Physics A: Mathematical and Theoretical*, vol. 40, no. 46, pp. R333–R441, oct 2007.

[58] D. Dhar, "An exactly solved model for interfacial growth," in *Phase transitions*, vol. 9, no. 1. Gordon Breach Sci publ ltd, 1987, pp. 51–51.

[59] P. Meakin, P. Ramanlal, L. M. Sander, and R. C. Ball, "Ballistic deposition on surfaces," *Physical Review A*, vol. 34, pp. 5091–5103, Dec 1986.

[60] N. Rajewsky, L. Santen, A. Schadschneider, and M. Schreckenberg, "The asymmetric exclusion process: Comparison of update procedures," *Journal of Statistical Physics*, vol. 92, pp. 151–194, 1997.

[61] S. A. Janowsky and J. L. Lebowitz, "Exact results for the asymmetric simple exclusion process with a blockage," *Journal of statistical physics*, vol. 77, no. 1-2, pp. 35–51, 1994.

[62] K. Mallick, S. Mallick, and N. Rajewsky, "Exact solution of an exclusion process with three classes of particles and vacancies," *Journal of Physics A: Mathematical and General*, vol. 32, no. 48, p. 8399, 1999.

[63] K. Mallick, "Shocks in the asymmetry exclusion model with an impurity," *Journal of Physics A: Mathematical and General*, vol. 29, no. 17, p. 5375, 1996.

[64] A. Parmeggiani, T. Franosch, and E. Frey, "Totally asymmetric simple exclusion process with langmuir kinetics," *Physical Review E*, vol. 70, p. 046101, Oct 2004.

[65] L. J. Cook, J. J. Dong, and A. LaFleur, "Interplay between finite resources and a local defect in an asymmetric simple exclusion process," *Physical Review E*, vol. 88, p. 042127, Oct 2013.

[66] K. Nagel and M. Schreckenberg, "A cellular automaton model for freeway traffic," *Journal de physique I*, vol. 2, no. 12, pp. 2221–2229, 1992.

[67] L. B. Shaw, R. Zia, and K. H. Lee, "Totally asymmetric exclusion process with extended objects: a model for protein synthesis," *Physical Review E*, vol. 68, no. 2, p. 021910, 2003.

[68] G. Tripathy and M. Barma, "Driven lattice gases with quenched disorder: Exact results and different macroscopic regimes," *Physical Review E*, vol. 58, pp. 1911–1926, Aug 1998.

[69] M. Ha, J. Timonen, and M. den Nijs, "Queuing transitions in the asymmetric simple exclusion process," *Physical Review E*, vol. 68, p. 056122, 2003.

[70] A. Valleriani, Z. Ignatova, A. Nagar, and R. Lipowsky, "Turnover of messenger rna: Polysome statistics beyond the steady state," *Europhysics Letters*, vol. 89, no. 5, p. 58003, 2010.

[71] M. Ha, H. Park, and M. den Nijs, "Dynamic instability transitions in one-dimensional driven diffusive flow with nonlocal hopping," *Physical Review E*, vol. 75, no. 6, p. 061131, 2007.

[72] F. Soriguera, I. Martinez, M. Sala, and M. Menendez, "Effects of low speed limits on freeway traffic flow," *Transportation Research Part C: Emerging Technologies*, vol. 77, pp. 257–274, 04 2017.

[73] D. Akin, V. P. Sisiopiku, and A. Skabardonis, "Impacts of weather on traffic flow characteristics of urban freeways in istanbul," *Procedia - Social and Behavioral Sciences*, vol. 16, pp. 89 – 99, 2011, 6th International Symposium on Highway Capacity and Quality of Service.

[74] D. E. Wolf, M. Schreckenberg, and A. Bachem, *Traffic and Granular Flow*. World Scientific, pp. 1–394.

[75] W.-M. Lu, K.-L. Tung, C.-H. Pan, and K.-J. Hwang, "The effect of particle sedimentation on gravity filtration," *Separation Science and Technology*, vol. 33, no. 12, pp. 1723–1746, 1998.

[76] E. Spruijt and P. M. Biesheuvel, "Sedimentation dynamics and equilibrium profiles in multicomponent mixtures of colloidal particles," *Journal of Physics: Condensed Matter*, vol. 26, no. 7, p. 075101, jan 2014.

[77] M. E. Fisher and A. B. Kolomeisky, "Molecular motors and the forces they exert," *Physica A: Statistical Mechanics and its Applications*, vol. 274, no. 1, pp. 241 – 266, 1999.

[78] S. E. Paulin and B. J. Ackerson, "Observation of a phase transition in the sedimentation velocity of hard spheres," *Physical Review Letters*, vol. 64, pp. 2663–2666, May 1990.

[79] J. Szavits-Nossan and K. Uzelac, "Totally asymmetric exclusion process with long-range hopping," *Physical Review E*, vol. 74, p. 051104, Nov 2006.

[80] J. Szavits Nossan and K. Uzelac, "Scaling properties of the asymmetric exclusion process with long-range hopping," *Physical Review E*, vol. 77, p. 051116, May 2008.

[81] G. M. Cooper and D. Ganem, "The cell: a molecular approach," *Nature Medicine*, vol. 3, no. 9, pp. 1042–1042, 1997.

[82] J. Szavits-Nossan and K. Uzelac, "Impurity-induced shocks in the asymmetric exclusion process with long-range hopping," *Journal of Statistical Mechanics: Theory and Experiment*, vol. 2009, no. 12, p. P12019, dec 2009.

[83] ——, "Absence of phase coexistence in disordered exclusion processes with bypassing," *Journal of Statistical Mechanics Theory and Experiment*, p. P05030, 05 2011.

[84] J. Otwinowski and S. Boettcher, "A totally asymmetric exclusion process with hierarchical long range connections," *Journal of Statistical Mechanics: Theory and Experiment*, vol. 2009, no. 07, p. P07010, 2009.

[85] A. Nagar, M. Ha, and H. Park, "Boundary-induced abrupt transition in the symmetric exclusion process," *Physical Review E*, vol. 77, no. 6, p. 061118, 2008.

[86] M. R. Evans and T. Hanney, "Nonequilibrium statistical mechanics of the zero-range process and related models," *Journal of Physics A: Mathematical and General*, vol. 38, no. 19, pp. R195–R240, apr 2005.

[87] A. Nagar, "Condensation transition in a model with attractive particles and non-local hops," *Journal of Statistical Mechanics: Theory and Experiment*, vol. 2009, no. 10, p. P10003, 2009.

[88] M. Ha and M. den Nijs, "Macroscopic car condensation in a parking garage," *Physical Review E*, vol. 66, no. 3, p. 036118, 2002.

[89] M. Ha, "Instability transitions and ensemble equivalence in diffusive flow," *Central European Journal of Physics*, vol. 7, no. 3, pp. 575–583, 2009.

[90] M. R. Evans, S. N. Majumdar, and G. Schehr, "Stochastic resetting and applications," *Journal of Physics A: Mathematical and Theoretical*, vol. 53, no. 19, p. 193001, apr 2020.

[91] A. Montanari and R. Zecchina, "Optimizing searches via rare events," *Physical Review Letters*, vol. 88, p. 178701, Apr 2002.

[92] F. Bartumeus and J. Catalan, "Optimal search behavior and classic foraging theory," *Journal of Physics A: Mathematical and Theoretical*, vol. 42, no. 43, p. 434002, oct 2009.

[93] M. E. Cates, "Diffusive transport without detailed balance in motile bacteria: does microbiology need statistical physics?" *Reports on Progress in Physics*, vol. 75, no. 4, p. 042601, mar 2012.

[94] M. Sedaghatmehr, V. P. Thirumalaikumar, I. Kamranfar, A. Marmagne, C. Masclaux-Daubresse, and S. Balazadeh, "A regulatory role of autophagy for resetting the memory of heat stress in plants," *Plant, Cell & Environment*, vol. 42, no. 3, pp. 1054–1064, 2019.

[95] S. C. Manrubia and D. H. Zanette, "Stochastic multiplicative processes with reset events," *Physical Review E*, vol. 59, no. 5, p. 4945, 1999.

[96] G. Oshanin, K. Lindenberg, H. S. Wio, and S. Burlatsky, "Efficient search by optimized intermittent random walks," *Journal of Physics A: Mathematical and Theoretical*, vol. 42, no. 43, p. 434008, oct 2009.

[97] E. Roldán, A. Lisica, D. Sánchez-Taltavull, and S. W. Grill, "Stochastic resetting in backtrack recovery by rna polymerases," *Physical Review E*, vol. 93, p. 062411, Jun 2016.

[98] A. Nagar, A. Valleriani, and R. Lipowsky, "Translation by ribosomes with mrna degradation: Exclusion processes on aging tracks," *Journal of Statistical Physics*, vol. 145, no. 5, pp. 1385–1404, 2011.

[99] P. Visco, R. J. Allen, S. N. Majumdar, and M. R. Evans, "Switching and growth for microbial populations in catastrophic responsive environments." *Biophysical journal*, vol. 98 7, pp. 1099–108, 2010.

[100] J. Tailleur and M. E. Cates, "Statistical mechanics of interacting run-and-tumble bacteria," *Physical Review Letters*, vol. 100, p. 218103, May 2008.

[101] B. Mukherjee, K. Sengupta, and S. N. Majumdar, "Quantum dynamics with stochastic reset," *Physical Review B*, vol. 98, p. 104309, Sep 2018.

[102] M. R. Evans and S. N. Majumdar, "Diffusion with stochastic resetting," *Physical Review Letters*, vol. 106, p. 160601, Apr 2011.

[103] ——, "Diffusion with resetting in arbitrary spatial dimension," *Journal of Physics A: Mathematical and Theoretical*, vol. 47, no. 28, p. 285001, jun 2014.

[104] ——, "Diffusion with optimal resetting," *Journal of Physics A: Mathematical and Theoretical*, vol. 44, no. 43, p. 435001, 2011.

[105] D. Boyer, M. R. Evans, and S. N. Majumdar, "Long time scaling behaviour for diffusion with resetting and memory," *Journal of Statistical Mechanics: Theory and Experiment*, vol. 2017, no. 2, p. 023208, 2017.

[106] J. Whitehouse, M. R. Evans, and S. N. Majumdar, "Effect of partial absorption on diffusion with resetting," *Physical Review E*, vol. 87, p. 022118, Feb 2013.

[107] S. N. Majumdar, S. Sabhapandit, and G. Schehr, "Random walk with random resetting to the maximum position," *Physical Review E*, vol. 92, p. 052126, Nov 2015.

[108] A. Pal, A. Kundu, and M. R. Evans, "Diffusion under time-dependent resetting," *Journal of Physics A: Mathematical and Theoretical*, vol. 49, no. 22, p. 225001, 2016.

[109] C. Christou and A. Schadschneider, "Diffusion with resetting in bounded domains," *Journal of Physics A: Mathematical and Theoretical*, vol. 48, no. 28, p. 285003, 2015.

[110] A. Pal, R. Chatterjee, S. Reuveni, and A. Kundu, "Local time of diffusion with stochastic resetting," *Journal of Physics A: Mathematical and Theoretical*, vol. 52, no. 26, p. 264002, jun 2019.

[111] L. Kusmierz, S. N. Majumdar, S. Sabhapandit, and G. Schehr, "First order transition for the optimal search time of lévy flights with resetting," *Physical Review Letters*, vol. 113, p. 220602, Nov 2014.

[112] M. Montero and J. Villarroel, "Monotonic continuous-time random walks with drift and stochastic reset events," *Physical Review E*, vol. 87, p. 012116, Jan 2013.

[113] A. Pal, L. Kusmierz, and S. Reuveni, "Home-range search provides advantage under high uncertainty," *arXiv: Statistical Mechanics*, 2019.

[114] T. T. da Silva and M. D. Fragoso, "The interplay between population genetics and diffusion with stochastic resetting," *Journal of Physics A: Mathematical and Theoretical*, vol. 51, no. 50, p. 505002, nov 2018.

[115] I. Eliazar, "Branching search," *Europhysics Letters*, vol. 120, no. 6, p. 60008, dec 2017.

[116] A. S. Bodrova, A. V. Chechkin, and I. M. Sokolov, "Nonrenewal resetting of scaled brownian motion," *Physical Review E*, vol. 100, p. 012119, Jul 2019.

[117] D. C. Rose, H. Touchette, I. Lesanovsky, and J. P. Garrahan, "Spectral properties of simple classical and quantum reset processes," *Physical Review E*, vol. 98, p. 022129, Aug 2018.

[118] S. Dhar, S. Dasgupta, A. Dhar, and D. Sen, "Detection of a quantum particle on a lattice under repeated projective measurements," *Physical Review A*, vol. 91, p. 062115, Jun 2015.

[119] S. Dhar, S. Dasgupta, and A. Dhar, "Quantum time of arrival distribution in a simple lattice model," *Journal of Physics A: Mathematical and Theoretical*, vol. 48, no. 11, p. 115304, feb 2015.

[120] J. Fuchs, S. Goldt, and U. Seifert, "Stochastic thermodynamics of resetting," *Europhysics Letters*, vol. 113, no. 6, p. 60009, 2016.

[121] A. Pal and S. Rahav, "Integral fluctuation theorems for stochastic resetting systems," *Physical Review E*, vol. 96, p. 062135, Dec 2017.

[122] M. Magoni, S. N. Majumdar, and G. Schehr, "Ising model with stochastic resetting," *Physical Review Research*, vol. 2, p. 033182, Aug 2020.

[123] S. Gupta, S. N. Majumdar, and G. Schehr, "Fluctuating interfaces subject to stochastic resetting," *Physical Review Letters*, vol. 112, p. 220601, Jun 2014.

[124] C. Godrèche, S. N. Majumdar, and G. Schehr, "Statistics of the longest interval in renewal processes," *Journal of Statistical Mechanics: Theory and Experiment*, vol. 2015, no. 3, p. P03014, mar 2015.

[125] A. Nagar and S. Gupta, "Diffusion with stochastic resetting at power-law times," *Physical Review E*, vol. 93, p. 060102, Jun 2016.

[126] S. Gupta and A. Nagar, "Resetting of fluctuating interfaces at power-law times," *Journal of Physics A: Mathematical and Theoretical*, vol. 49, no. 44, p. 445001, oct 2016.

[127] M. Kim, L. Santen, and J. D. Noh, "Asymmetric simple exclusion process in one-dimensional chains with long-range links," *Journal of Statistical Mechanics: Theory and Experiment*, vol. 2011, no. 04, p. P04003, 2011.

[128] S. N. Majumdar, S. Krishnamurthy, and M. Barma, "Nonequilibrium phase transition in a model of diffusion, aggregation, and fragmentation," *Journal of Statistical Physics*, vol. 99, no. 1-2, pp. 1–29, 2000.

[129] R. Rajesh and S. N. Majumdar, "Exact phase diagram of a model with aggregation and chipping," *Physical Review E*, vol. 63, no. 3, p. 036114, 2001.

[130] R. Rajesh and S. Krishnamurthy, "Effect of spatial bias on the nonequilibrium phase transition in a system of coagulating and fragmenting particles," *Physical Review E*, vol. 66, p. 046132, Oct 2002.

[131] H. Sachdeva, M. Barma, and M. Rao, "Condensation and intermittency in an open-boundary aggregation-fragmentation model," *Physical Review Letters*, vol. 110, p. 150601, April 2013.

[132] H. Sachdeva and M. Barma, "Analytical study of giant fluctuations and temporal intermittency," *Journal of Statistical Physics*, vol. 154, p. 950, December 2013.

[133] S. A. Janowsky and J. L. Lebowitz, "Finite-size effects and shock fluctuations in the asymmetric simple-exclusion process," *Physical Review A*, vol. 45, no. 2, pp. 618–625, 1992.

[134] O. Costin, J. L. Lebowitz, A. R. Speer, and A. Troiani, "The blockage problem," *Bulletin of the Institute of Mathematics Academia Sinica*, vol. 8, no. 1, pp. 49–72, 2013.

[135] R. Basu, V. , Sidoravicius, and A. Sly, "Last passage percolation with a defect line and the solution of the slow bond problem," *arxiv preprint:1408:3464v3*, vol. 110, 2016.

[136] J. Schmidt, V. Popkov, and A. Schadschneider, "Defect-induced phase transition in the asymmetric simple exclusion process," *Europhysics Letters*, vol. 110, p. 20008, 2015.

[137] K. Mallick, "The exclusion process: A paradigm for non-equilibrium behaviour," *Physica A: Statistical Mechanics and its Applications*, vol. 418, pp. 17 – 48, 2015.

[138] K. Dao Duc, Z. H. Saleem, and Y. S. Song, "Theoretical analysis of the distribution of isolated particles in totally asymmetric exclusion processes: Application to mrna translation rate estimation," *Physical Review E*, vol. 97, p. 012106, Jan 2018.

[139] D. E. Andreev, M. Arnold, S. J. Kiniry, G. Loughran, A. M. Michel, D. Rachinskii, and P. V. Baranov, "Tasep modelling provides a parsimonious explanation for the ability of a single uorf to derepress translation during the integrated stress response," *eLife*, vol. 7, p. e32563, jun 2018.

[140] S. Scott and J. Szavits-Nossan, "Power series method for solving tasep-based models of mrna translation," *bioRxiv*, 2019.

[141] I. Neri, N. Kern, and A. Parmeggiani, "Exclusion processes on networks as models for cytoskeletal transport," *New Journal of Physics*, vol. 15, no. 8, p. 085005, aug 2013.

[142] B. Gutenberg and C. F. Richter, "Frequency of earthquakes in california," *Bulletin of the Seismological Society of America*, vol. 34, no. 4, pp. 185–188, 1944.

[143] J. M. Carlson and J. S. Langer, "Mechanical model of an earthquake fault," *Physical Review A*, vol. 40, pp. 6470–6484, Dec 1989.

[144] E. T. Lu and R. J. Hamilton, "Avalanches and the distribution of solar flares," *The astrophysical journal*, vol. 380, pp. L89–L92, 1991.

[145] J. Touboul and A. Destexhe, "Can power-law scaling and neuronal avalanches arise from stochastic dynamics?" *PloS one*, vol. 5, no. 2, p. e8982, 2010.

[146] X. Gabaix, P. Gopikrishnan, V. Plerou, and H. Stanley, "A theory of power-law distributions in financial market fluctuations," *Nature*, vol. 423, pp. 267–70, 06 2003.

[147] M. Haase, C. G. HÃijbner, E. Reuther, A. Herrmann, K. MÃijllen, and T. BaschÃl', "Exponential and power-law kinetics in single-molecule fluorescence intermittency," *The Journal of Physical Chemistry B*, vol. 108, no. 29, pp. 10 445–10 450, 2004.

[148] G. Schlegel, J. Bohnenberger, I. Potapova, and A. Mews, "Fluorescence decay time of single semiconductor nanocrystals," *Physical Review Letters*, vol. 88, p. 137401, Mar 2002.

[149] M. F. L'Annunziata, *Radioactivity: introduction and history, from the quantum to quarks*. Elsevier, 2016.

[150] D. G. Kendall, "Stochastic processes occurring in the theory of queues and their analysis by the method of the imbedded markov chain," *The Annals of Mathematical Statistics*, vol. 24, no. 3, pp. 338–354, 09 1953.

[151] M. L. McManus, M. C. Long, A. Cooper, and E. Litvak, "Queuing theory accurately models the need for critical care resources," *Anesthesiology: The Journal of the American Society of Anesthesiologists*, vol. 100, no. 5, pp. 1271–1276, 2004.

[152] T. L. Saaty, *Elements of queueing theory: with applications*. McGraw-Hill New York, 1961, vol. 34203.

[153] D. Boyer and C. Solis-Salas, "Random walks with preferential relocations to places visited in the past and their application to biology," *Physical Review Letters*, vol. 112, p. 240601, Jun 2014.

[154] A. Proeme, R. A. Blythe, and M. R. Evans, "Dynamical transition in the open-boundary totally asymmetric exclusion process," *Journal of Physics A: Mathematical and Theoretical*, vol. 44, no. 3, p. 035003, 2011.

[155] L. Santen and C. Appert, "The asymmetric exclusion process revisited: Fluctuations and dynamics in the domain wall picture," *Journal of Statistical Physics*, vol. 106, no. 1, pp. 187–199, Jan 2002.

[156] R. B. Stinchcombe and S. L. A. de Queiroz, "Domain-wall theory and nonstationarity in driven flow with exclusion," *Physical Review E*, vol. 94, p. 012105, Jul 2016.

[157] A. B. Kolomeisky, G. M. SchÃijtz, E. B. Kolomeisky, and J. P. Straley, "Phase diagram of one-dimensional driven lattice gases with open boundaries," *Journal of Physics A: Mathematical and General*, vol. 31, no. 33, pp. 6911–6919, aug 1998.

[158] A. Nagar, S. N. Majumdar, and M. Barma, "Strong clustering of noninteracting, sliding passive scalars driven by fluctuating surfaces," *Physical Review E*, vol. 74, p. 021124, Aug 2006.

[159] D. Das and M. Barma, "Particles sliding on a fluctuating surface: Phase separation and power laws," *Physical Review Letters*, vol. 85, pp. 1602–1605, Aug 2000.

List of Publications

Refereed International Journals

1. S. Karthika and A. Nagar, *The effect of boundaries and impurity on a system with non-local hop dynamics*, J. Phys. A: Math. Theor. **52**, 085003 (2019).

2. S. Karthika and A. Nagar, *Effect of stochastic resetting in Totally asymmetric simple exclusion process*, J. Phys. A: Math. Theor. **53**, 115003 (2020).

Appendix A

Derivation of probability density

The probability density $f_\gamma(t, t-\tau)$ can be expressed as the product of the probabilities of two events:

$$f_\gamma(t, t-\tau) = \phi_0(\tau) G(t-\tau) \tag{A.1}$$

where $G(t-\tau)$ is the probability density for a reset at time $t-\tau$ and $\phi_0(\tau)$ is the probability that there is no reset in the time interval $[t-\tau, t]$. The latter can be calculated as $\phi_0(\tau) = \int_\tau^\infty d\tau' \phi(\tau') = (\tau/\tau_0)^{-\alpha}$.

Let us define $g_n(t); n \geq 0$ to be the probability for the n^{th} reset to take place at time t. The normalization condition implies that $\int_0^\infty dt\, g_n(t) = 1$. Here $g_0(t) = \delta(t)$ accounts for the initial condition of the empty lattice, starting with a reset. We also have

$$g_n(t) = \int_0^t d\tau \phi(t-\tau) g_{n-1}(\tau); n \geq 1. \tag{A.2}$$

Since the probability for the n^{th} reset at time t is given by the probability for the $(n-1)^{th}$ reset at an earlier time τ and the probability that the next reset happens after an interval $t-\tau$. By definition, we have

$$G(t) = \delta(t) + \sum_{n=1}^{\infty} g_n(t). \tag{A.3}$$

We can use Laplace transform to compute $g_n(t)$ in the limit of large t and thus calculate $G(t)$. One can show that at large times for $0 < \gamma < 1$, $G(t) \sim t^{\gamma-1}$. Plugging this into equation (A.1) and normalizing, we get

$$f_{\gamma<1}(t, t-\tau) = \frac{\sin(\pi\gamma)}{\pi} \tau^{-\gamma} (t-\tau)^{\gamma-1}. \tag{A.4}$$

When $\gamma > 1$, one can show that for large times ($t \gg \tau_0$), $G(t) = \frac{1}{\langle\tau\rangle}$, which when plugged into equation (A.1), gives us

$$f_{\gamma>1,\tau\geq\tau_0}(t, t-\tau) = \frac{\gamma-1}{\gamma\tau_0}(\tau/\tau_0)^{-\gamma}. \tag{A.5}$$